

DETERMINATION OF HERBICIDES IN WATER SAMPLES BY SPECTROSCOPIC TECHNIQUES



A Dissertation Submitted in Partial Fulfillment of the Requirements  
for the Degree of Doctor of Philosophy in Chemistry

Department of Chemistry

FACULTY OF SCIENCE

Chulalongkorn University

Academic Year 2020

Copyright of Chulalongkorn University

การตรวจวัดสารฆ่าวัชพืชในตัวอย่างน้ำด้วยเทคนิคทางสเปกโทรสโกปี



วิทยานิพนธ์นี้เป็นส่วนหนึ่งของการศึกษาตามหลักสูตรปริญญาวิทยาศาสตรดุษฎีบัณฑิต

สาขาวิชาเคมี ภาควิชาเคมี

คณะวิทยาศาสตร์ จุฬาลงกรณ์มหาวิทยาลัย

ปีการศึกษา 2563

ลิขสิทธิ์ของจุฬาลงกรณ์มหาวิทยาลัย

Thesis Title	DETERMINATION OF HERBICIDES IN WATER SAMPLES BY SPECTROSCOPIC TECHNIQUES
By	Miss Anna Prukjareonchook
Field of Study	Chemistry
Thesis Advisor	Assistant Professor LUXSANA DUBAS, Ph.D.
Thesis Co Advisor	Associate Professor THANYALAK CHAISUWAN, Ph.D.

---

Accepted by the FACULTY OF SCIENCE, Chulalongkorn University in Partial Fulfillment of the Requirement for the Doctor of Philosophy

..... Dean of the FACULTY OF SCIENCE  
(Professor POLKIT SANGVANICH, Ph.D.)

DISSERTATION COMMITTEE

..... Chairman  
(Associate Professor VUDHICHAJ PARASUK, Ph.D.)

..... Thesis Advisor  
(Assistant Professor LUXSANA DUBAS, Ph.D.)

..... Thesis Co-Advisor  
(Associate Professor THANYALAK CHAISUWAN, Ph.D.)

..... Examiner  
(Associate Professor FUANGFA UNOB, Ph.D.)

..... Examiner  
(Assistant Professor WARINTHORN CHAVASIRI, Ph.D.)

..... External Examiner  
(Assistant Professor Anawat Pinisakul, Ph.D.)

อรรณา พฤกษ์เจริญโชค : การตรวจวัดสารฆ่าวัชพืชในตัวอย่างน้ำด้วยเทคนิคทางสเปกโทรสโกปี. ( DETERMINATION OF HERBICIDES IN WATER SAMPLES BY SPECTROSCOPIC TECHNIQUES) อ.ที่ปรึกษาหลัก : ผศ. ดร.ลักขณา ดุบาส, อ.ที่ปรึกษาร่วม : รศ. ดร.ธัญญลักษณ์ ฉายสุวรรณ

อาหาราซินและพาราควอตถูกใช้อย่างกว้างขวางเพื่อควบคุมวัชพืชในพื้นที่ทำการเกษตร การตกค้างของสารฆ่าวัชพืชสามารถทำอันตรายต่อสิ่งแวดล้อมและสิ่งมีชีวิต ในงานวิจัยนี้ ตัวดูดซับคาร์บอนที่มีรูพรุนระดับนาโนที่เตรียมจากพอลิเบนซอกซาซินฐานเมลามีน หรือ NPC-PBZ-m เพื่อเป็นตัวดูดซับสำหรับอาหาราซินและพาราควอต NPC-PBZ-m ถูกสังเคราะห์โดยขั้นตอนซอล-เจลและการแยกสลายด้วยความร้อน ในการตรวจสอบลักษณะเฉพาะของตัวดูดซับจะใช้เทคนิค FTIR, BET, XPS, และ FE-SEM ในการตรวจวัดอาหาราซิน วิธีที่พัฒนาประกอบด้วย คอลัมน์เพิ่มความเข้มข้นของ NPC-PBZ-m ที่ใช้ร่วมกับการตรวจวัดเชิงสีโดยอาศัยปฏิกิริยา Konig และเทคนิค HPLC-UV ที่ความยาวคลื่น 222 นาโนเมตร ได้มีการศึกษาภาวะที่เหมาะสมของตัวแปรที่ส่งผลต่อประสิทธิภาพการดูดซับ ความสามารถในการนำคอลัมน์ NPC-PBZ-m กลับมาใช้ใหม่ได้ถึง 8 รอบ ในการวิเคราะห์เชิงสีโดยการวัดปริมาณ สารประกอบ polymethine สีส้มแดงซึ่งถูกพัฒนาขึ้นโดยใช้ 6% โดยน้ำหนักต่อปริมาตรของ p-Anisidine เทคนิค HPLC-UV และการตรวจวัดเชิงสี แสดงความสัมพันธ์ที่เป็นเส้นตรงที่ดีในช่วง 5-30 ไมโครกรัมต่อลิตรและ 10-30 ไมโครกรัมต่อลิตร กับค่าสัมประสิทธิ์ของสหสัมพันธ์เป็น 0.9988 และ 0.9979 ตามลำดับ ขีดจำกัดของวิธีในการตรวจพบ (MDL) และขีดจำกัดของวิธีของการวัดปริมาณ (MQL) ของการวิเคราะห์ด้วยเทคนิค HPLC-UV เป็น 1.05 ไมโครกรัมต่อลิตรและ 3.45 ไมโครกรัมต่อลิตร ในขณะที่การวิเคราะห์ด้วยเทคนิค UV-Vis เป็น 2.26 ไมโครกรัมต่อลิตรและ 7.46 ไมโครกรัมต่อลิตร ตามลำดับ ค่าการคืนกลับจากการเติมสารมาตรฐานที่ทราบค่าแน่นอนลงในตัวอย่างของเทคนิค HPLC-UV อยู่ในช่วง 98-105% ในขณะที่การตรวจวัดเชิงสีอยู่ในช่วง 100-107% นอกจากนี้ NPC-PBZ-m ที่ใช้ร่วมกับการตรวจวัดทางสีโดยอาศัยการทำปฏิกิริยากับกลูโคส แสดงประสิทธิภาพที่ดีสำหรับการตรวจวัดพาราควอต โดย NPC-PBZ-m จะถูกกระตุ้นด้วยสารละลายโพแทสเซียมไฮดรอกไซด์ 0.1 โมลาร์ก่อนใช้ อัตราส่วนที่เหมาะสมระหว่างน้ำหนักของ NPC-PBZ-m ต่อปริมาตรของโพแทสเซียมไฮดรอกไซด์ 0.1 โมลาร์เป็น 1 ต่อ 1 โดยน้ำหนักต่อปริมาตร สำหรับขั้นตอนการชะ 2 มิลลิลิตรของสารละลายกรดไฮโดรคลอริก 1 โมลาร์กับเมทานอลที่อัตราส่วน 70 ต่อ 30 โดยปริมาตร เป็นสารละลายที่เหมาะสมสำหรับการชะออก โดยมีการรายงานช่วงการตรวจวัดที่ได้จากวิธีนี้ในช่วง 0.05-1 ไมโครกรัมต่อมิลลิลิตร ที่มีค่าสัมประสิทธิ์ของสหสัมพันธ์เป็น 0.986

สาขาวิชา เคมี  
ปีการศึกษา 2563

ลายมือชื่อนิสิต .....  
ลายมือชื่อ อ.ที่ปรึกษาหลัก .....  
ลายมือชื่อ อ.ที่ปรึกษาร่วม .....

# # 5772217823 : MAJOR CHEMISTRY

KEYWORD: Atrazine determination, Paraquat determination, Nanoporous carbon,  
Polybenzoxazine, Solid phase extraction

Anna Prukjareonchook : DETERMINATION OF HERBICIDES IN WATER SAMPLES BY  
SPECTROSCOPIC TECHNIQUES. Advisor: Asst. Prof. LUXSANA DUBAS, Ph.D. Co-advisor:  
Assoc. Prof. THANYALAK CHAISUWAN, Ph.D.

Atrazine and paraquat are widely used to control weeds in the agricultural areas. The residue of herbicides can harm the environment and living things. In this research, nanoporous carbon derived from melamine based polybenzoxazine or NPC-PBZ-m was used as an adsorbent for atrazine and paraquat analysis. NPC-PBZ-m was synthesized by sol-gel and pyrolysis processes. The characteristics of sorbent were investigated by FTIR, BET, XPS, and FE-SEM. For atrazine determination, NPC-PBZ-m pre-concentration column combined with a colorimetric detection based on a König's reaction and HPLC-UV at 222 nm were developed. The parameters affecting the adsorption performance were optimized. The reusability of the NPC-PBZ-m column was over 8 cycles. For colorimetric analysis, the orange-red polymethine compound was developed by using 6 (%w/v) of p-Anisidine. The HPLC-UV and colorimetric analysis showed a good linearity in the ranges of 5–30 µg/L and 10–30 µg/L with correlation coefficients of 0.9988 and 0.9979, respectively. The method detection limit (MDL) and method quantitation limit (MQL) of HPLC-UV analysis method were 1.05 µg/L and 3.45 µg/L while UV-Vis analysis method were 2.26 µg/L and 7.46 µg/L, respectively. The recoveries from spiked samples for HPLC analysis was in the range of 98–105% while colorimetric analysis was in the range of 100–107%. Moreover, NPC-PBZ-m combined with colorimetric analysis using glucose reagent showed a good performance for paraquat determination. The NPC-PBZ-m was activated with 0.1 M KOH before use. The suitable ratio between weight of NPC-PBZ-m and the volume of 0.1 M KOH was 1:1 (% w/v). For the desorption step, 2 mL of the 70:30 (% v/v) of 1 M HCl:MeOH was used. The dynamic range was found to be from 0.05–1 µg/mL with correlation coefficient of 0.986.

Field of Study: Chemistry

Student's Signature .....

Academic Year: 2020

Advisor's Signature .....

Co-advisor's Signature .....

## ACKNOWLEDGEMENTS

My thesis would have been impossible and I would not have archived this far without all the support that I can receive from these people,

First, I would like to express my deep and sincere gratitude to my research advisor, Assistant Professor Dr. Luxsana Dubas, and my co-advisor, Associate Professor Dr. Thanyalak Chaisuwan, for their invaluable suggestion, support, motivation, inspiration, and confidence throughout this thesis process. Beside my advisors, I would like to gratefully my thesis committee members, Associate Professor Dr. Vudhichai Parasuk, Associate Professor Dr. Fuangfa Unob, Assistant Professor Dr. Warinthorn Chavasiri, and Assistant Professor Dr. Anawat Pinisakul for the helpful comments and suggestion in my research. Furthermore, I would like to thank Dr. Chadin Kulsing for any guidance and kindly support the HPLC-MS part in my work.

Second, The Scholarship from the Graduate School, Chulalongkorn University to commemorate the 72nd anniversary of his Majesty King Bhumibala Aduladeja and the 90th Anniversary Chulalongkorn University Fund (Ratchadaphiseksomphot Endowment Fund) are gratefully acknowledged.

My thankfulness is also sent to Dr. Nicharat Manmuanpom, Mr. Worawut Naewrittikul, and all members of my co-advisor group at the petroleum and petrochemical college, Chulalongkorn University. I also extend my gratitude to Miss Patcharaporn Muhry for the information on Konig's reaction mechanism. In addition, I would like to thank my friends, my seniors and all members of 1253 Laboratory for their kindness, cheer me up, friendship, and helpfulness.

Last, I would like to send a special thanks to my lovely family and my special friend, Mr. Jittawat Pradermwong, for their love, kindly support, encouragement and being besides me throughout the duration of my work.

Anna Prukjareonchook

## TABLE OF CONTENTS

	<b>Page</b>
ABSTRACT (THAI).....	iv
ABSTRACT (ENGLISH).....	v
ACKNOWLEDGEMENTS.....	vi
TABLE OF CONTENTS.....	vii
LIST OF FIGURES.....	xvii
LIST OF TABLES.....	xxii
LIST OF ABBREVIATIONS.....	xxiv
CHAPTER I INTRODUCTION.....	1
1.1 Statement of purpose.....	1
1.2 Objectives.....	4
1.3 Scopes of the research.....	4
1.4 Benefits of the research.....	5
CHAPTER II THEORY AND LITERATURE REVIEW.....	6
2.1 Atrazine.....	6
2.2 Paraquat.....	6
2.3 Polybenzoxazine.....	7
2.3.1 Benzoxazine monomer.....	7
2.3.2 Cationic ring-opening polymerization.....	9
2.3.3 Characterization of oxazine ring and ring-opening polymerization.....	11
2.3.4 The preparation of nanoporous carbon derived polybenzoxazine via sol-gel process.....	11

2.3.4.1 Sol-gel process.....	11
2.3.4.2 The nanoporous carbon material derived from polybenzoxazine	12
2.4 Alginate.....	14
2.5 Humic acid.....	15
2.6 Konig's reaction.....	16
2.7 Polymethine compound.....	17
2.8 Paraquat blue free radical reaction.....	18
2.9 Literature reviews.....	19
2.9.1 Solid phase extraction method for atrazine determination.....	19
2.9.2 Nanoporous carbon derived from melamine based polybenzoxazine.....	21
2.9.3 The adsorbents for paraquat adsorption.....	23
2.9.4 Atrazine and paraquat colorimetric detection.....	23
2.9.4.1 The atrazine detection based on Konig's reaction.....	24
2.9.4.2 The paraquat detection based on blue free radical reaction.....	25
CHAPTER III EXPERIMENTAL.....	28
3.1 Chemicals.....	28
3.2 Apparatus.....	29
3.3 The synthesis of nanoporous carbon derived from melamine based polybenzoxazine (NPC-PBZ-m) used as pre-concentration sorbent.....	31
3.3.1 Melamine based benzoxazine organogel synthesis.....	31
3.3.2 Melamine based benzoxazine organogel polymerization.....	32
3.3.3 Nanoporous carbon derived from melamine based polybenzoxazine (NPC-PBZ-m) preparation.....	33
3.4 Characterizations of nanoporous carbon derived from melamine based polybenzoxazine (NPC-PBZ-m).....	34



3.4.1 Fourier Transform Infrared Spectrometer (FTIR).....	34
3.4.2 Quantachrome-Autosorb-1 MP Surface Area and Pore Size Analyzer .....	34
3.4.3 X-ray Photoelectron Spectroscopy (XPS) .....	34
3.4.4 Field Emission Scanning Electron Microscope (FE-SEM) .....	34
3.5 Solutions preparation .....	35
3.5.1 100 and 500 µg/mL of atrazine standard stock solutions.....	35
3.5.2 Working atrazine standard solutions.....	35
3.5.2.1 5–30 µg/L of atrazine working solutions.....	35
3.5.2.2 0.1–5 µg/mL of atrazine working solutions .....	35
3.5.3 A series of atrazine standard solution (0.005–5 µg/mL) in sample blank solvent.....	36
3.5.4 Paraquat, glyphosate, 2,4-dichlorophenoxyacetic (2,4-D) and chlorpyrifos standard stock solutions .....	36
3.5.5 The mixture standard solutions of pesticides .....	36
3.5.5.1 HPLC-UV analysis method .....	36
3.5.5.2 UV-Vis based on König's reaction .....	37
3.5.6 5 M sodium hydroxide solution.....	38
3.5.7 6 (% w/v) <i>p</i> -Anisidine solution .....	39
3.5.8 8 and 10 (% v/v) aniline solutions .....	39
3.5.9 1 (% w/v) sulfanilic acid solution .....	39
3.5.10 0.5 (% w/v) 4-aminophenol.....	39
3.5.11 1 M glucose solution.....	39
3.5.12 1 M potassium hydroxide solution .....	39
3.5.13 1 M HCl-MeOH (70:30, % v/v) .....	39

3.6 Atrazine pre-concentration.....	39
3.6.1 NPC-PBZ-m column preparation .....	40
3.6.1.1 Investigation of NPC-PBZ-m particle size.....	41
3.6.1.2 Investigation of NPC-PBZ-m weight .....	42
3.6.1.3 Investigation of adsorption flow rate .....	42
3.6.1.4 Investigation of elution volume and elution flow rate .....	42
3.6.1.5 Reusability of NPC-PBZ-m pre-concentration column .....	42
3.6.2 Selectivity of HPLC-UV analysis .....	43
3.6.3 Enrichment factor determination .....	44
3.6.4 The precision and interference of NPC-PBZ-m column on atrazine adsorption.....	45
3.6.4.1 The Repeatability (%RSD <sub>r</sub> ) and reproducibility (%RSD <sub>R</sub> ) of pre- concentration procedure.....	45
3.6.4.2 The effect of pesticides on atrazine adsorption on NPC-PBZ-m pre-concentration column .....	46
3.7 Optimization of parameters affecting on atrazine-colorimetric detection based on Konig's reaction.....	47
3.7.1 Optimization the volume of pyridine and conc. HCl volume (step 1).....	49
3.7.1.1 Effect of pyridine volume .....	49
3.7.1.2 Effect of conc. HCl volume .....	50
3.7.2 Effect of reaction temperature, heating time, and NaOH concentration on glutaconic dialdehyde (yellow product) formation (step 2) .....	50
3.7.2.1 Effect of reaction temperature.....	51
3.7.2.2 Effect of heating time .....	51
3.7.2.3 Effect of NaOH concentration.....	51

3.7.3 Preliminary study of various coupling reagents study .....	52
3.7.3.1 Aniline .....	52
3.7.3.2 Sulfanilic acid .....	52
3.7.3.3 4-aminophenol.....	52
3.7.4 Optimization of the volume of conc. HCl, <i>p</i> -Anisidine concentration, and reaction time (step 3).....	52
3.7.4.1 Effect of conc. HCl volume for the coupling step .....	52
3.7.4.2 Effect of <i>p</i> -Anisidine concentration .....	53
3.7.4.3 Effect of reaction time on the orange-red polymethine formation .....	53
3.7.5 Characterization of an orange-red polymethine compound.....	53
3.7.5.1 HPLC-UV analysis system.....	53
3.7.5.2 UPLC-MS analysis system .....	55
3.7.6 The analytical performance of atrazine via the Konig's reaction using <i>p</i> -Anisidine as coupling reagent. ....	56
3.7.6.1 The matrix effect .....	57
3.7.6.2 Working range, Instrument detection limit (IDL), and limit of quantitation (LOQ) .....	57
3.7.6.3 Effect of other pesticides on atrazine colorimetric detection (Konig's reaction).....	57
3.8 Quantitative Analysis .....	58
3.8.1 Interferences in the performance of the developed method .....	58
3.8.2 Matrix effect for assessing the performance of method .....	58
3.9 Application to environmental water samples for atrazine determination.....	59
3.9.1 The preparation of water samples.....	59

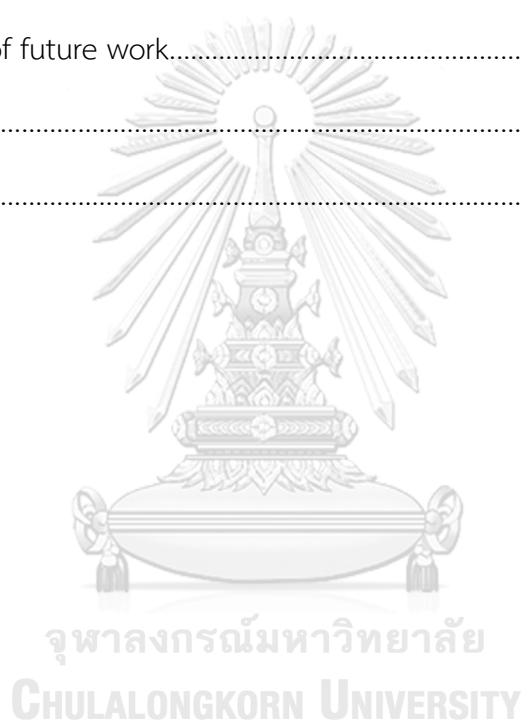
3.9.2 Quantitative analysis of atrazine in real water sample.....	59
3.10 Preparation of Si-HA-Alg materials (Si-HA-Alg).....	61
3.10.1 Preparation of agar mold contained CaCl <sub>2</sub> .....	61
3.10.2 Preparation of Si-HA-Alg materials .....	62
3.10.2.1 Effect of the percentage of silica particles and humic acid sodium salt (HA).....	63
3.10.2.2 Percentage of alginate study .....	64
3.11 The preliminary test for paraquat adsorption by NPC-PBZ-m.....	64
3.11.1 The effect of KOH activation, DI washing step after activation and agitation direction on paraquat adsorption on NPC-PBZ-m .....	64
3.11.2 The stability of paraquat in KOH activation .....	65
3.11.3 The study of solvent for paraquat desorption.....	66
3.12 The optimization of paraquat blue free radical reaction for colorimetric method .....	66
3.12.1 The concentration and volume of glucose .....	67
3.12.2 The concentration and volume of NaOH.....	67
3.12.3 The suitable of reaction time .....	67
3.12.4 Limit of detection (LOD) and limit of quantitation (LOQ) for paraquat blue free radical reaction .....	67
3.13 Optimization conditions for paraquat-NPC-PBZ-m batch adsorption study.....	67
3.14 The performance of NPC-PBZ-m for paraquat determination .....	68
3.15 The suggestion of this proposed method to enhance the efficiency for paraquat detection.....	69
3.15.1 Weight of NPC-PBZ-m study.....	69
3.15.2 The ratio of NPC-PBZ-m weight to KOH volume (mg/mL) study .....	69

CHAPTER IV RESULTS AND DISCUSSION .....	70
4.1 Characterization of nanoporous carbon derived from melamine based polybenzoxazine (NPC-PBZ-m) sorbent .....	70
4.1.1 Melamine based polybenzoxazine (PBZ-m) characterization .....	71
4.1.2 The textural properties of nanoporous carbon derived from melamine based polybenzoxazine (NPC-PBZ-m).....	72
4.1.3 The functionality of nitrogen- and carbon-containing on nanoporous carbon derived from melamine based polybenzoxazine (NPC-PBZ-m) ...	73
4.1.4 The surface morphology of nanoporous carbon derived from melamine based polybenzoxazine (NPC-PBZ-m).....	74
4.2 Optimization parameters affecting on NPC-PBZ-m pre-concentration efficiency .....	75
4.2.1 Effect of pH on atrazine-NPC-PBZ-m adsorption .....	76
4.2.2 Effect of NPC-PBZ-m particle size .....	76
4.2.3 Effect of NPC-PBZ-m weight .....	77
4.2.4 Effect of sample flow rate .....	78
4.2.5 Effect of eluent volume (methanol) and elution flow rate .....	79
4.2.6 Reusability of NPC-PBZ-m pre-concentration column.....	81
4.3 Selectivity of HPLC-UV analysis.....	81
4.4 Enrichment factor.....	83
4.5 The precision and interferences of NPC-PBZ-m column for atrazine adsorption .....	84
4.5.1 Repeatability ( $RSD_r$ ) and reproducibility ( $RSD_R$ ) of pre-concentration procedure.....	84
4.5.2 Effect of other pesticides on atrazine adsorption on NPC-PBZ-m pre-concentration column.....	85

4.6 Optimization parameters affecting on atrazine-colorimetric detection.....	87
4.6.1 Investigation of pyridine and conc. HCl volume (step 1).....	88
4.6.1.1 Effect of pyridine volume .....	88
4.6.1.2 Effect of conc. HCl volume .....	89
4.6.2 Effect of temperature, heating time, and sodium hydroxide (NaOH) concentration (step 2).....	89
4.6.2.1 Effect of reaction temperature.....	90
4.6.2.2 Effect of heating time.....	90
4.6.2.3 Effect of NaOH concentration.....	90
4.6.3 Preliminary study of various coupling reagents.....	92
4.6.3.1 Aniline .....	92
4.6.3.2 Sulfanilic acid .....	93
4.6.3.3 4-aminophenol.....	93
4.6.4 Optimization of <i>p</i> -Anisidine as the coupling reagent (step 3).....	95
4.6.4.1 Volume of conc. HCl for coupling step .....	97
4.6.4.2 Effect of <i>p</i> -Anisidine concentration .....	97
4.6.4.3 Effect of reaction time on orange-red polymethine compound formation .....	98
4.6.5 Characterization of an orange-red polymethine compound.....	100
4.6.6 The analytical performance of atrazine via the Konig's reaction using <i>p</i> - Anisidine as coupling reagent .....	103
4.6.6.1 Matrix effect.....	104
4.6.6.2 Dynamic range, Instrument detection limit (IDL), limit of quantitation (LOQ) for UV-Vis measurement.....	104
4.6.6.3 Effect of other pesticides on UV-Vis method (Konig's reaction) .	106

4.7 Quantitative analysis.....	107
4.7.1 Interferences in the performance of the developed method .....	109
4.7.2 Matrix-match calibration curves on HPLC-UV measurement .....	111
4.8 Application to environmental water samples for atrazine determination.....	112
4.9 The preparation of silica-humic acid entrapped calcium alginate hydrogel (Si-HA-Alg).....	115
4.9.1 Effect of the percentage of silica particles and humic acid sodium salt (HA) .....	115
4.9.2 Percentage of alginate study.....	116
4.10 The effect of KOH activation, DI washing step after activation and agitation direction on paraquat adsorption on NPC-PBZ-m .....	118
4.11 The stability of paraquat in KOH activation .....	120
4.12 The study of desorption solvent for paraquat determination .....	120
4.13 The optimization of paraquat blue free radical reaction for colorimetric method .....	121
4.13.1 The concentration and volume of glucose study .....	122
4.13.2 The concentration and volume of NaOH study.....	122
4.13.3 The suitable of reaction time .....	123
4.13.4 Instrument detection limit (IDL) and limit of quantitation (LOQ) for paraquat blue free radical reaction.....	124
4.14 Optimization conditions for paraquat-NPC-PBZ-m batch adsorption .....	124
4.14.1 Effect of KOH concentration on activation step .....	124
4.14.2 Study of the volume of desorbing solvent on the paraquat determination.....	125
4.15 The performance of proposed method for paraquat detection .....	126

4.16 The suggestion of this proposed method to enhance the efficiency for paraquat detection.....	127
4.16.1 Effect of NPC-PBZ-m weight on paraquat adsorption.....	127
4.16.2 The ratio of NPC-PBZ-m weight to KOH volume (mg/mL) affecting on paraquat adsorption .....	128
CHAPTER V CONCLUSION .....	129
5.1 Conclusion .....	129
5.2 Suggestion of future work.....	130
REFERENCES .....	131
VITA.....	143





## LIST OF FIGURES

	Page
<b>Figure 2.1</b> Chemical structure of atrazine [28].....	6
<b>Figure 2.2</b> Chemical structure of paraquat [7].....	6
<b>Figure 2.3</b> The structure of Benzoxazine [44]. ....	7
<b>Figure 2.4</b> The mechanism of benzoxazine monomer formation [48,51].....	8
<b>Figure 2.5</b> The monomeric type of monofunctional (Class A) and difunctional with bisphenol-monoamine (Class B) and phenol-diamine (Class C) [44].....	9
<b>Figure 2.6</b> Ring-opening polymerization by phenolic compound initiation [56].....	10
<b>Figure 2.7</b> Proposed of initiation mechanism with acid catalyst [56]. ....	11
<b>Figure 2.8</b> The sequence of sol-gel processing step for porous solid preparation [60]. .....	12
<b>Figure 2.9</b> Precursors and the polybenzoxazine reaction [47]. ....	13
<b>Figure 2.10</b> Phase separation in DMF (a) and dioxane (b) solvents [61]. ....	14
<b>Figure 2.11</b> Sodium alginate molecular structure [63].....	15
<b>Figure 2.12</b> Model of humic acid structure [68]. ....	16
<b>Figure 2.13</b> The probable color reaction of polymethine dye [36]. ....	17
<b>Figure 2.14</b> Polymethine dye (PD) structure [72]. ....	18
<b>Figure 2.15</b> Paraquat reduction-oxidation [41]. ....	18
<b>Figure 2.16</b> Visible spectra of paraquat (A) and diquat (B) reduction with sodium dithionite in alkaline solution [73]. ....	18
<b>Figure 2.17</b> Synthesis of benzoxazine monomer based on bisphenol-A and melamine [58]. ....	22
<b>Figure 3.1</b> The proposed reaction of melamine based polybenzoxazine (PBZ-m) synthesis. ....	33

<b>Figure 3.2</b> The NPC-PBZ-m pre-concentration unit. ....	40
<b>Figure 3.3</b> The recycling of NPC-PBZ-m pre-concentration unit. ....	43
<b>Figure 3.4</b> The proposed reaction mechanism of orange-red polymethine compound. .....	48
<b>Figure 3.5</b> The proposed method for atrazine analysis. ....	60
<b>Figure 3.6</b> Agar mold 0.8 (% w/v) containing of 0.8 M CaCl <sub>2</sub> solution. ....	61
<b>Figure 3.7</b> The experimental design to investigate 3 factors: activation, washing and agitation direction, on the paraquat adsorption efficiency. (A): activation, (W): washing step, (S) orbital shaker (x-y direction), and (R) rotating shaker, (NA): no activation, and (NW): no washing step. ....	65
<b>Figure 3.8</b> The experimental step for paraquat determination by using paraquat blue free radical reaction. ....	68
<b>Figure 4.1</b> The oxazine ring and Mannich base bridge structures. ....	71
<b>Figure 4.2</b> FTIR spectra of Melamine based benzoxazine organogel and melamine based polybenzoxazine (PBZ-m). ....	72
<b>Figure 4.3</b> N <sub>2</sub> adsorption-desorption isotherms (A) and pore size distributions (B) of NPC-PBZ-m. ....	73
<b>Figure 4.4</b> XPS narrow scan spectra of N1s (A) and C1s (B) and proposed structure of NPC-PBZ-m (C). ....	74
<b>Figure 4.5</b> SEM micrographs of PBZ-m (A) and NPC-PBZ-m (B) at 100,000X magnification. ....	75
<b>Figure 4.6</b> Effect of pH on atrazine-NPC-PBZ-m batch adsorption. ....	76
<b>Figure 4.7</b> Effect of NPC-PBZ-m particle size. ....	77
<b>Figure 4.8</b> Effect of NPC-PBZ-m weight. ....	78
<b>Figure 4.9</b> Effect of sample flow rate. ....	79
<b>Figure 4.10</b> Effect of elution flow rate. ....	80

<b>Figure 4.11</b> Reusability of NPC-PBZ-m column based on optimum conditions.....	81
<b>Figure 4.12</b> Chromatogram of atrazine spiked in various solutions: MeOH (A), MeOH-NPC-PBZ-m (B), Lopburi (C) and Nakhon Pathom (D), fish farm water (E), and pond water (F). Blue line : non-spiked solvent or water samples; orange line : spiked solvent or water samples. ....	82
<b>Figure 4.13</b> Linear relationship of atrazine concentration before and after pre-concentration. ....	84
<b>Figure 4.14</b> The proposed reaction mechanism of Konig's reaction (step 1). ....	88
<b>Figure 4.15</b> Effect of pyridine volume (A) and conc. HCl volume (B) in step 1.....	89
<b>Figure 4.16</b> Effect of reaction temperature (A) and heating time (B).....	90
<b>Figure 4.17</b> Effect of NaOH concentration.....	91
<b>Figure 4.18</b> The proposed reaction mechanism of Konig's reaction (step 2). ....	92
<b>Figure 4.19</b> The study of volume of conc. HCl for aniline (A), concentration of aniline (B), volume of conc. HCl for sulfanilic acid (C), concentration of sulfanilic acid (D), volume of conc. HCl for 4-aminophenol (E), concentration of 4-aminophenol (F). ....	94
<b>Figure 4.20</b> UV-Vis spectra (A) and solution color of polymethine compounds coupling with aniline, sulfanilic acid, and 4-aminophenol (B). ....	95
<b>Figure 4.21</b> The proposed reaction mechanism of Konig's reaction (step 3). ....	96
<b>Figure 4.22</b> Effect of conc. HCl volume (A) and p-Anisidine concentration (B) on orange-red polymethine compound formation.....	98
<b>Figure 4.23</b> Effect of reaction time on orange-red polymethine compound formation. ....	99
<b>Figure 4.24</b> The peak chromatograms of atrazine standard solution (A), orange-red polymethine compound (B), and pyridine and p-Anisidine reagents (C).....	101
<b>Figure 4.25</b> TIC and EIC of Atrazine (A) and orange-red polymethine compound (B). ....	103

<b>Figure 4.26</b> The linear relationship between atrazine concentration and the absorbance intensity of polymethine compound at 500 nm and the color chart for atrazine determination. ....	105
<b>Figure 4.27</b> Effect of other pesticides on the color of polymethine compound development: atrazine (A); paraquat (P); glyphosate (G); 2,4-D (D); chlorpyrifos (C). AX is the mixture of atrazine with the other pesticides (X). The absorbance of orange-red polymethine compound performed at 1 µg/mL of atrazine. ....	107
<b>Figure 4.28</b> Effect of other pesticides on the colorimetric analysis. Atrazine (A); paraquat (P); glyphosate (G); 2,4-D (D); chlorpyrifos (C). AX is the mixture of atrazine with the other pesticides (X). ....	110
<b>Figure 4.29</b> The different amount of silica (Si) (0-2 % w/v) and humic acid (HA) (0-2 % w/v) contained in alginate bead (Alg) affecting paraquat adsorption efficiency. The concentration of alginate (Alg) was fixed at 2 (% w/v). ....	116
<b>Figure 4.30</b> Alginate content affecting on paraquat adsorption (A) and humic acid leaching (B). ....	117
<b>Figure 4.31</b> The effects of three factors on the paraquat adsorption efficiency investigation. (A): activation, (W): washing step, (S) shaking adsorption (x-y direction), and (R) rotating adsorption, (NA): no activation, and (NW): no washing step. ....	120
<b>Figure 4.32</b> Effect of HCL solution (A) and mixture of HCL-MeOH at ratio 70:30 (B) on paraquat desorption. ....	121
<b>Figure 4.33</b> Glucose concentration (A) and volume of glucose 1 M (B) on paraquat blue free radical reaction. ....	122
<b>Figure 4.34</b> NaOH concentration (A) and volume of NaOH 5 M (B) on paraquat blue free radical reaction. ....	123
<b>Figure 4.35</b> The effect of reaction time on paraquat blue free radical determination. ....	123
<b>Figure 4.36</b> Effect of KOH concentration on activation step on paraquat adsorption. ....	125

<b>Figure 4.37</b> Number of desorption fraction study on paraquat desorption.....	126
<b>Figure 4.38</b> Correlation curve between paraquat concentration against absorbance signal of blue radical at 600 nm.....	127
<b>Figure 4.39</b> Effect of NPC-PBZ-m weight (A) and ratio of NPC-PBZ-m weight to 0.1 M KOH volume (B) on paraquat adsorption. ....	128



## LIST OF TABLES

	<b>Page</b>
<b>Table 2.1</b> The chemical properties of atrazine and paraquat .....	7
<b>Table 2.2</b> SPE method for atrazine determination.....	20
<b>Table 2.3</b> Coupling reagents for Konig's reaction.....	24
<b>Table 2.4</b> The structure and standard reduction potential of reducing agents for paraquat blue free radical formation.....	26
<b>Table 3.1</b> List of chemical and supplier.....	28
<b>Table 3.2</b> List of apparatus.....	30
<b>Table 3.3</b> Mixture standard solutions of pesticides preparation.....	37
<b>Table 3.4</b> Mixture standard solutions of pesticides affecting on atrazine sensitivity based on Konig's reaction.....	38
<b>Table 3.5</b> HPLC-UV condition.....	41
<b>Table 3.6</b> The preparation of mixture solution on pyridine volume study.....	50
<b>Table 3.7</b> Conditions of HPLC-UV.....	54
<b>Table 3.8</b> Mobile phase of HPLC-UV.....	54
<b>Table 3.9</b> Conditions of UPLC-MS.....	55
<b>Table 3.10</b> Mobile phase of UPLC-MS.....	56
<b>Table 3.11</b> The composition of silica gel and humic acid on alginate sorbent study	63
<b>Table 3.12</b> The alginate sorbent preparation for alginate content study.....	64
<b>Table 4.1</b> Textural properties of NPC-PBZ-m .....	73
<b>Table 4.2</b> The optimum conditions of NPC-PBZ-m pre-concentration procedure.....	80
<b>Table 4.3</b> The effect of matrix from NPC-PBZ-m and sample blank on an external calibration curve preparation.....	83
<b>Table 4.4</b> Effect of pesticides on atrazine adsorption of NPC-PBZ-m column.....	86

<b>Table 4.5</b> The structure and log Pow of other pesticides .....	87
<b>Table 4.6</b> The optimum conditions of colorimetric method based on Konig's reaction .....	99
<b>Table 4.7</b> Matrix effect of NPC-PBZ-m sorbent on calibration curve of colorimetric method .....	104
<b>Table 4.8</b> Effect of other pesticides on UV-Vis method determination based on Konig's reaction.....	106
<b>Table 4.9</b> Analytical performance of the HPLC-UV and UV-Vis .....	108
<b>Table 4.10</b> Mean recoveries of atrazine for both HPLC-UV and UV-Vis.....	109
<b>Table 4.11</b> Effect of other pesticides on atrazine determination .....	110
<b>Table 4.12</b> Matrix-matched calibration curve of water samples on HPLC-UV determination.....	111
<b>Table 4.13</b> Matrix-matched calibration curves of water samples on UV-Vis determination.....	112
<b>Table 4.14</b> The recovery and precision in water samples determined by proposed methods .....	113

## LIST OF ABBREVIATIONS

AOAC	Association of Official Analytical Chemists
°C	degree celcius
cm <sup>-1</sup>	wavenumber
g	gram
M	Molar
mg	milligram
mL	milliliter
mL/min	milliliter per minute
NPC-PBZ-m	carbon nanoporous melamine based polybenzoxazine
MDL	method detection limit
MLQ	method quantitation limit
nm	nanometer
LOD	limit of detection
LOQ	limit of quantitation
Si-HA-Alg	silica-humic acid entrapped calcium alginate hydrogel
v/v	volume by volume
% v/v	percentage volume by volume
% w/v	percentage weight by volume
% RSD	Relative standard deviation percentage
µg/mL	microgram per milliliter
µg/L	microgram per liter
2,4-D	2,4-Dichlorophenoxyacetic



## CHAPTER I

### INTRODUCTION

#### 1.1 Statement of purpose

Agricultural sector is an important part of Thailand's development and economy which employs up to 35 percent of the workforce in our country [1]. In 2017, Office of Agricultural Economics (OAE) established the holding land in Thailand was 149,253,717 rais which is calculated as 46.54 percent of total land utilization [2]. However, the agricultural production in Thailand still relies on herbicides usage. Paraquat (1,1'-dimethyl-4,4'-bipyridinium dichloride) and atrazine (6-chloro-N-ethyl-N-(1-methylethyl)-1,3,5-triazine-2,4-diamine) are the two most herbicides applied to prevent unwanted weeds growing and improve crop productivity. For this reason, the contamination of herbicides in natural water resources via surface runoff can occur and be harmful to living things.

Paraquat has been reported as quick-acting and non-selective killer chemicals [3]. In case of atrazine is used to prevent pre- and post-emergence grass and broad-leaved weeds especially for maize, sorghum, pineapple, and sugarcane production [4,5]. Due to its utility, many of these herbicides were imported into Thailand. In 2019, The Office of Agricultural Regulation (OAR) reported that the amounts of paraquat and atrazine were brought into our country as 9,943,932.80 kg and 3,470,312.00 kg, respectively [6]. Because the high dosage of herbicide was applied in agricultural areas, the contamination of these chemicals is poisonous to humans' life and other living things. Paraquat has been reported as an etiological factor of Parkinson's disease [7], while atrazine is well known as an endocrine disruptor. It can interfere with the synthesis, transportation, metabolism, binding or elimination of natural blood-borne hormones [8,9]. In addition, it is also considered as a carcinogenic agent [10,11]. The Pollution Control Department (PCD), Ministry of Natural Resources and Environment of Thailand has established an allowance of the highest paraquat concentration in water

at 0.5 mg/L for freshwater animals [12]. The US Environmental Protection Agency (USEPA) and the Water Environmental Partnership in Asia (WEPA) have established the maximum contamination limit (MCL) for atrazine in drinking water and ground water at 3 µg/L [11,13].

In Thailand, the risk of environment contamination associated with these herbicides have been documented by means of the residue amount detection in natural water resources. The level of paraquat contaminated in ground water and surface water were 1.5-18.9 µg/L and 9.3-87.0 µg/L, respectively [14]. In case of atrazine contamination, previous work reported that an atrazine can be detected in Chao Praya River at level of 0.058-0.086 µg/L [15]. Moreover, the higher level of atrazine contaminated in tap water and drinking water in Thailand were found to be 12.29 µg/L and 18.78 µg/L, respectively [16]. In addition, atrazine contamination in stream water and sediment at Huay Kapo watershed was also reported at 4.7 µg/L and 27.42 µg/kg, respectively [17]. It indicates that pesticide contamination is the crucial problem in Thailand.

Due to the low level of these herbicides in natural water resources, the method which can provide high sensitivity and selectivity was adopted for determination in water samples. In previous work, various techniques were employed to determine paraquat such as liquid chromatography/mass spectrometry (LC/MS) [18], ionic-liquid microextraction coupled with HPLC [19], capillary electrophoresis (CE) [20], and electrochemical method [21]. For atrazine detection, enzyme-linked immunosorbent assay or ELISA [22], gas chromatography/mass spectrometry [23] and solid phase extraction coupled with HPLC/GC [24] have been reported. Although these techniques can detect the herbicides at low concentration, they still have some limitations including high-cost instruments, require a specialist and water sample need to be transferred to laboratory which may increase the chance of sample contamination and degradation. As mentioned, it is quite hard for local authorities' monitoring.

To overcome the limitations, the purpose of this work is to develop an easy-usable method by using the pre-concentration step and colorimetric method for paraquat and atrazine determination without any expensive instrument. For pre-concentration method, the suitable adsorbent should be prepared for herbicides adsorption.

For paraquat sorbent, humic acid [25], alginate bead [26], and silica based material [27] were used as sorbent because they can interact with paraquat via electrostatic interaction. Therefore, silica-humic acid entrapped calcium alginate hydrogel materials (Si-HA-Alg) was prepared and used for paraquat pre-concentration.

In case of atrazine, owing to aromatic ring structure and hydrophobic properties [28], carbon-based sorbents were chosen for adsorption in previous works [29,30]. However, the cost of sorbent is high and the reusability has not reported. Therefore, the carbon-based sorbent which is prepared from polybenzoxazine is interesting because of its excellent properties such as molecular design flexibility, high porosity, high surface area, and low density [31]. For the monomer preparation, the starting materials are composed of phenol, amine, and formaldehyde which are synthesized via a sol-gel process based on ring-opening polymerization. Due to molecular design flexibility, the amine source for synthesis was considered. Because of a similar structure of atrazine and melamine compounds, the sorbent was prepared by using melamine as an amine source according to the previous study [32]. Thus, the carbon nanoporous derived melamine based polybenzoxazine (NPC-PBZ-m) was used for atrazine pre-concentration in this work. The adsorption interaction between atrazine and NPC-PBZ-m sorbent is expected as  $\pi$ - $\pi$  interaction.

After the pre-concentration procedure, a colorimetric method was performed. For paraquat detection, paraquat blue free radical was generated by many reducing agents such as ascorbic acid, sodium borohydride, and sodium dithionite [33-35]. Unfortunately, the stability of these reagents was quite poor. Therefore, glucose was

chosen as a reducing agent in this work. The color of reaction will change from colorless to blue. While atrazine detection, the colorimetric method was developed based on Konig's reaction to generate polymethine compound by using various coupling agent such as *p*-aminoacetophenone (PMP), sulfanilic acid, aniline, and 4-aminoacetanilide [36-40]. However, the obtained polymethine compounds from these reagents have maximum wavelength between 440-480 nm which is difficult to interpret by naked-eye because some reagents have their own color. Thus, *p*-Anisidine was selected as a coupling agent in this work. The color of reaction was changed from colorless to orange-red which has a maximum wavelength at 500 nm. Moreover, the paraquat blue free radical and orange-red polymethine compounds were detected by UV-Visible spectrophotometer.

## 1.2 Objectives

1.2.1 To prepare the silica-humic acid entrapped calcium alginate hydrogel materials (Si-HA-Alg) for paraquat pre-concentration

1.2.2 To synthesize the nanoporous carbon derived melamine based polybenzoxazine (NPC-PBZ-m) for atrazine pre-concentration

1.2.3 To optimize the various parameters affecting on pre-concentration step for paraquat (batch) and atrazine (flow) adsorption

1.2.4 To optimize the various parameters affecting on colorimetric method for paraquat (glucose reaction) and atrazine (Konig's reaction) determination

## 1.3 Scopes of the research

For paraquat determination, silica-humic acid entrapped calcium alginate hydrogel materials (Si-HA-Alg) and NPC-PBZ-m adsorbent were tested. The adsorption and desorption conditions were optimized by using the batch adsorption. The NPC-PBZ-m sorbent found to be the suitable material was selected for further analysis. Many parameters such as NPC-PBZ-m activation and adsorption-desorption conditions

were studied. The optimal condition of the colorimetric detection using glucose, as a reducing agent, was also investigated by UV-Visible spectrophotometer.

For atrazine determination, nanoporous carbon derived melamine based polybenzoxazine (NPC-PBZ-m) sorbent was synthesized and the material was characterized by fourier transform infrared spectrometer using KBr pellets (KBr-FTIR), Brunauer-Emmett-Teller (BET) surface area analyzer, X-ray photoelectron spectroscopy (XPS), and field emission scanning electron microscope (FE-SEM). The pre-concentration unit was prepared by packing NPC-PBZ-m sorbent into SPE empty cartridge operating with a syringe pump. Various parameters affecting pre-concentration such as particle sizes and weight of NPC-PBZ-m, adsorption-elution flow rate, and other herbicides interference were investigated by high-performance liquid chromatography-ultraviolet detector (HPLC-UV). For colorimetric detection, the parameters that can affect the sensitivity of Konig's reaction was also optimized by using UV-Visible spectrophotometer. The efficiency of the proposed method was tested with natural water samples from various resources.

#### **1.4 Benefits of the research**

This work aims to develop the paraquat and atrazine determination which is composed of two sections as pre-concentration and determination steps. The proposed method provides an easy preparation of sorbents and the colorimetric method can be detected by UV-Visible spectrophotometer.

## CHAPTER II

### THEORY AND LITERATURE REVIEW

#### 2.1 Atrazine

Atrazine (6-chloro-*N*-ethyl-*N*-(1-methylethyl)-1,3,5-triazine-2,4-diamine), is an herbicide that is heavily used worldwide to control broadleaf and grassy weed [5]. The residue of atrazine can persist in water and soil for several years which can induce contamination in the environment. This herbicide has been adequate as an endocrine disruptor which may interfere with the metabolism, transportation, binding action or elimination of natural blood-borne hormones [8,9]. Moreover, the hazard of atrazine to humans was also reported as it can increase breast cancer in women and effect on semen quality and fertility in men [10,11]. The chemical structure of atrazine was shown in **Figure 2.1**.

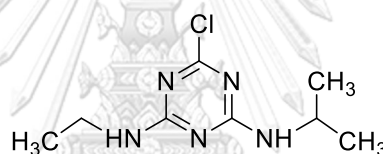


**Figure 2.1** Chemical structure of atrazine [28].

#### 2.2 Paraquat

Paraquat (1,1'-dimethyl-4,4'-dipyridinium dichloride) which is well known in commercial name as Gramoxone is a quaternary ammonium bipyridyl compound. Paraquat is reported as a non-selective and quick-acting herbicide which can interrupt the process of photosynthetic electron transfer in a plant cell [3,41]. The harmful effects of paraquat are reported as it can contribute to the neurodegenerative disorder that led to enhance a risk of Parkinson's disease [7]. The structure of paraquat consisted of two pyridine rings which illustrated the cationic characteristic as shown **Figure 2.2**.

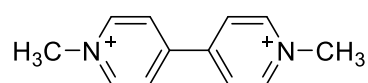


**Figure 2.2** Chemical structure of paraquat [7].

The physical properties of atrazine and paraquat are listed in **Table 2.1**

**Table 2.1** The chemical properties of atrazine and paraquat

Properties	Atrazine [42]	Paraquat [43]
Molecular weight (g/mol)	215.68	186.20 (paraquat) and 257.20 (paraquat dichloride)
Physical state	Solid; White	Solid; white (pure), yellow (technical)
Water solubility at 20 °C	34.7 mg/L	561 g/L
Melting point (°C)	173–175	175–180

## 2.3 Polybenzoxazine

### 2.3.1 Benzoxazine monomer

Benzoxazine is a new class of phenolic resin which is a molecule composed of a benzene ring attached with an oxazine ring, a six-membered heterocyclic ring instituted with nitrogen (N) and oxygen (O) atoms, as shown in **Figure 2.3**. They exhibit many attractive properties over traditional phenolic resin such as high char yields, excellent mechanical-chemical properties, and molecular design flexibility [44-47].

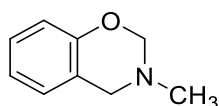


**Figure 2.3** The structure of Benzoxazine [44].

The benzoxazine monomer was synthesized via Mannich condensation reaction from three starting materials which are phenolic compound, formaldehyde, and amine [44,48,49]. The reaction starts with a lone pair electron of nitrogen in amine compound added to carbonyl of formaldehyde compound. This reaction is known as

nucleophilic addition. An obtained iminium ion further reacts with phenolic compounds via electrophilic addition reaction. Finally, the benzoxazine monomer is formed via the dehydration reaction between formaldehyde and mannich bases as shown in **Figure 2.4**. Moreover, the kinetic of benzoxazine synthesis reaction has been studied in previous work [50]. The results indicated that phenol compound played as the key of starting material and the step of reaction between phenol and iminium ion was a controlling step.

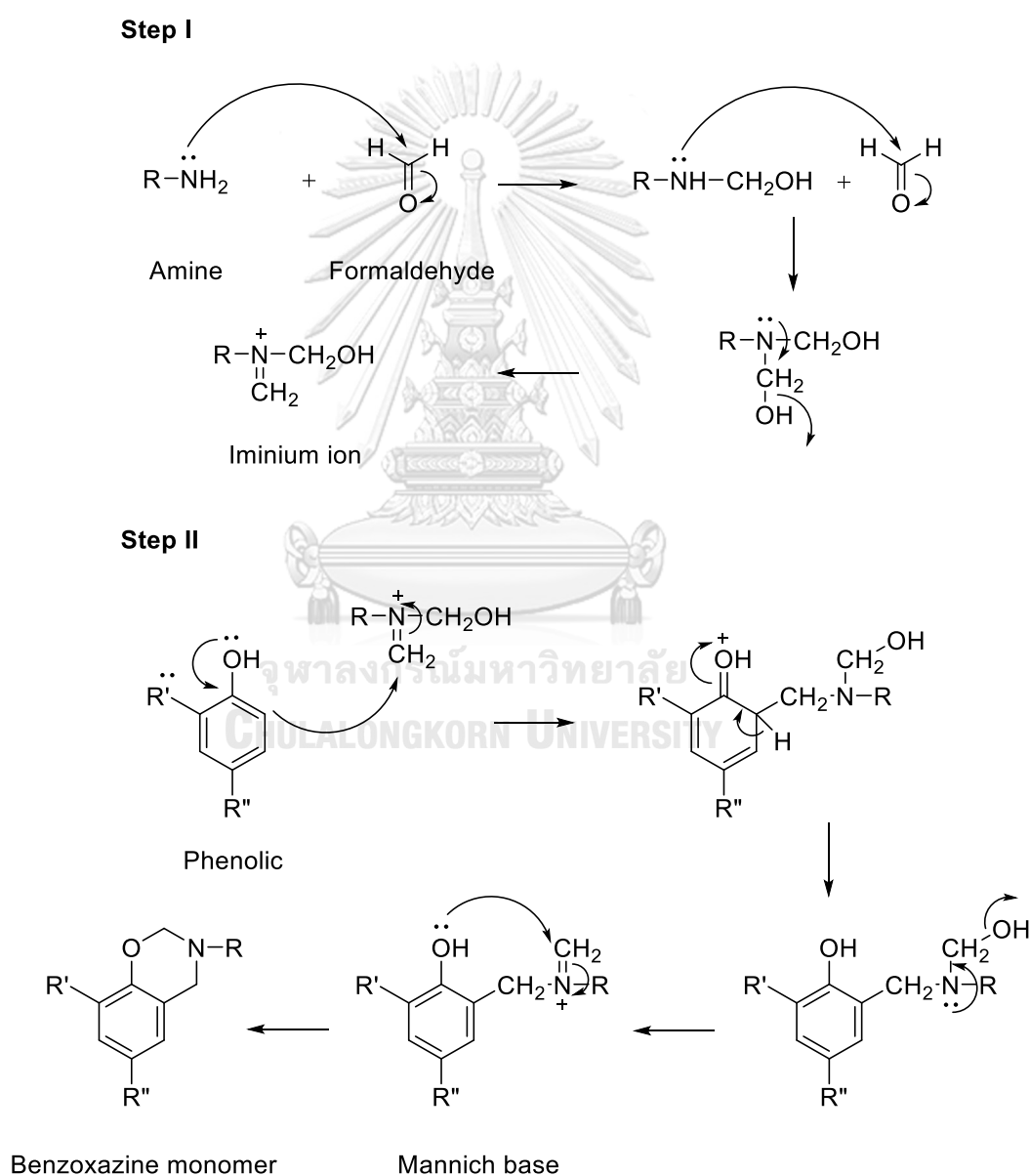


**Figure 2.4** The mechanism of benzoxazine monomer formation [48,51].



As the variety of formaldehyde is not much, the benzoxazine molecule can be designed by tuning a type of phenolic and amine compound. The monomer of benzoxazine can be synthesized as mono-, bi- or multi- functionals which is classified by the number of functional groups in amine or phenol compound usage. The example of monomeric type has been described in **Figure 2.5**. However, Ning *et al.* demonstrated that a crosslinked network structure with good mechanical integrity of polybenzoxazine was obtained when bi- or multi- functional benzoxazine precursors was used [52].

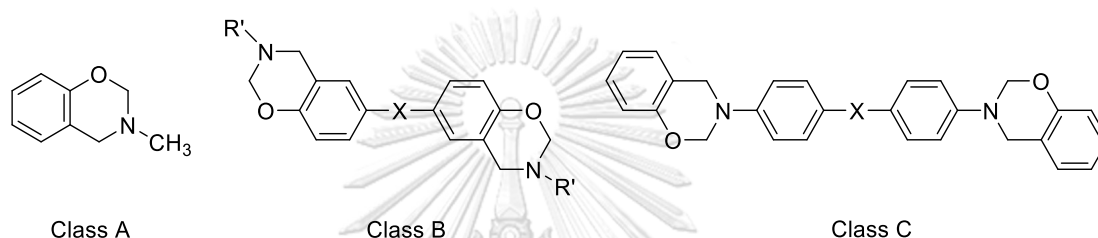


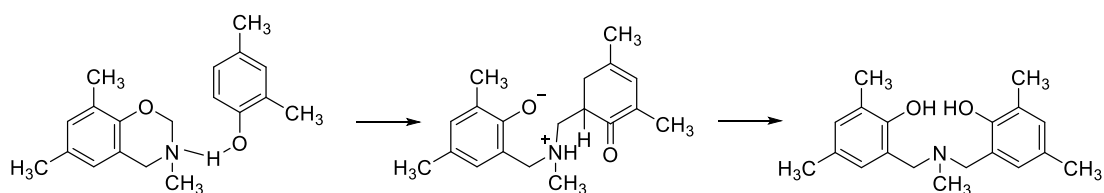
**Figure 2.5** The monomeric type of monofunctional (Class A) and difunctional with bisphenol-monoamine (Class B) and phenol-diamine (Class C) [44].

### 2.3.2 Cationic ring-opening polymerization

The structure of oxazine ring in benzoxazine molecule (**Figure 2.3**) was assumed to present in a distorted semi-chair structure which could produce the ring-opening polymerization [53,54]. In addition, the presence of N and O atoms which have strong basicity on the structure can offer the ring opening via cationic mechanism. Moreover, the reaction rate of polymerization can be accelerated by adding the catalyst which reduces time and temperature for curing steps.

In 1985, Riess *et al.* studied the kinetic of polymerization that was initiated by phenolic compounds [55,56]. For ortho- reaction, the ring-opening polymerization can occur via the intramolecular hydrogen-bonding while a para-reaction was performed with a partial phenol dissociation. The reaction can be seen in **Figure 2.6**.

- Intermolecular hydrogen-bonding (ortho reaction)



- Partial phenol dissociation (para reaction)

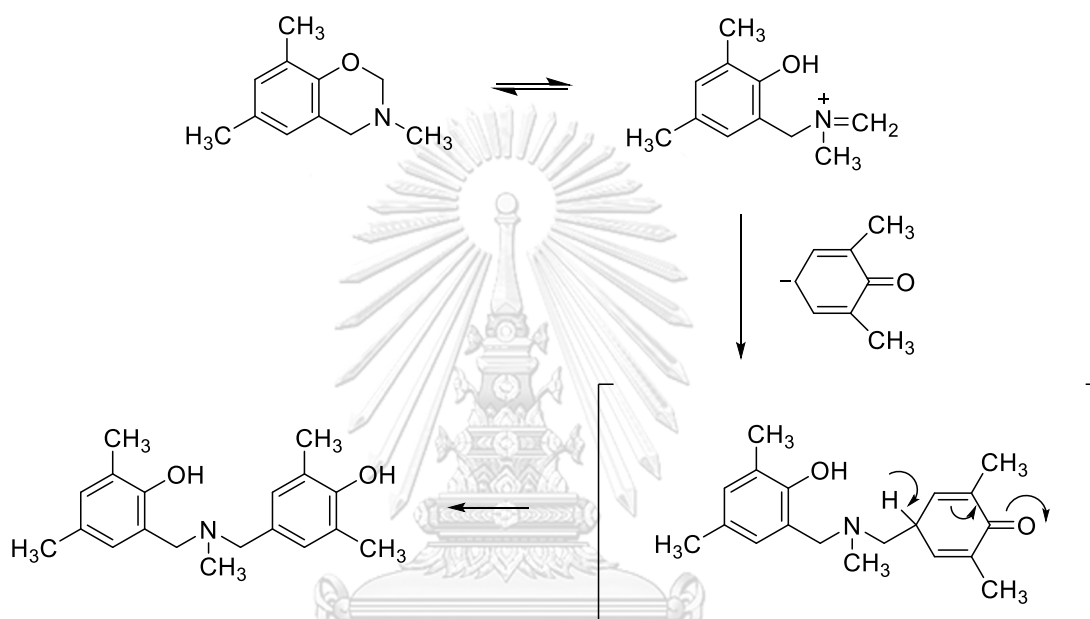


**Figure 2.6** Ring-opening polymerization by phenolic compound initiation [56].

Many initiators, as cationic, anionic, and a free radical, have been reported as a catalyst for benzoxazine polymerization [53]. The results showed several Lewis acids initiators such as phosphorus pentachloride ( $\text{PCl}_5$ ), aluminium chloride ( $\text{AlCl}_3$ ), and Titanium chloride ( $\text{TiCl}_4$ ) has effectively performed the ring-opening polymerization at moderate temperature. Moreover, an acid compound was also reported as a catalyst for ring-opening polymerization [54,57].

In 1999, Dunker *et al.* proposed that the ring-opening polymerization can occur via protonation of oxygen atom to form an iminium ion followed by electrophilic aromatic substitution [57]. The details of mechanism were showed in **Figure 2.7**. The protonated benzoxazines can perform a tautomerization of ring chain with iminium species under the acid medium. As the mechanism of reaction can be expected that

the usage of Lewis acids can improve the rate of initiation for benzoxazine polymerization.

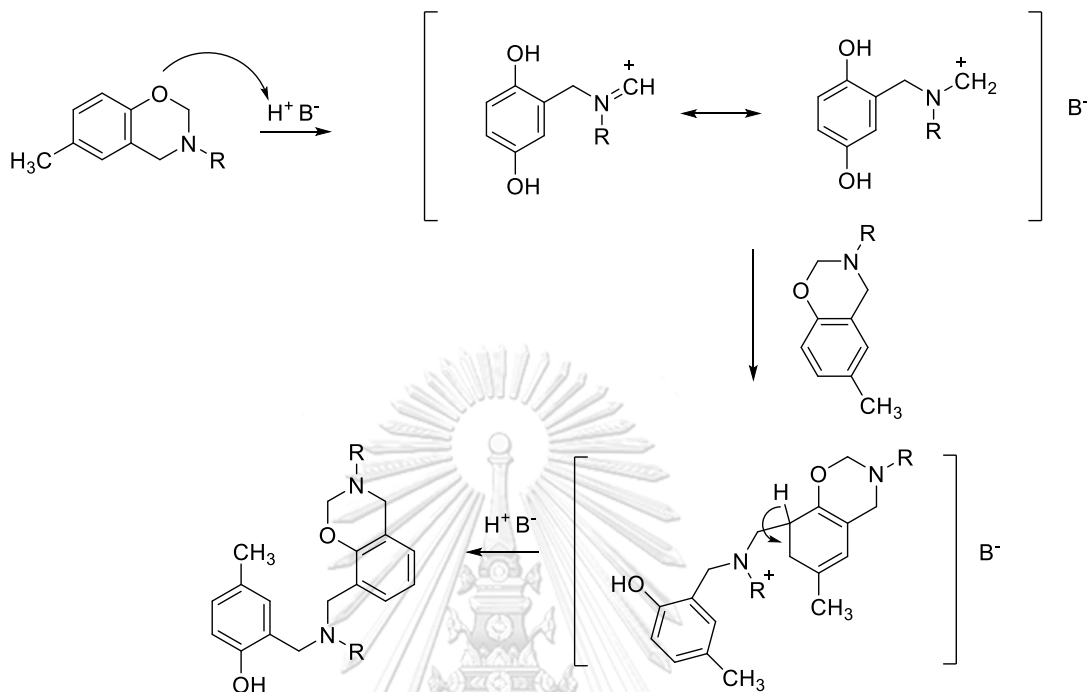


Figure 2.7 Proposed of initiation mechanism with acid catalyst [56].

### 2.3.3 Characterization of oxazine ring and ring-opening polymerization

The oxazine ring formation and ring-opening polymerization was confirmed using Fourier transform infrared spectroscopy or FTIR. The peak characteristic of oxazine ring show asymmetric stretching bands of C-N-C ( $1180\text{ cm}^{-1}$ ), C-O-C ( $1260\text{ cm}^{-1}$ ), and  $\text{CH}_2$  wagging of oxazine ( $1370\text{--}1380\text{ cm}^{-1}$ ) [58,59]. Moreover, tri-substituted benzene ring of in-plane C-C stretching and out-of-plane C-H deformation was noticed at  $1500$  and  $949\text{ cm}^{-1}$ , respectively [53].

### 2.3.4 The preparation of nanoporous carbon derived polybenzoxazine via sol-gel process

#### 2.3.4.1 Sol-gel process

The one route for preparation of a porous material is the sol-gel process. The reaction involves chemical reactions and physical processes, which are phase separation, dissolution, evaporation etc., tend to the formation of porous solid

precursor in the liquid solvent. The sequences of the sol-gel process including the following steps as shown in **Figure 2.8**.

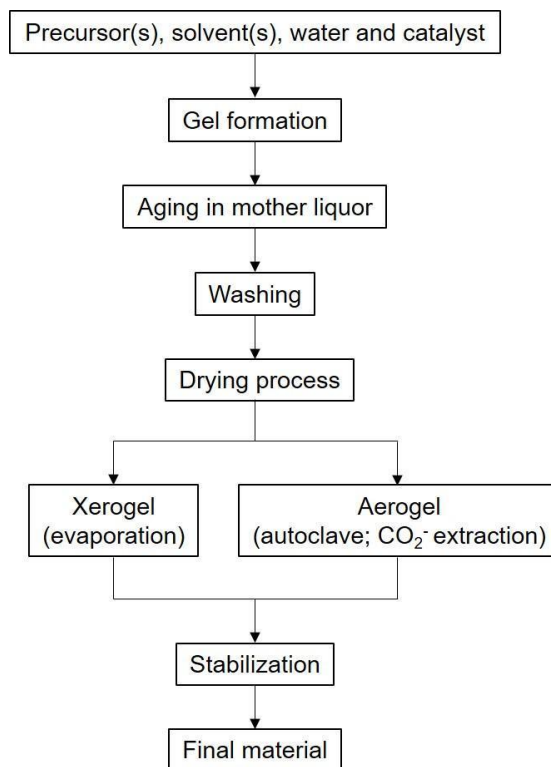


**Figure 2.8** The sequence of sol-gel processing step for porous solid preparation [60].

#### 2.3.4.2 The nanoporous carbon material derived from polybenzoxazine

A sol-gel processing was adopted in previous works for preparation the benzoxazine organogel as detail follow

In 2009, Lorjai *et al.* prepared a carbon aerogel from polybenzoxazine via solvent-less technique followed by sol-gel process method [47]. A monomer was synthesized using bisphenol-A, aniline, and paraformaldehyde at molar ratio was 1:2:4. After that, a benzoxazine precursor was dissolved in xylene and heated the solution at 130 °C for 96 h. The obtained partially cured benzoxazine was dried at ambient temperature to remove xylene out. At this step, the polybenzoxazine aerogel was obtained. The mechanism of synthetic reaction was shown in **Figure 2.9**. Then, the carbon aerogel was prepared further via a pyrolysis process by performing in a quartz

reactor under nitrogen flow at 500 cm<sup>3</sup>. The ramp cycle of temperature was set from 30 to 250 °C for 60 min, 250 to 600 °C for 300 min, 600 to 800 °C for 60 min and held at 800 °C for 60 min. Finally, the furnace was cooled to room temperature under a nitrogen atmosphere.

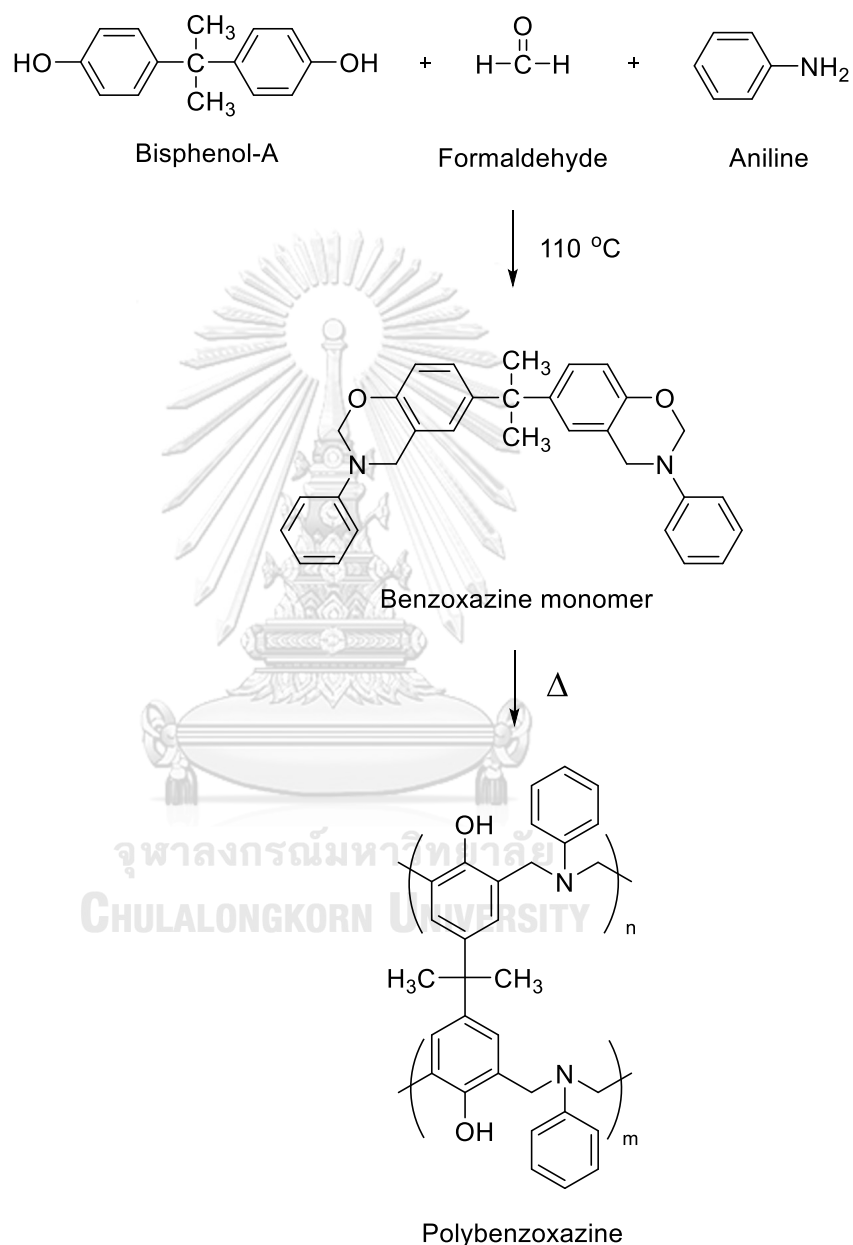


**Figure 2.9** Precursors and the polybenzoxazine reaction [47].

In 2014, Thubsuang *et al.* studied the synthesis of 3D interconnected macroporous carbon xerogels derived from polybenzoxazine via sol-gel process [61].

The effect of organic solvents, as dimethylformamide (DMF) and dioxane, on the cluster growth behaviors during sol-gel process and pore characteristics were reported. The result showed that when dioxane was used, the longer gelation time and smallest cluster size were obtained. It can be explained by the good miscibility of a precursor in dioxane causing a difficulty for phase separation. Therefore, a dense with small porous material was obtained. However, the DMF solvent can generate a 3D interconnected macroporous structure due to the solubility between benzoxazine and DMF showed a poor miscibility. Moreover, the ring-opening of oxazine ring prefers to occur in DMF solvent than dioxane because DMF has more dielectric constants. The phase separation and porous structure were illustrated in **Figure 2.10**.

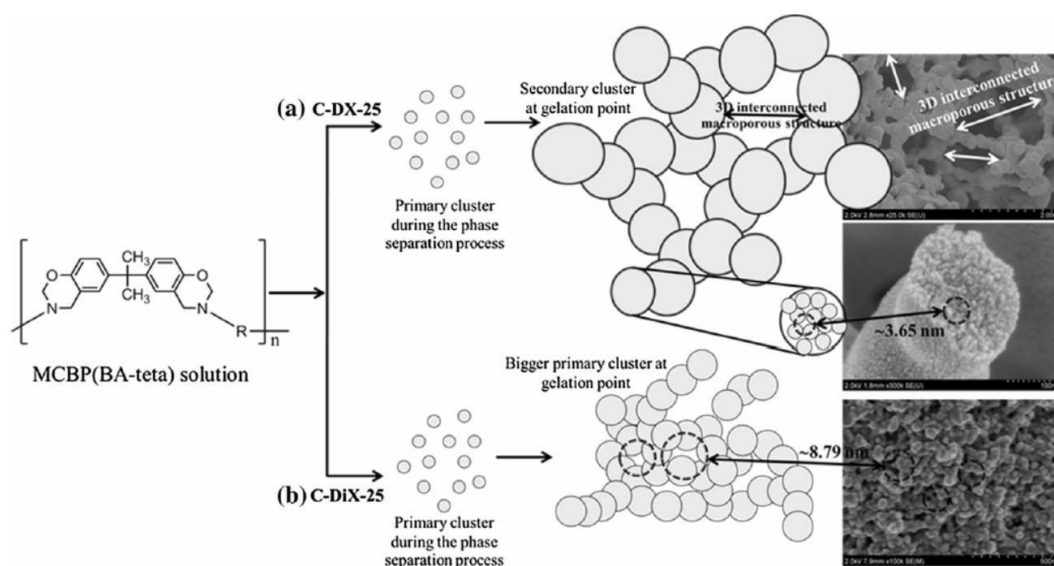


**Figure 2.10** Phase separation in DMF (a) and dioxane (b) solvents [61].

## 2.4 Alginate

Alginate or sodium alginic acid is an anionic linear polysaccharide which is produced from brown algae. The structure is composed of (1-4)-linked  $\beta$ -D-mannuronic acid (M) and  $\alpha$ -L-guluronic acids (G). Alginate has some unique properties such as simple preparation, hydrophilicity, biocompatibility, high adsorption potential and non-toxic substance [62]. The structure of alginate was shown in **Figure 2.11**.

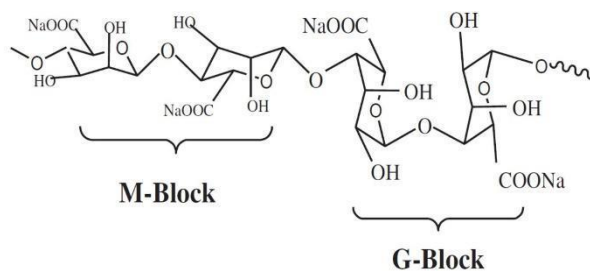


**Figure 2.11** Sodium alginate molecular structure [63].

A divalent cation can allow the gel formation which the pattern of molecular was either MM, GG or GM dimeric form. The gel formation starts with a monovalent cation of soluble alginate, as sodium ion ( $\text{Na}^+$ ), was replaced with divalent cation to provide a 3D network structure. Montanucci *et al.* [64] reported the guluronic acid (G-block) prefers to bind with cation than mannuronic acid (M-block). The affinity of divalent cation was also reported in ascending order of  $\text{Mg}^{2+}$ ,  $\text{Ca}^{2+}$ ,  $\text{Sr}^{2+}$ , and  $\text{Ba}^{2+}$ . Moreover, the GG and GM patterns of gelation were obtained when using calcium ion ( $\text{Ca}^{2+}$ ).

## 2.5 Humic acid

The major component in soil and waters is humic substances (HS) which result from the decomposition of organic matter and particular plants [65,66]. HS are classified into three fractions based on their solubility in water which are humic acids, fulvic acids, and humin. Fulvic acids are soluble at any given pH while humin is insoluble. For humic acids, they greatly dissolve in basic medium, partially soluble in water and insoluble at pH medium lower than 2 [67,68].

Humic acids or HAs are organic macromolecules that have hydrophilic and hydrophobic sites on their structure which exhibit a large ability to interact with herbicides via ionic bonding, cation exchange, and Van der Waal forces [65,69]. **Figure 2.12** illustrates the model structure of HAs which has numerous oxygen-containing functional groups such as carboxyl ( $\text{COOH}$ ), carbonyl ( $\text{C}=\text{O}$ ) and hydroxyl ( $\text{OH}$ ). Moreover, the solubility of humic acid in aqueous media can be increased with the number of these groups [67,69].

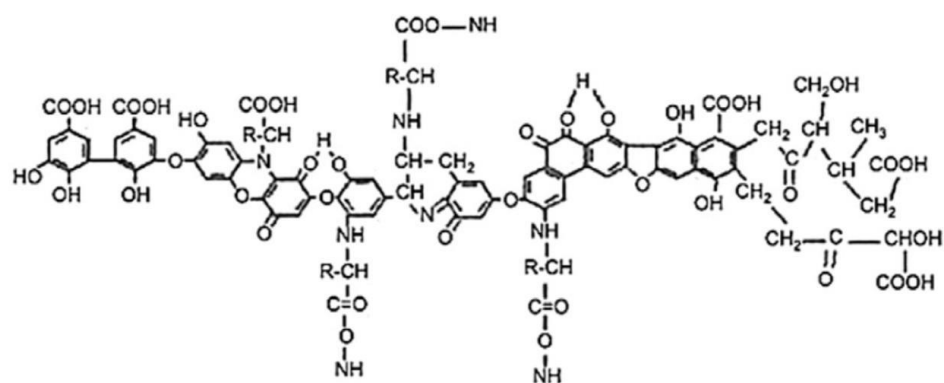


Figure 2.12 Model of humic acid structure [68].

## 2.6 Konig's reaction

For atrazine detection, the simple and sensitive spectrophotometric method has been reported based on Konig's reaction [36]. At first, the atrazine compound reacted with pyridine and converted to a quaternary pyridinium halide. Then, the hydroxyl group from alkali reagent adds to the pyridinium halide compound to create a carbinol base and glutaconic dialdehyde, respectively. Finally, *p*-aminoacetophenone reagent was coupled with glutaconic dialdehyde in acidic medium to obtain a yellow-orange polymethine dye which has a maximum absorbance at 470 nm. The reaction was demonstrated in Figure 2.13.



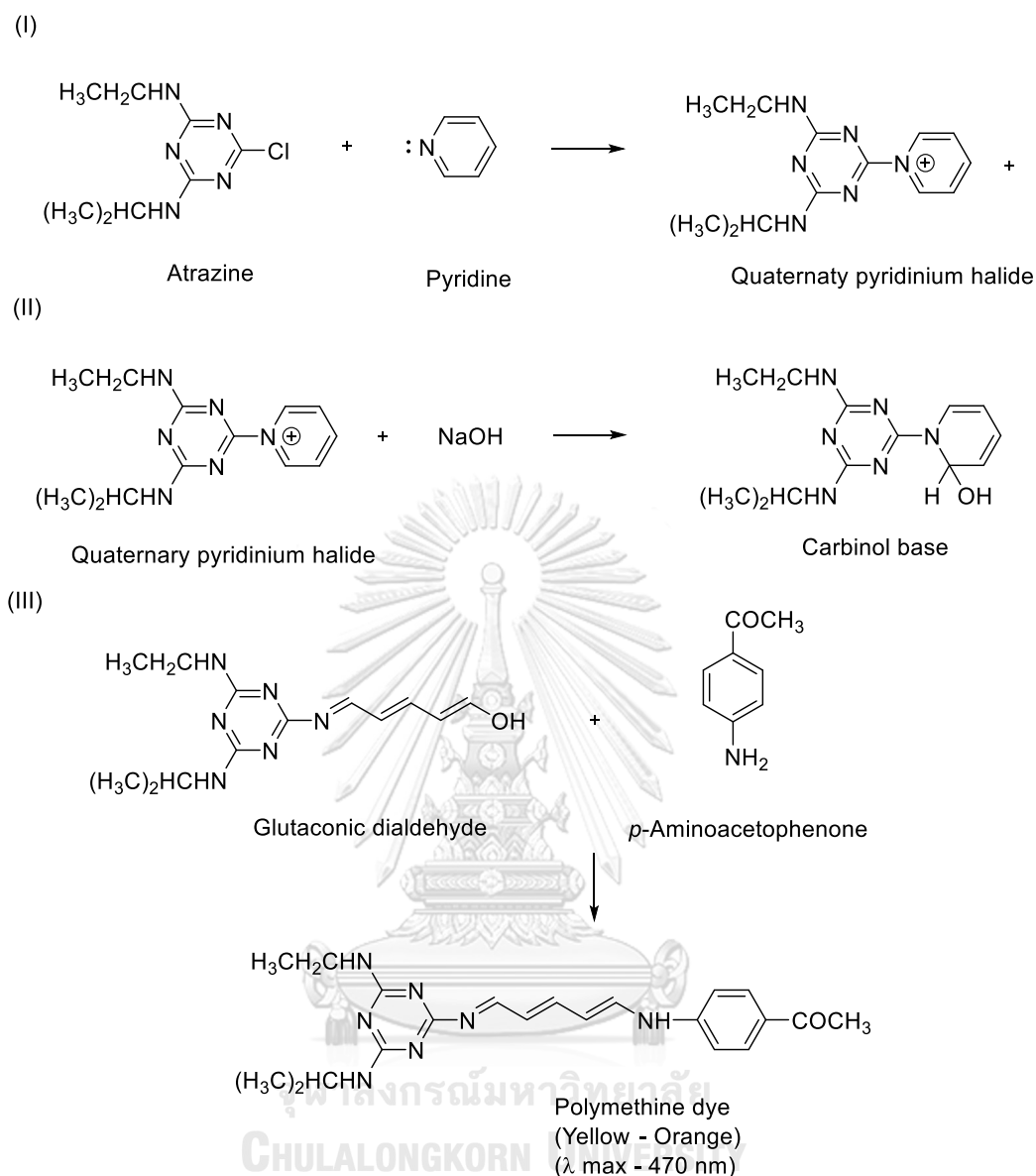


Figure 2.13 The probable color reaction of polymethine dye [36].

## 2.7 Polymethine compound

The polymethine dyes (PD) is an efficient spectral-fluorescent probe which was widely used in various fields because it has unique properties in terms of photophysical and photochemical application. They give an adsorption broad spectral range from 400 to 800 nm [70]. The color of polymethine depending on the length of chain, the end-group topology, and electron shell occupation that tend to it can absorb light in Ultraviolet, Visible, and near-IR spectral regions [71]. The structure of PD contains a  $\pi$ -electron conjugated system (polymethine chromophore) as shown in **Figure 2.14**.

which composed of an electron-acceptor end group (A), an electron-donor end group (D), and the chain of methine groups (-CH=).

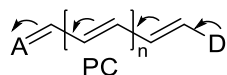


Figure 2.14 Polymethine dye (PD) structure [72].

## 2.8 Paraquat blue free radical reaction

For paraquat detection, the spectrophotometric method is usually converting a paraquat substance in general form ( $PQ^{2+}$ ) using suitable reducing agents to obtain a paraquat blue free radical ion ( $PQ^{\bullet+}$ ) in alkali condition. The mechanism of paraquat reduction-oxidation was shown in Figure 2.15. The absorption spectrum of paraquat radical has both sharp and broad peaks at 394 nm and 600 nm, respectively which was illustrated in Figure 2.16.

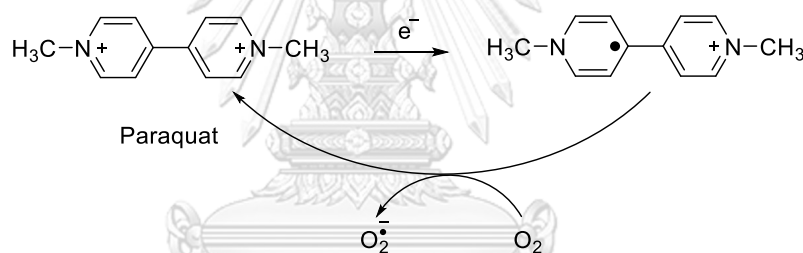


Figure 2.15 Paraquat reduction-oxidation [41].

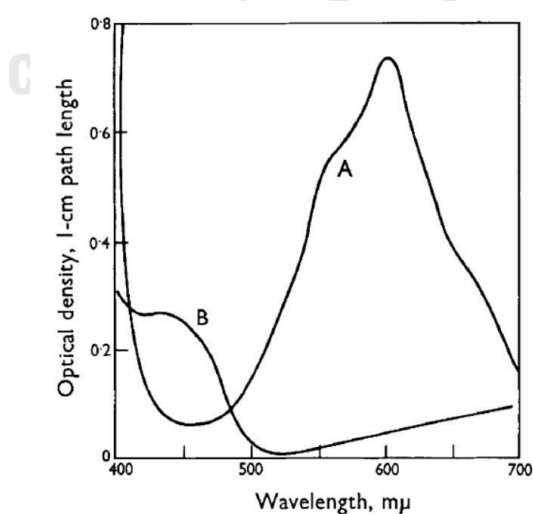


Figure 2.16 Visible spectra of paraquat (A) and diquat (B) reduction with sodium dithionite in alkaline solution [73].

## 2.9 Literature reviews

Since the contamination level of two herbicides, atrazine and paraquat, in environmental water were reported at trace level. Therefore, the high sensitivity and selectivity techniques were required for atrazine or paraquat analysis such as liquid chromatography/mass spectrometry or LC/MS [18], electrochemistry [21], enzyme-linked immunosorbent assay or ELISA [22], and gas chromatography mass spectrometry [23] were established. However, among these techniques required an expert user and high-cost instrument which restrict the local authorities monitoring.

### 2.9.1 Solid phase extraction method for atrazine determination

Many studies using a solid phase extraction or SPE to pre-concentrate the amount of these herbicides before measuring with an instrument are detailed in **Table 2.2**.

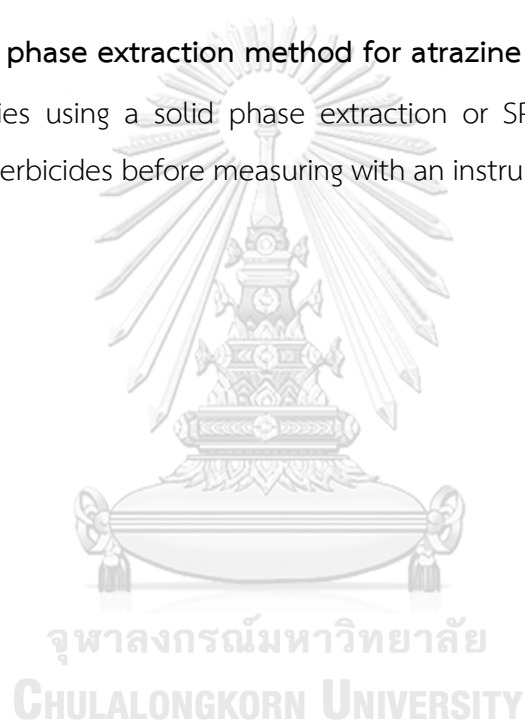


**Table 2.2** SPE method for atrazine determination

Adsorbent	Methodology	Method requirement	Reusability	Ref.
Heat-treated diatomaceous earth	SPE-HPLC	The suitable pH of water sample needs to be adjusted (pH = 2)	7 cycles	[74]
Molecular imprinted polymer or MIP	SPE-HPLC combined with subcritical water extraction (SWE)	LC/MS-MS and SPE vacuum manifold requirements	No report	[75]
Molecular imprinted polymer or MIP	SPE-HPLC	Rotary evaporator and SPE vacuum manifold requirements	No report	[76]
Amino modified mesostructured cellular foam or AF-MCF	dSPE-HPLC	Need centrifugation and N <sub>2</sub> evaporation steps	6 cycles	[77]
Ionic liquid-magnetic graphene composite	MDSPE-HPLC	Absorbent was prepared under severe condition and requirement the evaporation step	No report	[78]

It can be seen that many researchers use MIP as a solid sorbent for atrazine pre-concentration. The recognition properties of MIP material can be improved by using target analyte as a template to generate lock and key model which can enhance the extraction efficiency. However, the formation of this polymer tends to be relatively

dense leading to the difficulty in mass transport. Therefore, the vacuum manifold unit was required in previous works. Moreover, the evaporation step after elution can increase the operation time.

Many reports using carbon nanoporous material as sorbent for atrazine adsorption because it has many advantages such as the large surface area, unique porous structure, and high electrical conductivity because of their intrinsic  $\pi$ - $\pi$  conjugation. The pore structures were classified into three types which are micropores (<2 nm), mesopores (2-50 nm), and macropores (> 50 nm) [79].

In 2006, Zhou *et al.* determined an atrazine using multiwalled carbon nanotubes as a sorbent. However, the developed SPE cartridge needs to operate with a vacuum pump for a maximum flow rate [80]. The hydrophobic interactions between atrazine and multiwalled carbon nanotubes was reported [81].

In 2015, Liado *et al.* demonstrated that atrazine can be adsorbed on activated carbon via  $\pi$ - $\pi$  interaction which the micropore volume plays a significant role on the adsorption capacity [29]. Moreover, Lupul *et al.* investigated the atrazine removal performance of activated carbon (AC) when activation condition is different. They found that the highest affinity of atrazine towards the surface sorbent obtained when the carbon was activated at high temperature under a nitrogen flow [82]. Furthermore, the  $\pi$ - $\pi$  interaction between functionalized nylon6/polypyrrole core-shell nanofibers and atrazine were reported by Yang *et al.* [83].

Therefore, the suitable materials for atrazine adsorption should have a pyrrole group and be able to form  $\pi$ - $\pi$  interaction within their structure. Furthermore, some physicochemical properties of adsorbent materials such as a lot of active binding sites, high porosity and surface area but still has a good pore accessibility are required.

### **2.9.2 Nanoporous carbon derived from melamine based polybenzoxazine**

Due to the phenolic and amine compound that can be tuned for polybenzoxazine synthesis, these two compositions should be considered to obtain a suitable carbon nanoporous material for atrazine adsorption. As Ning *et al.* [52] demonstrated a bifunctional benzoxazine monomeric has a good mechanical property,

the bisphenol-A was selected to prepare benzoxazine precursor. Since the structure of atrazine is similar to the structure of melamine compounds, the adsorption interaction can occur via  $\pi$ - $\pi$  interactions or hydrogen bonding. Therefore, the melamine was used as an amine source for benzoxazine precursor preparation.

In 2013, Shi *et al.* prepared a film material from a low-viscosity polybenzoxazine using bisphenol-A, melamine, and formaldehyde as precursors [58]. They demonstrated that the introducing of melamine on the network structure can provide a high chemical and thermal stability. The molar equivalent for melamine, bisphenol-A, and formaldehyde was 1:1:6, respectively. The synthesis was illustrated in **Figure 2.17**.

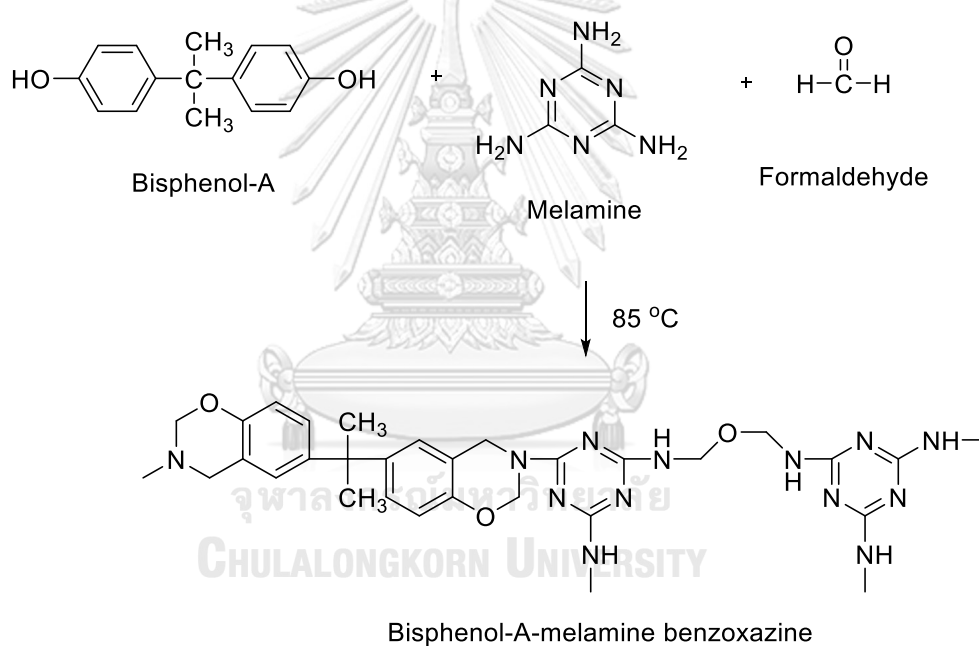


**Figure 2.17** Synthesis of benzoxazine monomer based on bisphenol-A and melamine [58].

In 2018, Rattanopas *et al.* prepared a nanoporous carbon derived from melamine based polybenzoxazine by using sodium chloride templates (NaCl) [32]. The preparation starts with dissolving bisphenol-A, melamine, and formaldehyde at mol ratio 1:1:6 in mixing solvent of water and ethanol at ratio of 1:1 under the acid conditions. To increase surface area, sodium chloride was used as a porous template.

The result of BET showed that surface area was enhanced up to 1516 m<sup>2</sup>/g. Moreover, when acid amounts increase, the lower average pore diameter will be obtained.

### 2.9.3 The adsorbents for paraquat adsorption

Due to the anionic properties of polysaccharide sodium alginate and humic acid, these chemical substances have been used to prepare the adsorbents for paraquat adsorption application.

In 2008, Ruiz *et al.* [26] used the calcium alginate beads to remove paraquat dichloride via electrostatic interaction. They found that the pH was a main factor affecting adsorption. At pH 3.0, high concentration of H<sup>+</sup> competed with the adsorption of paraquat whereas at pH 7.0, the lower adsorption competition was observed.

In 2010, Brigante *et al.* [25] studied the paraquat adsorption on humic acid-goethite adsorbent. The results indicated paraquat can bind with negative charge of carboxylates and phenolates groups of humic acid tends to form ionic pairs or outer-sphere complexes. The adsorption efficiency increases by decreasing electrolyte concentration and increasing pH.

In addition, silica gel is widely used for adsorption application because it has stability, physical strength, high surface area and high porosity. In 2011, Brigante *et al.* [27] prepared a binary system of titania-modified silica for paraquat adsorption with the reaction occurring via an electrostatic interactions and charge-transfer reaction. Moreover, the paraquat was detected by using silica gel as adsorbents [84].

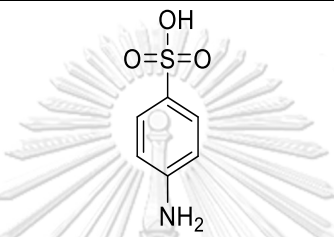
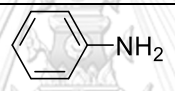
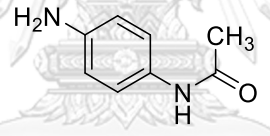
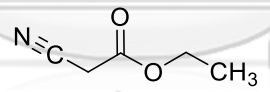
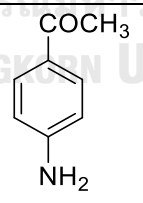
### 2.9.4 Atrazine and paraquat colorimetric detection

The colorimetric method is an interesting alternative method because the detection is simplicity and rapidity which requires only a unit of spectrophotometer. The method was operated based on changing from a colorless compound to a colored compound which can be observed by UV-Visible spectrophotometer and naked-eye. The use of Konig's reaction and paraquat blue free radical reaction have been reported for atrazine and paraquat detection in this research.

### 2.9.4.1 The atrazine detection based on Konig's reaction

As the polymethine dye (PD), a product of Konig's reaction, can absorb light in wide range of visible region depending on their structure, many coupling reagents for atrazine detection have been reported in previous works as shown in **Table 2.3**.

**Table 2.3** Coupling reagents for Konig's reaction

Coupling reagents	Structure	Dynamic range [Ref.]
Sulfanilic acid		0.50-2.50 µg/mL [37] 0.07-0.7 µg/mL [38] 0.1-25 µg/mL [39]
Aniline		0.08-12 µg/mL [39]
<i>p</i> -Aminoacetanilide		0.012-0.12 µg/mL [40]
Ethyl cyanoate		No reported [85]
<i>p</i> -Aminoacetophenone		0.16-1.6 µg/mL [36]

In 1966, Radke *et al.* evaluated the pyridine-alkali compound for determination of atrazine. The experiment was performed based on Konig's reaction using ethyl cyanoate as a coupling agent. They found that stability of pyridine-alkaline, a glutamic dialdehyde, was poor and it can be improved by reacting the pyridine-alkali with ethyl cyanoacetate. Then, the stable red color compound was developed. The maximum absorbance was demonstrated at 550 nm [85].



In 1998, Kesari *et al.* [36] developed a simple method for determination atrazine in environmental and biological samples. They used *p*-Aminoacetophenone as a coupling reagent to generate polymethine dye (PD) The maximum absorbance value was reported at 470 nm which is close to the maximum wavelength of obtained polymethine dye when sulfanilic acid (450 nm) and aniline (480nm) were used [39].

In 2013, the sensitivity of Konig's reaction on atrazine determination can be improved by using a micellar medium as reported by Tiwari *et al* [40]. Even though the lowest of dynamic range was reported, the step up coming for polymethine dye extraction by C<sub>18</sub> cartridge after coupling with *p*-Aminoacetanilide was required in this work. In the same way, the step of polymethine dye extraction was also reported by Tamrakar and co-workers when sulfanilic acid was used as a coupling reagent [38]. In these works, the maximum wavelength for atrazine analysis was also measured at 460 nm.

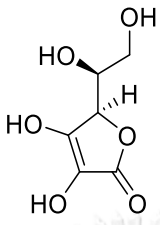
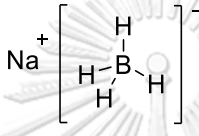
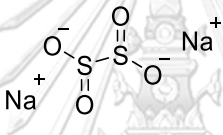
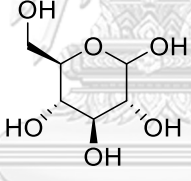
In 2016, Martins *et al.* reported the atrazine determination method by flow injection techniques (FIA) [37]. Even the advantages of FIA are high sample throughput, small volume of reagent used and lower amount of residual, the batch experiment of heating step needs to be carried out before measuring by FIA system. The reported maximum wavelength was applied at 445 nm.

Among these works, the heating condition in Konig's reaction has been required to perform at high temperature or boiling conditions. Moreover, the performance of these methods to use as naked-eye detection have not been evaluated.

#### **2.9.4.2 The paraquat detection based on blue free radical reaction**

Several reducing agents such as ascorbic acid [33], sodium borohydride [34], and sodium dithionite [35] have been applied to detect paraquat. The structure and standard reduction potential of these reagents was indicated in **Table 2.4**.

**Table 2.4** The structure and standard reduction potential of reducing agents for paraquat blue free radical formation

Reducing reagents	Structure	Standard reduction potential or $E^0$ (V)	Ref.
Ascorbic acid		-0.390	[86]
Sodium borohydride		-1.240	[87]
Sodium dithionite		-1.120	[87]
Glucose		-0.050	[88]

In 1991, Shivhare *et al.* [33] determined a paraquat in water, grain, and plant materials. The method used ascorbic acid as a reducing agent and the dynamic range was obtained from 1.2-9.6  $\mu\text{g/mL}$  with the color of blue radical is stable for 12 hours. However, the experiment in this work was developed by starting the reaction with paraquat high concentration (12-96  $\mu\text{g/mL}$ ).

In 1997, Rai *et al.* [34] detected paraquat via blue free radical using sodium borohydride as a reducing agent. Even the dynamic range of detection was low as 0.05-0.5  $\mu\text{g/mL}$ , this reagent has some disadvantages in terms of it can damage skin and eye. In the same year, the glucose was conducted to determine paraquat in many samples such as plants, fruits, water, blood and urine [89]. They found that the suitable temperature for fully color development was within the range of 70-100  $^{\circ}\text{C}$ .

In 2016, Kuan *et al.* [35] prepared a paper-based device for clinical paraquat poisoning diagnosis. The reaction was performed using sodium dithionite and ascorbic acid. They reported the detection limits in normal human serum for ascorbic acid and sodium dithionite assays were 3.86 and 13.80 mg/L. However, the stability of sodium dithionite was quite low and should be freshly prepared.

In this research, the nanoporous carbon derived from melamine based polybenzoxazine (NPC-PBZ-m) was prepared for atrazine adsorption related to previous work. The application of polybenzoxazine material for atrazine adsorption has never been reported. While silica-humic acid-alginate beads were prepared to use as paraquat adsorbent. Moreover, Konig's reaction and paraquat blue free radical were developed for atrazine and paraquat detection by using UV-Visible spectrophotometer.



## CHAPTER III

### EXPERIMENTAL

In this work, the atrazine determination is composed of three steps including the NPC-PBZ-m sorbent synthesis and characterization (**section 3.3 and 3.4**) followed by pre-concentration (**section 3.6**) and colorimetric detection steps based on Konig's reaction (**section 3.7**)

#### 3.1 Chemicals

All chemicals in this research were analytical reagent grade (AR) and listed in **Table 3.1**. Chemicals were used without further purification.

**Table 3.1** List of chemical and supplier

Chemicals	Suppliers
1. Bisphenol-A (97%)	Sigma-Aldrich
2. Melamine (99%)	Sigma-Aldrich
3. Pyridine anhydrous (99.8%)	Sigma-Aldrich
4. Atrazine	Sigma-Aldrich
5. Paraquat, Analytical standard	Sigma-Aldrich
6. Glyphosate, Analytical standard	Sigma-Aldrich
7. 2,4-Dichlorophenoxyacetic acid	Sigma-Aldrich
8. Chlorpyrifos, Analytical standard	Sigma-Aldrich
9. Formaldehyde solution (37%)	Merck
10. Sodium hydroxide, A.R. Grade	Merck
11. Methanol, HPLC grade	Merck
12. Methanol (absolute)	Merck

Chemicals	Suppliers
13. Hydrochloric acid (37% w/w)	Merck
14. <i>p</i> -Anisidine (>98%)	TCI
15. Aniline (synthesis grade)	PanReac AppliChem
16. Sulfanilic acid (ACS reagent 99%)	Sigma-Aldrich
17. 4-aminophenol (≥98%)	Sigma-Aldrich
18. Ethanol (absolute)	RCl Labscan
19. Dimethyl sulfoxide (DMSO) anhydrous (≥99.9%)	Merck
20. Alginate powder	Sigma-Aldrich
21. Agar (Food grade)	-
22. Calcium alginate	Merck
23. Humic acid sodium salt (Technical grade)	Sigma-Aldrich
24. Potassium hydroxide	Merck
25. D-glucose	Daejung
26. DI and Milli-Q water	-

### 3.2 Apparatus

The apparatus used in this study are listed in **Table 3.2**.

**Table 3.2** List of apparatus

Apparatus	Company, model
1. High-performance liquid chromatography-ultraviolet detector (HPLC-UV)	Agilent 1260 Infinity II Quaternary pump
2. ZORBAX Eclipse Plus C18 (150 mm × 4.6 mm i.d., particle size 5 µm)	Agilent
3. UV-Visible spectrophotometer (UV-Vis)	Hewlett Packard 8453
4. Fourier transform infrared spectrometer	Nicolet 6700
5. Surface area and pore size analyzer	Quantachrome-Autosorb-1MP
6. X-ray photoelectron spectroscope (XPS)	Kratos Axis Ultra DLD
7. Field emission scanning electron microscope (FE-SEM)	JEOL JSM-7610F
8. Syringe pump	ProSense BV model NE-1000
9. Empty cartridge polypropylene column (Bond Elut Reservoir, 1 mL)	Agilent, Part No:12131007
10. Syringe adapter	Agilent, Part No:12131001
11. Polyethylene frit	Agilent, Part No:12131019
12. Syringe (10 and 50 mL)	Nipro Sales (Thailand) Co., Ltd.
13. PTFE syringe filter (13 mm, 0.20 µm)	National scientific
14. Cellulose acetate (CA) membrane filter (47 mm, 0.45 µm)	Vertical Chromatography Co., Ltd.
15. Cellulose filter paper (125 mm)	Thomas Baker

Apparatus	Company, model
16. 2 mL vial Amber I-D	National scientific
17. Polypropylene tube, 13 mL	Becthai
18. Household blender	Anitech
18. Test sieve (30-40, 40-60 mesh)	Rung Arun Machinery (1989) Company Limited
19. Rotating shaker (ROTAX 6.8 Overhead mixer)	Velp scientifica
20. Orbital shaker (HS 500)	Janke & kunkel ika werk

### 3.3 The synthesis of nanoporous carbon derived from melamine based polybenzoxazine (NPC-PBZ-m) used as pre-concentration sorbent

The synthesis of NPC-PBZ-m composes of three steps in detail

#### 3.3.1 Melamine based benzoxazine organogel synthesis

To obtain a melamine based benzoxazine monomer via a sol-gel process, three starting materials which are melamine, bisphenol-A and formaldehyde were mixed with a molar ratio of 1:1:6, respectively [32,58]. The solvent system is the mixture of ethanol and water at v/v ratio of 1:1. Then, bisphenol-A was added and stirred until it was completely dissolved, followed by adding formaldehyde and melamine into the mixture solution under continuous stirring. This solution was stirred and heated in an oil-bath for 30 minutes at 80 °C to get a clear solution. Then, the reaction mixture was cooled down. A 2.70 mL of conc. HCl, as an acid catalyst, was added dropwise while mixture was stirring. After that, the reaction mixture was transferred into a glass vial and sealed in a closed system to settle in an oil bath at 95 °C for 2 days. At this step, an opaque benzoxazine organogel was formed. To remove acid catalyst, a gel was

then immersed in deionized water until pH was nearly neutral and dried in the oven overnight at 80 °C. Finally, the melamine based benzoxazine organogel was obtained.

### 3.3.2 Melamine based benzoxazine organogel polymerization

Next, an opaque melamine based benzoxazine organogel was polymerized under temperature programmed conditions in the following steps: 100 °C for 30 minutes, 220 °C for 8 hours, holding at 220 °C for 15 minutes and cool down to 30 °C for 2 hours in an air-circulating oven to receive melamine based polybenzoxazine (PBZ-m). The proposed reaction of PBZ-m synthesis is shown in **Figure 3.1**.





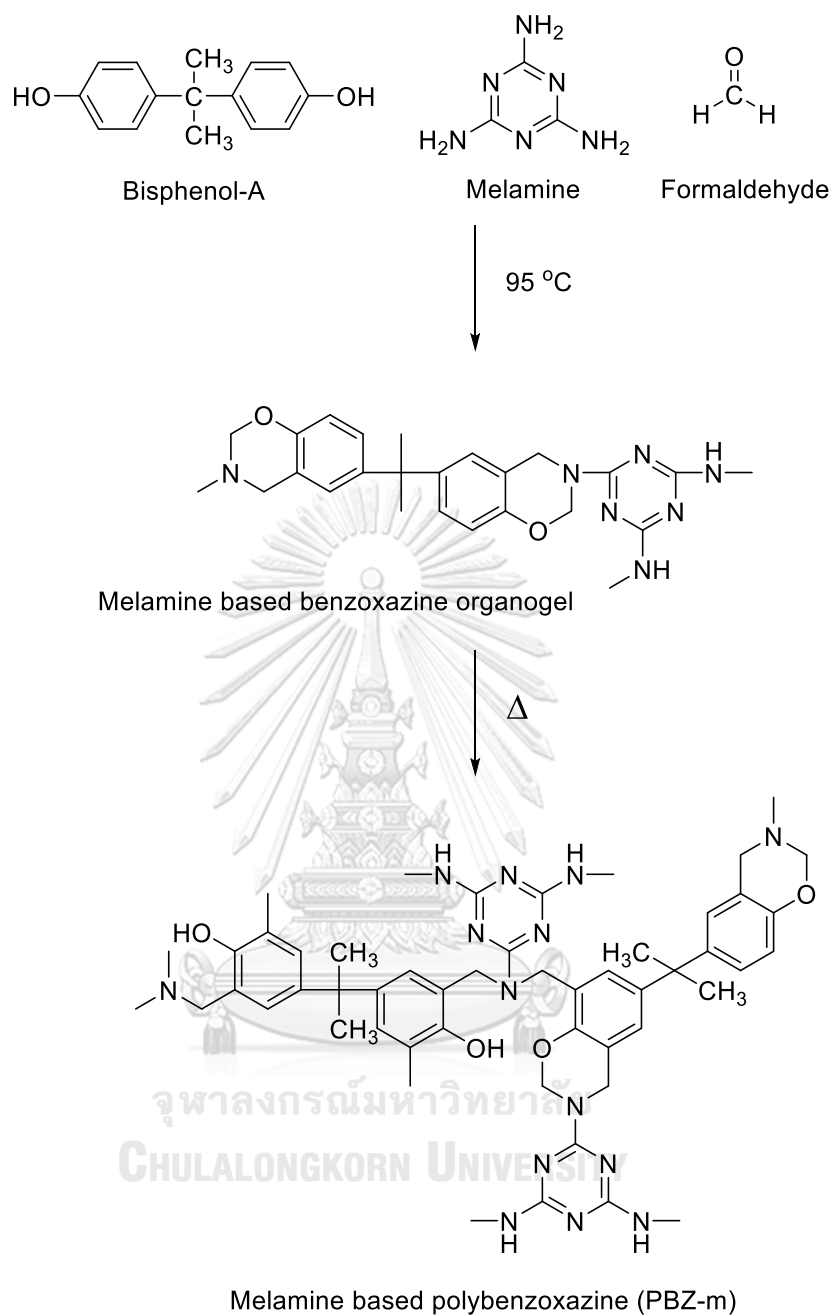


**Figure 3.1** The proposed reaction of melamine based polybenzoxazine (PBZ-m) synthesis.

### 3.3.3 Nanoporous carbon derived from melamine based polybenzoxazine (NPC-PBZ-m) preparation

Afterwards, PBZ-m was pyrolyzed under nitrogen atmosphere ( $N_2$ ) at a flow rate of 600 mL/min by purging with  $N_2$  gas for 30 minutes before performing the temperature programmed. The temperature was raised to 200 °C for 1 hour, 600 °C for

6 hours, 800 °C for 2 hours, and held at 800 °C for 2 hours. Then, the oven temperature was decreased to room temperature under N<sub>2</sub> conditions. The obtained nanoporous carbon particles were washed with methanol and dried at 110 °C for 1 hour. The obtained material was denoted as NPC-PBZ-m.

### **3.4 Characterizations of nanoporous carbon derived from melamine based polybenzoxazine (NPC-PBZ-m)**

#### **3.4.1 Fourier Transform Infrared Spectrometer (FTIR)**

The successful synthesis and polymerization of melamine based benzoxazine organogel were investigated using FTIR-KBr pellet technique. The oxazine ring functional groups between melamine based benzoxazine organogel and melamine based polybenzoxazine (PBZ-m) were pursued.

#### **3.4.2 Quantachrome-Autosorb-1 MP Surface Area and Pore Size Analyzer**

The N<sub>2</sub> adsorption-desorption isotherms was conducted to study the textural properties of NPC-PBZ-m (Quantachrome-Autosorb-1 MP). The sample was degassed at 250°C for 8 hours under vacuum before the measurement. The Brunauer-Emmett-Teller (BET) algorithm was applied to receive a specific surface area ( $S_{\text{BET}}$ ) [90] and total pore volume ( $V_{\text{tot}}$ ) was calculated at a relative pressure of 0.992. The Barrett-Joyner-Halenda (BJH) method [91] and the density functional theory (DFT) method were performed to determine the pore size distributions of mesopores, respectively. The  $t$ -plot method was conducted to analyze micropore volume ( $V_{\text{micro}}$ ) [92].

#### **3.4.3 X-ray Photoelectron Spectroscopy (XPS)**

The functionality of carbon- and nitrogen-containing the nanoporous carbon derived from melamine based polybenzoxazine (NPC-PBZ-m) sorbent was observed using an X-ray photoelectron spectroscopy (XPS).

#### **3.4.4 Field Emission Scanning Electron Microscope (FE-SEM)**

To investigate the surface morphology of NPC-PBZ-m, the FE-SEM was used, and NPC-PBZ-m sorbent was coated with platinum under vacuum condition prior to investigation using 100,000X magnification.

### 3.5 Solutions preparation

#### 3.5.1 100 and 500 $\mu\text{g}/\text{mL}$ of atrazine standard stock solutions

A 50 mL of 500  $\mu\text{g}/\text{mL}$  atrazine standard stock solutions was obtained by dissolving  $0.0250 \pm 0.0001$  g of atrazine in methanol and this solution was diluted with methanol to prepare a 100  $\mu\text{g}/\text{mL}$  atrazine standard stock solution. The standard stock solutions were stored at 4 °C when not in use.

#### 3.5.2 Working atrazine standard solutions

##### 3.5.2.1 5–30 $\mu\text{g}/\text{L}$ of atrazine working solutions

Atrazine standard solutions were prepared in sample matrices. Based on our preliminary study, the sample matrix causes the difference in the atrazine content after pre-concentration. Therefore, this study developed a calibration curve for detection of the atrazine using a linear regression analysis by adding a series of atrazine standard solutions to the matrix solution, an agricultural water sample.

The 5-30  $\mu\text{g}/\text{L}$  of atrazine working solutions were prepared in the agricultural water sample collected from a rice field where there is no any atrazine herbicide (Lopburi province, Thailand). These solutions were used for investigating the optimal conditions of the NPC-PBZ-m pre-concentration unit.

To study the matrix effect in different water samples, 5-30  $\mu\text{g}/\text{L}$  of atrazine working solutions were also prepared in water collected from different sources including agricultural water from Lopburi province, Nakhon Pathom province and pond water from Bangkok, Thailand.

##### 3.5.2.2 0.1–5 $\mu\text{g}/\text{mL}$ of atrazine working solutions

The external calibration curves to find the concentrations after pre-concentration process by both HPLC-UV analysis and colorimetric method based on Konig's reaction detected by UV-Vis analysis were prepared. 0.1-5  $\mu\text{g}/\text{mL}$  of atrazine standard solutions were prepared in methanol by pipetting the appropriated volume of stock solutions.

### 3.5.3 A series of atrazine standard solution (0.005–5 µg/mL) in sample blank solvent

In order to estimate the IDL and LOQ of the HPLC analysis, the agricultural water sample blank was pumped through the NPC-PBZ-m pre-concentration column. Then, methanol eluent was used as the solvent to prepare the series of standard solutions concentration ranging from 0.005–5 µg/mL by diluting the appropriated volumes of atrazine standard stock solutions with methanol.

### 3.5.4 Paraquat, glyphosate, 2,4-dichlorophenoxyacetic (2,4-D) and chlorpyrifos standard stock solutions

A 50 mL of 500 µg/mL paraquat and glyphosate standard stock solutions were prepared by dissolving 0.0250 g of each pesticide in Milli-Q water. The 50 mL of 500 µg/mL 2,4-Dichlorophenoxyacetic (2,4-D) standard stock solution was prepared by dissolving 0.0250 g of 2,4-D in methanol before making up volume with milli-Q water. A 50 mL of 500 µg/mL chlorpyrifos standard stock solution was prepared in methanol. All the standard solutions were stored at 4°C when not in use.

### 3.5.5 The mixture standard solutions of pesticides

#### 3.5.5.1 HPLC-UV analysis method

To study the effect of other pesticides towards an atrazine adsorption on NPC-PBZ-m sorbent, two-level concentrations, 1.5 and 7.5 µg/mL, of paraquat, glyphosate, 2,4-D and chlorpyrifos standard solutions were mixed with 0.015 µg/mL of atrazine standard solution followed by making up volume to 1000 mL with agricultural water (1:100 and 1:500). The preparation of these standard mixture solutions was shown in **Table 3.3**.

**Table 3.3** Mixture standard solutions of pesticides preparation

Other pesticides standard solutions ( $\mu\text{g/mL}$ )	Atrazine standard solution ( $\mu\text{g/mL}$ )	Pesticides mixture solutions (concentration ratios)
Paraquat (1.5)	Atrazine (0.015)	Atrazine: Paraquat (1:100)
Paraquat (7.5)		Atrazine: Paraquat (1:500)
Glyphosate (1.5)		Atrazine: Glyphosate (1:100)
Glyphosate (7.5)		Atrazine: Glyphosate (1:500)
2,4-D (1.5)		Atrazine: 2,4-D (1:100)
2,4-D (7.5)		Atrazine: 2,4-D (1:500)
Chlorpyrifos (1.5)		Atrazine: Chlorpyrifos (1:100)
Chlorpyrifos (7.5)		Atrazine: Chlorpyrifos (1:500)

### 3.5.5.2 UV-Vis based on Konig's reaction

To study the effect of other pesticides towards atrazine sensitivity based on Konig's reaction, three-level concentrations (10, 50, and 100  $\mu\text{g/mL}$ ), of paraquat, glyphosate, 2,4-D and chlorpyrifos standard solutions were mixed with 1  $\mu\text{g/mL}$  of atrazine standard solution followed by making up volume to 5 mL with methanol (1:10, 1:50, and 1:100). The preparation of these standard mixture solutions was shown in **Table 3.4**.

**Table 3.4** Mixture standard solutions of pesticides affecting on atrazine sensitivity based on Konig's reaction

Other pesticides standard solutions ( $\mu\text{g/mL}$ )	Atrazine standard solution ( $\mu\text{g/mL}$ )	Pesticides mixture solutions (concentration ratios)	Abbreviation
Paraquat (10)	Atrazine (1)	Atrazine: Paraquat (1:10)	AP-10
Paraquat (50)		Atrazine: Paraquat (1:50)	AP-50
Paraquat (100)		Atrazine: Paraquat (1:100)	AP-100
Glyphosate (10)		Atrazine: Glyphosate (1:10)	AG-10
Glyphosate (50)		Atrazine: Glyphosate (1:50)	AG-50
Glyphosate (100)		Atrazine: Glyphosate (1:100)	AG-100
2,4-D (10)		Atrazine: 2,4-D (1:10)	AD-10
2,4-D (50)		Atrazine: 2,4-D (1:50)	AD-50
2,4-D (100)		Atrazine: 2,4-D (1:100)	AD-100
Chlorpyrifos (10)		Atrazine: Chlorpyrifos (1:10)	AC-10
Chlorpyrifos (50)		Atrazine: Chlorpyrifos (1:50)	AC-50
Chlorpyrifos (100)		Atrazine: Chlorpyrifos (1:100)	AC-100

### 3.5.6 5 M sodium hydroxide solution

The solution of sodium hydroxide (NaOH) was used in Konig's reaction (step 2) and paraquat blue free radical reaction. A 5 M sodium hydroxide solution was prepared by dissolving approximately  $5.0000 \pm 0.1000$  g of sodium hydroxide in 25 mL of DI water.

### 3.5.7 6 (% w/v) *p*-Anisidine solution

The freshly prepared solution of *p*-Anisidine was used as a coupling reagent in Konig's reaction for atrazine colorimetric detection. A 6 (% w/v) of *p*-Anisidine solution was prepared by dissolving  $0.6000 \pm 0.0100$  g of *p*-Anisidine with 10 mL of methanol. The pale yellow of *p*-Anisidine solution was obtained.

### 3.5.8 8 and 10 (% v/v) aniline solutions

A 5 mL of 8 and 10 (% v/v) aniline solutions were freshly prepared by diluting aniline reagent in methanol.

### 3.5.9 1 (% w/v) sulfanilic acid solution

A  $0.0500 \pm 0.0010$  g of sulfanilic acid was dissolved in conc. HCl 1.8 mL followed by sonication for 10 min and adjusted volume to 5 mL with DI water.

### 3.5.10 0.5 (% w/v) 4-aminophenol

A  $0.0250 \pm 0.0005$  g of 4-aminophenol was dissolved in 5 mL of mixture solvent (DMSO-ethanol, ratio 1:2.3). This solution was freshly prepared before using.

### 3.5.11 1 M glucose solution

A  $0.2000 \pm 0.0050$  g of glucose was dissolved in 5 mL of DI water.

### 3.5.12 1 M potassium hydroxide solution

A  $11.2200 \pm 0.0200$  g of potassium hydroxide (KOH) was dissolved in 200 mL of DI water. Moreover, 0.1, 0.15, 0.3, and 0.5 M of KOH solutions were prepared by diluting 1 M of KOH with DI water.

### 3.5.13 1 M HCl-MeOH (70:30, % v/v)

1 M of HCl was prepared by diluting conc. HCl with DI water and mixing with methanol solution at volume ratio was 70:30.

## 3.6 Atrazine pre-concentration

In this work, the synthesized NPC-PBZ-m sorbent was packed in the SPE empty cartridge column to use as pre-concentration column. The adsorption and elution steps are performed by using a syringe pump. All parameters that can affect atrazine

pre-concentration were investigated using agricultural water, as a matrix water sample ( $n = 3$ ). The preparation of atrazine in water samples was described in **section 3.5.2.1**. The optimal conditions for pre-concentration and colorimetric detection were investigated as described below.

Firstly, the study of the pH effect on the atrazine adsorption, the batch experiments were conducted. A 10 mL of 5  $\mu\text{g}/\text{mL}$  atrazine standard solutions was prepared in DI water by adjusting to pH 3, 7, and 9 using either 0.1 M of HCl and NaOH. Then, this solution was filled in a polypropylene-plastic tube containing  $0.0100 \pm 0.0010$  g of NPC-PBZ-m. The adsorption tube was shaken using a rotating shaker for 24 hours. After that, the filtrate was measured by UV-Vis spectrophotometer.

### 3.6.1 NPC-PBZ-m column preparation

To prepare the pre-concentration column, NPC-PBZ-m sorbent was dry-packed in a polypropylene column (Bond Elut Reservoir, 1 mL) with polyethylene frit at the bottom. The pre-concentration unit of NPC-PBZ-m sorbent unit was connected to a syringe pump as shown in **Figure 3.2**.

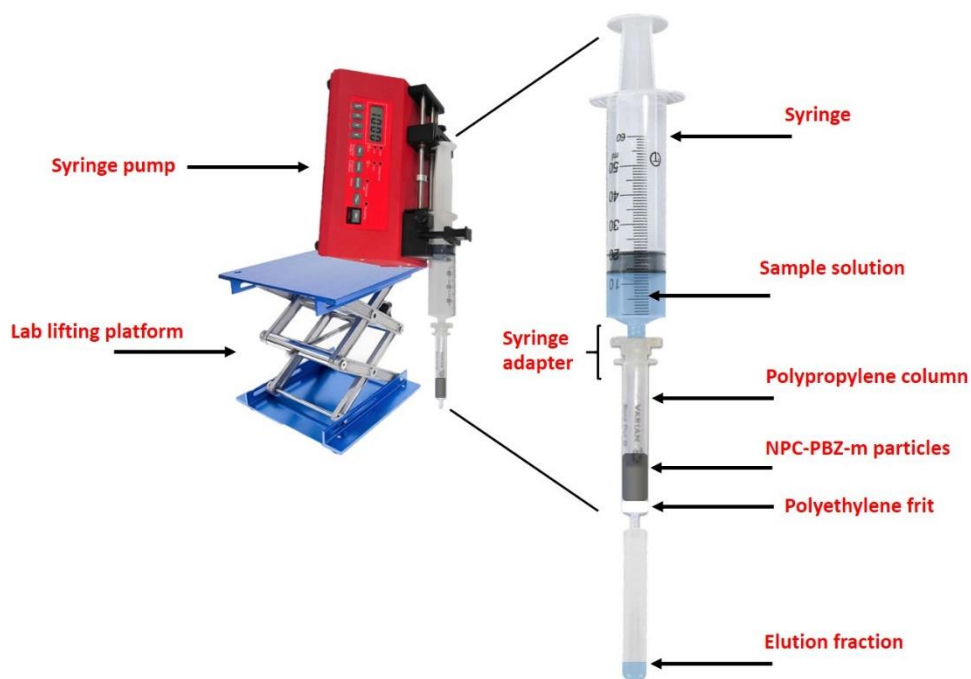


**Figure 3.2** The NPC-PBZ-m pre-concentration unit.



To increase the packing density, 50 mL of Deionized water (DI) was pumped through the column at the flow rate of 10 mL/min. The step for atrazine pre-concentration using syringe pump was described as follows

The NPC-PBZ-m pre-concentration column was conditioned and equilibrated at a flow rate of 1 mL/min with 5 mL of methanol and 10 mL of methanol/water (1:1, v/v), respectively. Then, 300 mL of atrazine in water sample was loaded into the column unless stated. Afterwards, the column was washed with 3 mL of deionized water and dried with air flow, respectively. To desorb an atrazine, a certain volume of methanol was flown through the column (unless stated). The atrazine amount in eluent was measured by HPLC-UV. The condition of HPLC-UV was shown in **Table 3.5**.

**Table 3.5** HPLC-UV condition

Parameters	Condition
Separation column	ZORBAX Eclipse Plus C18 (150 mm × 4.6 mm i.d., particle size 5 μm)
Mobile phase	Methanol/water (60/40, v/v)
Flow rate	1.5 mL/min
Injection volume	20 μL
Detection wavelength	222 nm [93]

### 3.6.1.1 Investigation of NPC-PBZ-m particle size

Since the particle size of solid sorbent can affect the adsorption performance, two particle sizes of NPC-PBZ-m were prepared by grinding with a household blender and sieving into the range of 30 – 40 and 40 – 60 mesh by test sieve. 300 mg of the NPC-PBZ-m sorbent was packed into an empty cartridge polypropylene column. A 300 mL of atrazine in a water sample (25 μg/L) was pumped through the column by using a syringe pump. To get the clear result, every 1 mL of

methanol elution was collected for 10 fractions to evaluate the atrazine pre-concentration.

### **3.6.1.2 Investigation of NPC-PBZ-m weight**

The weight of NPC-PBZ-m can affect the atrazine adsorption-desorption on pre-concentration procedure. For NPC-PBZ-m weights study, 100 - 400 mg of the suitable particle size of NPC-PBZ-m was found in **section 3.6.1.1**. A 300 mL of atrazine in a water sample (25  $\mu\text{g/L}$ ) was pumped through the column. The adsorbed atrazine was eluted with 1 mL of methanol. The appropriate NPC-PBZ-m weight is expected to give the highest atrazine content in the eluent.

### **3.6.1.3 Investigation of adsorption flow rate**

The effect of flow rate on atrazine adsorption was studied. Three flow rates, 5, 10 and 12 mL/min were applied to the NPC-PBZ-m pre-concentration column. Two levels of concentration of atrazine in water samples, 10 and 25  $\mu\text{g/L}$ , were used. Afterwards, the adsorbed atrazine was eluted with 3 mL of methanol. The appropriate atrazine adsorption flow rate was adopted for further experiment.

### **3.6.1.4 Investigation of elution volume and elution flow rate**

The volume of methanol eluent can affect the amount of atrazine in the elution fraction. A 25  $\mu\text{g/L}$  of atrazine in water sample was passed through a pre-concentration column followed by eluting with methanol varied volume from 3-5 mL. An elution flow rate was fixed at 1 mL/min.

Due to the elution flow rate affecting atrazine desorption efficiency, the 25  $\mu\text{g/L}$  of atrazine in water sample was loaded into pre-concentration column before elution with methanol at 3 mL. Two elution flow rates, 0.5 and 1 mL/min, were examined to obtain the suitable condition.

### **3.6.1.5 Reusability of NPC-PBZ-m pre-concentration column**

The possibility of NPC-PBZ-m pre-concentration column reusable was also evaluated for this work. A 300 mL of 30  $\mu\text{g/L}$  atrazine in water sample was loaded into NPC-PBZ-m pre-concentration column, which the solution preparation is described

in **section 3.5.2.1**. The scheme of adsorption-desorption step on the NPC-PBZ-m column is indicated in **Figure 3.3**. After each cycle was done, the column was washed with 30 mL of methanol. To operate the new cycle, NPC-PBZ-m column was started with 50 mL of deionized water packing for operation with the similar step in every cycle. After that, the column was conditioned and equilibrated as mentioned before sample water loading. The process was performed under optimization conditions.

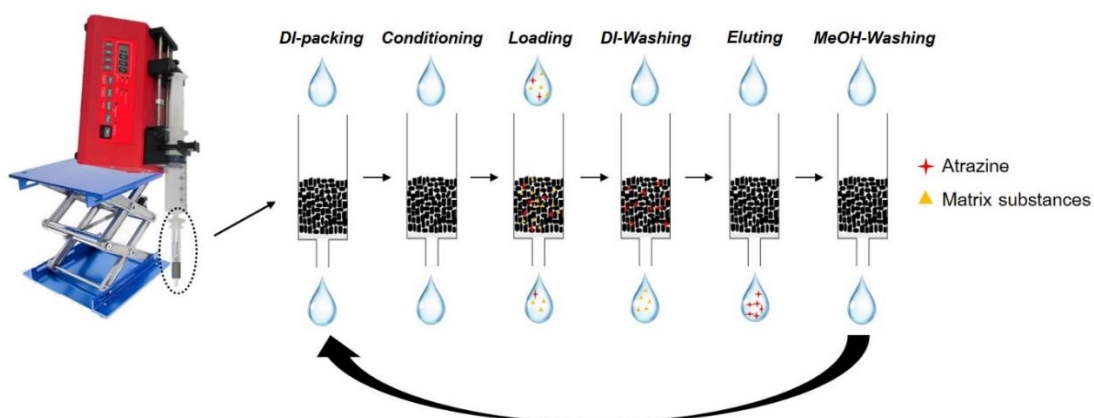


**Figure 3.3** The recycling of NPC-PBZ-m pre-concentration unit.

The performance of NPC-PBZ-m reusability was considered by monitoring the difference between the content of atrazine in eluent that was received from each cycle compared with the first cycle. The percent relative difference (< 10%) was calculated by the following formula

$$\% \text{relative difference} = \left( \frac{|P_{\text{cycle}N} - P_{\text{cycle}1}|}{P_{\text{cycle}1}} \right) \times 100 \dots \dots \dots (3.1)$$

$P_{\text{cycle}N}$  : the peak area after pre-concentration step at n-cycle (n = 2 to 8)

$P_{\text{cycle}1}$  : the peak area after pre-concentration step at first-cycle

### 3.6.2 Selectivity of HPLC-UV analysis

The proposed method was applied to determine an atrazine in water samples which have differences in matrix substances using HPLC-UV. Therefore, the selectivity of the analysis method has to be evaluated based on investigating the characteristic of chromatograms in different types of water samples. The retention time of atrazine

and other interference peaks in different water sample were evaluated with the chromatogram of atrazine which was prepared in methanol solvent.

In order to determine the concentration of atrazine after pre-concentration process, the suitability of methanol solvent type for calibration curve preparation was also investigated in this section. Three different types of solvents including methanol, methanol-NPC-PBZ-m, and methanol sample blank which each solvent preparation was described in detail

Methanol was collected from absolute methanol solvent from Merck. In case of methanol-NPC-PBZ-m, this solvent was collected from flow the methanol solvent passed through the NPC-PBZ-m column while the methanol sample blank was obtained when filling the water sample into column before passing the methanol solvent through the column. These methanol solvents were used to prepare a series of standard solutions (0.1-5 µg/mL) as described in **section 3.5.2.2**.

To estimate the effect of matrix substance on the response signal of target analyte for calibration curve construction, a signal suppression/enhancement effect (SSE) value was used [94]. The slopes of the calibration curves were compared and the accepted SSE value was set in range between 0.8 and 1.2 and SSE calculation was performed by following formula

$$SSE = \frac{\text{Slope}_{\text{matrix}}}{\text{Slope}_{\text{solvent}}} \dots \dots \dots (3.2)$$

### 3.6.3 Enrichment factor determination

A 5-30 µg/L of atrazine in agricultural water samples were prepared as described in **section 3.5.2.1** and performed the pre-concentration procedure under optimal conditions followed by HPLC-UV determination. The amount of atrazine in elution fractions was quantified by using an external calibration curve which the preparation is explained in **section 3.6.2**. The linear relationship between atrazine concentration before and after pre-concentration were investigated. The enrichment factor was calculated by the following formula

$$\text{Enrichment factor} = \frac{C_f}{C_i} \dots\dots\dots(3.3)$$

$C_f$  : the atrazine concentration ( $\mu\text{g/mL}$ ) after pre-concentration

$C_i$  : the atrazine concentration ( $\mu\text{g/L}$ ) before pre-concentration

Because the concentration of atrazine after pre-concentration by using HPLC-UV, the instrument detection limit (IDL) and limit of quantitation (LOQ) of this technique should be investigated. A series of atrazine standard solutions from 0-5  $\mu\text{g/mL}$  were prepared as described in **section 3.5.2.2**. The calibration curve was plotted between atrazine concentrations against peak area. IDL and LOQ were calculated by the following formula

$$\text{IDL} = \bar{X} + 3\text{SD} \dots\dots\dots(3.4)$$

$$\text{LOQ} = \bar{X} + 10\text{SD} \dots\dots\dots(3.5)$$

$\bar{X}$  : the average signal of sample blank

SD : the standard deviation of sample blank signal

### 3.6.4 The precision and interference of NPC-PBZ-m column on atrazine adsorption

To assess the precision and interference of NPC-PBZ-m column on atrazine pre-concentration step, 300 mL of atrazine water sample was loaded through 200 mg of NPC-PBZ-m column by syringe pump. The adsorption and elution flow rate were fixed at 10 and 1 mL/min, respectively. After that, the methanol eluent was flown through the column to desorb an atrazine compound. The experiment was set as shown in **Figure 3.2** and performed under a selected condition. After pre-concentration, the amount of atrazine in the elution fraction was determined by using HPLC-UV.

#### 3.6.4.1 The Repeatability (%RSD<sub>r</sub>) and reproducibility (%RSD<sub>R</sub>) of pre-concentration procedure

For repeatability and reproducibility test, the column was loaded with 300 mL of 30  $\mu\text{g/L}$  atrazine in water sample into the same NPC-PBZ-m column ( $n = 8$ )

and separate NPC-PBZ-m column ( $n = 3$ ) to pre-concentrate under optimal conditions, respectively. The amount of atrazine in elution fraction was determined using external standard curve which was prepared from methanol solvent. The precision of the pre-concentration step was evaluated in terms of repeatability relative standard deviation ( $RSD_r$ , %) and reproducibility relative standard deviation ( $RSD_R$ , %). The relative standard deviation was calculated by the following formula

$$\%RSD = \left( \frac{SD}{\bar{X}} \right) \times 100 \dots \dots \dots (3.6)$$

SD : the standard deviation of atrazine elution concentration

$\bar{X}$  : the average of atrazine elution concentration

#### 3.6.4.2 The effect of pesticides on atrazine adsorption on NPC-PBZ-m pre-concentration column

To evaluate the adsorptive selectivity of NPC-PBZ-m sorbent, other pesticides which are often applied with atrazine in agricultural fields such as paraquat, glyphosate, 2,4 D and chlorpyrifos were employed [95,96]. The standard of mixture pesticides in water samples were loaded into the NPC-PBZ-m pre-concentration column under optimal conditions ( $n = 3$ ), which the solution preparation is described in **section 3.5.5.1** The concentration of atrazine after pre-concentration was compared by using percent relative error ( $< 5\%$ ) for all interference species. The calculation performed by the following formula

$$\%relative\ error = \left( \frac{|C_{mea} - C_a|}{C_a} \right) \times 100 \dots \dots \dots (3.7)$$

$C_{mea}$  : the atrazine concentration after pre-concentration with other pesticides

$C_a$  : the atrazine concentration after pre-concentration without other pesticides

### 3.7 Optimization of parameters affecting on atrazine-colorimetric detection based on Konig's reaction

In this proposed method, a colorimetric method for atrazine determination was performed based on Konig's reaction that was adapted from the Shah and co-worker's study [39]. First, atrazine reacts with pyridine in a slightly acid medium under heat to form a quaternary pyridinium halide (step 1). Afterwards, an unstable yellow product, glutaconic dialdehyde, is developed after adding NaOH solution (step 2). Finally, glutaconic dialdehyde is converted into an orange-red polymethine compound by coupling with *p*-Anisidine (step 3). The proposed reaction mechanism of orange-red polymethine compound is shown in **Figure 3.4**.



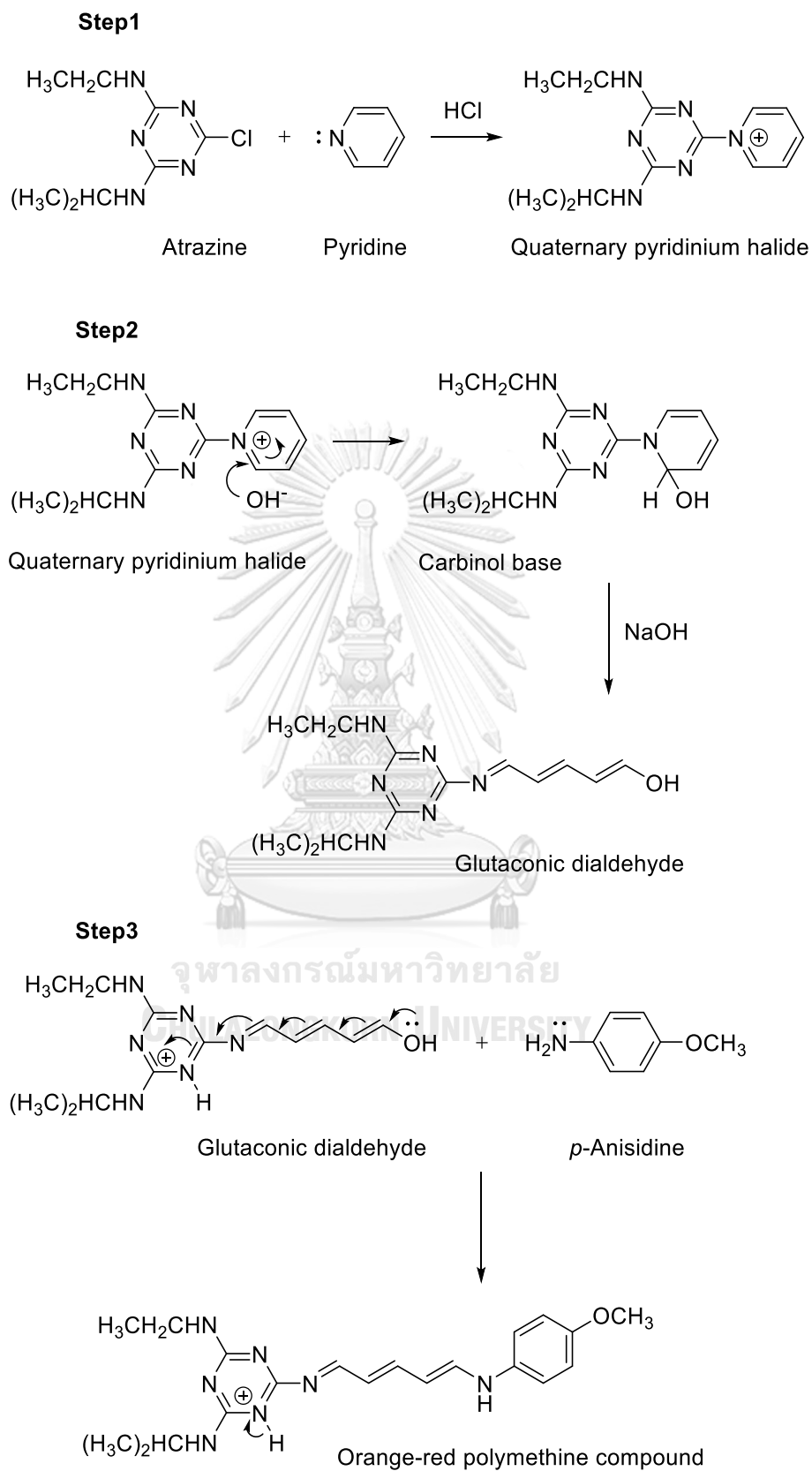


Figure 3.4 The proposed reaction mechanism of orange-red polymethine compound.



### 3.7.1 Optimization the volume of pyridine and conc. HCl volume (step 1)

To form the pyridinium quaternary halide as shown in step 1 (**Figure 3.4**), Konig's reaction begins with a pyridine compound interacting with atrazine in an acid medium. Therefore, the suitable volume of pyridine and conc. HCl should be investigated. In this step, the optimal conditions were investigated by measuring a final product, polymethine compound that was generated by coupling with 0.1 mL of 10 (% v/v) aniline. Two concentrations level of atrazine standard solutions (1 and 5  $\mu\text{g/L}$ ), with fixed volume at 0.5 mL were adopted to evaluate the suitable conditions. The preparations of atrazine standard solutions were described in **section 3.5.2.2**. The absorbance of polymethine compounds was measured at 487 nm by using UV-Vis.

#### 3.7.1.1 Effect of pyridine volume

The previous study reported the suitable condition of pyridinium quaternary halide formation occurred in acid medium [85]. Therefore, the pH of reaction was fixed at 4. To adjust the mixture solution to pH 4, the amount of conc. HCl varied depending on pyridine volume. The preparation of mixture solution was shown in **Table 3.6**, which the volume of pyridine was varied ranging from 0.2-0.5 mL were studied. The difference of reaction volume was equalized by adding methanol. The reaction temperature and heating time were fixed at 70 °C and 30 minutes, respectively. Then, 0.5 mL of 5 M NaOH and 0.15 mL of conc. HCl were added followed by coupling with aniline reagent.

**Table 3.6** The preparation of mixture solution on pyridine volume study

Atrazine standard solution ( $\mu\text{g/mL}$ ), 0.5 mL	Volume of pyridine (mL)	Volume of conc. HCl (mL)	Volume of MeOH (mL)
1 and 5	0.200	0.100	0.350
	0.250	0.100	0.300
	0.300	0.125	0.225
	0.400	0.150	0.150
	0.500	0.150	-

### 3.7.1.2 Effect of conc. HCl volume

After the optimized volume of pyridine is obtained in the previous study, the volume of conc. HCl varied from 0-0.15 mL were studied. The mixture solution was prepared by mixing 0.5 mL of atrazine standard solution with suitable volume of pyridine. The reaction was heated in a water bath with fixed reaction temperature and heating time at 70 °C and 30 minutes, respectively. Then, 0.5 mL of 5 M NaOH and 0.15 mL of conc. HCl were added following by the coupling step with aniline reagent.

### 3.7.2 Effect of reaction temperature, heating time, and NaOH concentration on glutaconic dialdehyde (yellow product) formation (step 2)

Because the orange-red polymethine compound was generated via the reaction between glutaconic dialdehyde and *p*-Anisidine, various parameters such as temperature, heating time, and NaOH concentration that can affect the glutaconic dialdehyde formation (step 2) were investigated. The 0.5 mL of 1 and 5  $\mu\text{g/mL}$  atrazine standard solutions were separately used to evaluate the suitable condition for all parameters. The preparation of atrazine standard solution was described in **section**

**3.5.2.2.** The absorbance of glutaconic dialdehyde was measured at 437 nm by using UV-Vis [85].

The examination was performed by mixing atrazine with a suitable volume of pyridine and conc. HCl (**section 3.7.1**) in a glass tube with screw cap. Then, the reaction tube was heated in a water bath with controlling temperature and time. After that, the solution was cooled down to room temperature before adding the NaOH solution. In this step, the color of the solution is changed from colorless to yellow. Due to the glutaconic aldehyde compound (yellow product) being unstable, the signal was instantly measured as soon as possible after the solution of sodium hydroxide was added.

#### **3.7.2.1 Effect of reaction temperature**

The suitable temperature on glutaconic dialdehyde formation was examined. The mixture solutions of atrazine with pyridine and conc. HCl at optimized volume was heated for 30 minutes with temperature varied from 35 – 70 °C. The concentration of 0.5 mL of NaOH was fixed at 5 M.

#### **3.7.2.2 Effect of heating time**

The appropriate time on glutaconic dialdehyde formation was also studied. After the optimized temperature was obtained, the heating time was investigated between 10-60 minutes. The concentration of 0.5 mL of NaOH was fixed at 5 M.

#### **3.7.2.3 Effect of NaOH concentration**

The hydroxyl group was required to form a carbinol base and glutaconic dialdehyde compound as shown in **Figure 3.4** (step2). The suitable concentration of NaOH should be investigated. The experiment was performed by mixing 0.5 mL of atrazine solution with optimized volume of pyridine and conc. HCl followed by heating in a water bath at suitable temperature and time. The concentration of NaOH was studied in a range from 2-8 M with the volume fixed at 0.5 mL.

### 3.7.3 Preliminary study of various coupling reagents study

Aniline, sulfanilic acid, and 4-aminophenol were initially tested. To test the color sensitivity, atrazine standard solutions at level 1 and 5  $\mu\text{g}/\text{mL}$  coupling with these reagents were measured by UV-Vis. The experiments were described in detail below

#### 3.7.3.1 Aniline

The volume of conc. HCl for aniline coupling reaction was investigated ranging from 0.255-0.700 mL. Moreover, the concentration of aniline was studied in range of 2-20 (% v/v).

#### 3.7.3.2 Sulfanilic acid

The studied volume of conc. HCl and concentration of sulfanilic acid were varied in the range of 0.2-0.5 mL and 0.2-1.0 (% w/v).

#### 3.7.3.3 4-aminophenol

The volume of conc. HCl varied from 0.15 to 0.40 mL and the concentration of 4-aminophenol solution in the range of between 0.1 – 1.0 (% w/v) were tested.

### 3.7.4 Optimization of the volume of conc. HCl, *p*-Anisidine concentration, and reaction time (step 3)

To obtain a suitable sensitivity of orange-red polymethine compound formation in step 3, many parameters that can affect the reaction such as volume of conc. HCl, *p*-Anisidine concentration, and reaction time were also investigated under the optimal conditions of step 1 and 2, which were obtained from **section 3.7.1 and 3.7.2**. The absorbance of the orange-red polymethine compound was measured at 500 nm by using UV-Vis.

#### 3.7.4.1 Effect of conc. HCl volume for the coupling step

The solution of glutaconic dialdehyde (step 2) was adjusted to suitable pH before coupling with *p*-Anisidine reagent. The yellow product (glutaconic dialdehyde) was generated by using a 0.5 mL of atrazine standard solution (1 and 5  $\mu\text{g}/\text{mL}$ ). Then, the volume of conc. HCl ranging from 0.10-0.20 mL was added into the

glutaconic dialdehyde solution followed by coupling with 6 (% w/v) of *p*-Anisidine (0.25 mL). The suitable volume of conc. HCl was adopted for further studies.

#### 3.7.4.2 Effect of *p*-Anisidine concentration

The sensitivity of orange-red polymethine compounds depends on the concentration of coupling reagent. Therefore, the *p*-Anisidine concentration should be investigated. A 0.5 mL of atrazine standard solutions (1 and 5 µg/mL) was used under optimal conditions. Then, the pH of solution was adjusted with optimized volume of conc. HCl followed by dropping with a *p*-Anisidine solution. The studied concentration range of *p*-Anisidine was from 2-15 (% w/v). To allow the reaction to occur completely, the signal of the orange-red polymethine compound was measured by UV-Vis at 500 nm after the reaction was settled for 1 hour.

#### 3.7.4.3 Effect of reaction time on the orange-red polymethine formation

The color of orange-red polymethine compound was generated after *p*-Anisidine adding into the solution (step 3). To ensure the formation of polymethine compounds can occur completely, the suitable reaction time on orange-red polymethine formation should be investigated. A 0.5 mL of atrazine standard solutions (0.5, 1 and 2 µg/mL) was used to evaluate the reaction based on optimal conditions for all parameters. The reaction time was studied from 1-60 minutes after *p*-Anisidine adding. The absorbance of an orange-red polymethine compound was measured by UV-Vis at 500 nm.

#### 3.7.5 Characterization of an orange-red polymethine compound

To characterize the orange-red polymethine compound structure (**Figure 3.4**), the chromatogram of atrazine, *p*-Anisidine, pyridine, and an orange-red polymethine dye compounds were investigated by HPLC-UV and UPLC-MS.

##### 3.7.5.1 HPLC-UV analysis system

For HPLC-UV measurement, three levels, 5, 25, and 50 µg/mL, of atrazine standard solution was prepared and used to perform the reaction under optimum condition. Moreover, the chromatograms of pyridine and *p*-Anisidine reagents

were also investigated. The chromatogram of these compounds was investigated in a wavelength of 222 nm for atrazine, *p*-Anisidine, and pyridine while an orange polymethine compound was detected at 500 nm. Moreover, the UV-Vis spectrum of peak chromatogram was also illustrated. The condition and mobile phase of HPLC-UV was shown in **Table 3.7 and 3.8**, respectively.

**Table 3.7** Conditions of HPLC-UV

Parameters	Conditions
Column	C18 (150 mm × 4.6 mm i.d., particle size 5 μm)
Flow rate	0.5 mL/min
Injection volume	5 μL
Detection wavelength (nm)	222, 500 nm

**Table 3.8** Mobile phase of HPLC-UV

Time (min)	Water (%A) <sup>a</sup>	Methanol (%B) <sup>a</sup>
0.00	40.0	60.0
5.00	20.0	80.0
35.00	20.0	80.0
35.10	40.0	60.0
40.00	40.0	60.0

<sup>a</sup> Water and methanol mobile phase containing 0.1% formic acid

### 3.7.5.2 UPLC-MS analysis system

To confirm the proposed structure of an orange-red polymethine compound, the mass per charge ratio or  $m/z$  of the proposed structure was pursued by UPLC-MS. The conditions and gradient mobile phase for UPLC/MS was adapted from HPLC-UV condition. 5  $\mu\text{g/mL}$  of atrazine performed the reaction under optimum conditions and atrazine standard solutions were injected to the UPLC-MS system. The electrospray ionization mode (positive mode) was adopted to estimate the  $m/z$  ratio. The condition and mobile phase of UPLC-MS was shown in **Table 3.9** and **3.10**, respectively.

**Table 3.9** Conditions of UPLC-MS

Parameters	Conditions
Column	C18 (150 mm $\times$ 4.6 mm i.d., particle size 5 $\mu\text{m}$ )
Flow rate	0.3 mL/min
Injection volume	3 $\mu\text{L}$
Mass range detection	100 – 1000 $m/z$ ratio

**Table 3.10** Mobile phase of UPLC-MS

Time (min)	Water (%A) <sup>a</sup>	Methanol (%B) <sup>a</sup>
0.00	40.0	60.0
3.00	40.0	60.0
5.00	20.0	80.0
15.00	0.0	100.0
20.00	0.0	100.0
20.10	40.0	60.0
25.00	40.0	60.0

<sup>a</sup> Water and methanol mobile phase containing 0.1% formic acid

### 3.7.6 The analytical performance of atrazine via the Konig's reaction using *p*-Anisidine as coupling reagent.

To solely evaluate the performance of Konig's reaction to determine an atrazine compound based on colorimetric analysis, the concentration of atrazine was varied from 0.1-5 µg/mL. The preparation of atrazine working standard solution was detailed in **section 3.5.2.2**. The experiment was performed under the optimum conditions. The intensity of the orange-red polymethine compound was measured by UV-Vis. Parameters such as matrix effect, working range, instrument detection limit, and limit of quantitation were investigated under the optimum conditions. The calibration curve was plotted between concentration against the absorbance value of the orange-red polymethine compound at 500 nm. Moreover, the color chart for atrazine determination was also investigated.



### 3.7.6.1 The matrix effect

Due to the solvent of elution was methanol, any organic matter from NPC-PBZ-m material may leak out and the response of colorimetric detection could be interfered. Therefore, the calibration curve of Konig's reaction was constructed in two methanol solvent systems which are methanol solvent (MeOH) and methanol that pass through the NPC-PBZ-m unit (MeOH-NPC-PBZ-m). A 0-5 µg/mL of atrazine standard solution was prepared in two methanol solvents (MeOH and MeOH-NPC-PBZ-m). The matrix effects from NPC-PBZ-m material in elution fraction towards the colorimetric detection were estimated by comparing the two slopes of the calibration as described in **section 3.6.2**.

### 3.7.6.2 Working range, Instrument detection limit (IDL), and limit of quantitation (LOQ)

Instrument detection limit (IDL), and limit of quantitation (LOQ) for colorimetric detection based on Konig's reaction were determined using standard deviation of linear regression line and slope of calibration. The IDL and LOQ values were calculated the following formula

$$IDL = \frac{3SD}{\text{Slope}} \dots \dots \dots (3.8)$$

$$LOQ = 3.3 \times IDL \dots \dots \dots (3.9)$$

Slope : the slope of calibration

SD : the standard deviation of linear regression line

### 3.7.6.3 Effect of other pesticides on atrazine colorimetric detection (Konig's reaction)

The selectivity of colorimetric method toward an atrazine detection when the presence of paraquat, glyphosate, 2,4-D or chlorpyrifos were also investigated. The preparation of mixture standard solution of these pesticides and atrazine are detailed in **section 3.5.5.2**. These standard solutions performed the colorimetric reaction under optimal conditions (n = 3), which were studied as described in **section 3.7**. The concentration ratio of each pesticide towards atrazine affecting the

performance of colorimetric method was evaluated by using percent relative error (< 5%). The calculation performed by the following formula in **section 3.6.4.2**.

### 3.8 Quantitative Analysis

To evaluate the applicability of the proposed method, agricultural water sample (Lopburi province, Thailand) spiked with atrazine concentration from 5-30  $\mu\text{g/L}$  were performed with optimum conditions ( $N=3$ ) for both HPLC and Konig's reaction. Several parameters including linearity, method detection limit (MDL), method quantitation limit (MQL), interference and matrix on the developed method were estimated.

#### 3.8.1 Interferences in the performance of the developed method

The effect of other pesticides for the whole process since pre-concentration step until colorimetric detection should be investigated. A 300 mL of 0.015  $\mu\text{g/mL}$  atrazine and mixture standard solutions with other herbicides and pesticide: paraquat, glyphosate, 2,4-D and chlorpyrifos at 1.5 and 7.5  $\mu\text{g/mL}$ . After these solutions were pre-concentrated under the optimum conditions, the elution fractions were tested with both HPLC-UV and UV-Vis method based on Konig's reaction ( $n = 3$ ). The elution fraction of atrazine, atrazine-paraquat (AP), atrazine-glyphosate (AG), atrazine-2,4-D (AD), and atrazine-chlorpyrifos (AC) were detected colorimetric method (Konig's reaction) based on the optimum conditions. The absorbance of orange-red polymethine compounds in each mixture solution (AP, AG, AD, and AC) was compared against atrazine solution (A) to estimate the limit of concentration level over than atrazine. The percent relative error (< 5%) was set as a maximum acceptable value. The calculation was performed as described in **section 3.6.4.2**.

#### 3.8.2 Matrix effect for assessing the performance of method

To assess the performance of proposed methods for different types of water samples analysis, three environmental waters which are pond and agricultural waters were collected from different resources of Thailand. Pond water was collected in the area of Chulalongkorn University campus, Bangkok. In case of agricultural water, the sample was collected from Lopburi and Nakhon Pathom province. 0-30  $\mu\text{g/mL}$  of atrazine standard solution was spiked in water samples. A 300 mL of each spiked water

sample was pumped through the NPC-PBZ-m preconcentration unit under the optimum condition. After that, the elution fraction was measured by using HPLC-UV and performed a colorimetric method followed by detecting with UV-Vis at 500 nm. To estimate the effect of matrices in different water, the linear relationships between the absorbance intensities and atrazine concentrations were evaluated and the slope of each water sample was compared. The acceptable slope ratio was set in range between 0.8 and 1.2 as described in **section 3.6.2**.

### **3.9 Application to environmental water samples for atrazine determination**

The proposed method was applied to analyze atrazine in real water samples. All steps since sample collection until atrazine colorimetric detection was described in this section.

#### **3.9.1 The preparation of water samples**

All water samples were collected in high density polyethylene or HDPE plastic containers and filtered through cellulose filter paper and 0.45  $\mu\text{m}$  of CA membrane filters (47mm diameter, Vertical) to remove any suspended organic matters before spiked with atrazine standard solution.

#### **3.9.2 Quantitative analysis of atrazine in real water sample**

After water sample preparation, 300 mL of environmental water samples were spiked with atrazine standard solution at 8, 10, 20, and 25  $\mu\text{g/L}$ . Then, the solution was pumped through the NPC-PBZ-m column for pre-concentration using a syringe pump after condition and equilibrating the column. The flow rate of adsorption was fixed at 10 mL/min. After pre-concentration, the column was washed with 2 mL of DI water and air dried, respectively. For atrazine elution, 3 mL of methanol was applied to column under flow rate at 1 mL/min. Next, the elution fraction was detected in both HPLC-UV and colorimetric analysis based on Konig's reaction. The concentration of atrazine was calculated using a calibration curve which was prepared using a Lopburi agricultural water.

For HPLC-UV determination, 0.9 mL of elution solution was mixed with 0.1 mL milli-Q water to avoid the effect of sample-mobile different polarity. The condition of

the HPLC-UV instrument was described in **Table 3.5**. In case of colorimetric analysis, 0.5 mL of elution was mixed with 0.2 mL of pyridine and 0.1 mL of conc. HCl followed by heating in a water bath at 40 °C for 20 minutes. Then, the glutaconic dialdehyde (yellow product) was performed by adding 0.5 mL of 5 M NaOH into a reaction. Next, 0.15 mL of conc. HCl and 0.25 mL of 6 (% w/v) of *p*-Anisidine were added to generate orange-red polymethine compounds. To allow the product generation completely, the reaction was allowed to settle at 20 minutes and determined by UV-Visible spectrophotometer at 500 nm. Moreover, the %recovery and %RSD was evaluated. **Figure 3.5** showed a whole step of this proposed method.

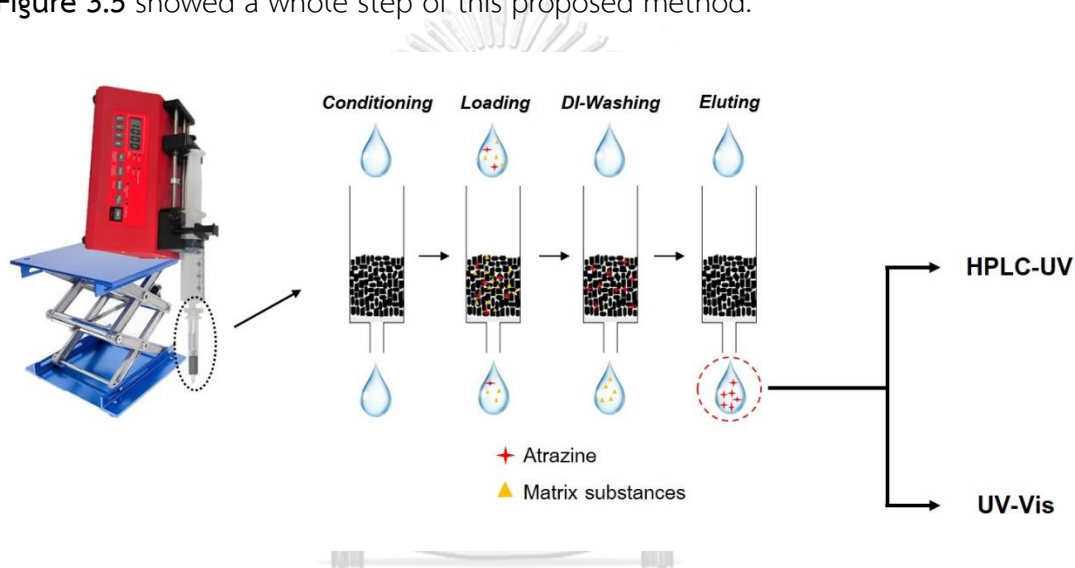


**Figure 3.5** The proposed method for atrazine analysis.

For paraquat determination, alginate bead composite which is silica-humic acid entrapped calcium alginate hydrogel (Si-HA-Alg) was prepared to use as a sorbent for paraquat adsorption (section 3.10). The preliminary test for paraquat adsorption on NPC-PBZ-m (section 3.11) and optimization reaction of paraquat blue free radical were investigated (section 3.12). Moreover, the optimization factors affecting paraquat-NPC-PBZ-m adsorption and method performance were tested (section 3.13 and 3.14).

### 3.10 Preparation of Si-HA-Alg materials (Si-HA-Alg)

In the batch adsorption procedure, the complicated step after adsorption is the materials removal step when the fine particles of adsorbents were used. Therefore, the enlarged Si-HA-Alg beads were designed to be prepared in agar- mold containing  $\text{CaCl}_2$  as shown in Figure 3.6. The preparation step of Si-HA-Alg using agar mold described below.

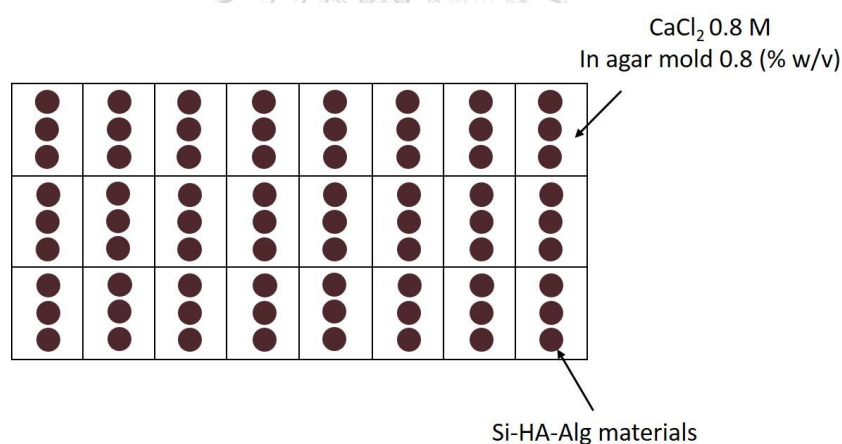


Figure 3.6 Agar mold 0.8 (% w/v) containing of 0.8 M  $\text{CaCl}_2$  solution.

#### 3.10.1 Preparation of agar mold contained $\text{CaCl}_2$

At first,  $58.800 \pm 0.0050$  g of  $\text{CaCl}_2$  was added in 500 mL of 80 °C DI water with continuous stir for 10 minutes. Next, the  $4.000 \pm 0.0050$  g agar powder was slowly added under stirring until the solution turns a pale-yellow clear solution obtained. Before transferring into a plastic mold, the temperature of solution was brought to 50 °C. Finally, the agar was set at ambient temperature for 3 hours before usage. Lastly,

the pit, a mold of Si-HA-Alg, was made by punching the agar mold with a plastic straw before filling with 1 mL of Si-HA-Alg mixture solutions.

### 3.10.2 Preparation of Si-HA-Alg materials

Firstly, certain weight of sodium alginate was dissolved in 20 mL of DI water and stirred until completely dissolved. Then, a suitable amount of silica gel and humic acid sodium salt were slowly added. To obtain a homogeneous solution, the mixture solution was continuously stirred for 6 hours before dropping into a pit of agar mold by using 1 mL of plastic syringe. After filling the mixture solution into agar mold, a solid hydrogel bead was slowly formed. The mold was left at room temperature for 24 hours to ensure the crosslinking entirely occurred. After that, remove the Si-HA-Alg bead from agar mold and wash with DI water. Finally, the obtained bead was dried in the oven at 50 °C for 1 day.

Generally, the adsorption efficiency was evaluated by adding a piece of the adsorbent into a 10 mL of 0.5 µg/mL paraquat solutions in a polypropylene tube. The adsorption process was performed by using a rotator at 30 rpm/min for 3 hours. Then, the content of paraquat in the filtrate was measured by performing the reaction of paraquat blue free radical which provides a maximum wavelength at 600 nm.

This reaction is used to measure the signal of paraquat blue free radical in the filtrate. 100 µL of 1 M glucose and 50 µL of 5 M NaOH reagents were dropped into 1.5 mL of the filtrate. The absorbance of the blue color was measured by UV-Vis. Moreover, the reaction of 0-4 µg/mL paraquat solution was performed and the signal of blue free radical was plotted against the paraquat concentration. The linear relationship with correlation coefficient of 0.9997 was obtained. Therefore, the adsorption performance can be estimated by comparing the absorbance intensity between 0.5 µg/mL of paraquat standard solution with the filtrate.

The adsorption percentage was calculated as the following equation [97]

$$\text{Percentage of adsorption} = \left( \frac{A_i - A_t}{A_i} \right) \times 100 \dots (3.10)$$

$A_i$  : the absorbance intensity of paraquat solution

$A_t$  : the absorbance intensity of filtration solution after adsorption

Many parameters including percentage of alginate, silica gel, and humic acid sodium salts amount were investigated to get an appropriate composition of sorbent. The experiment was described in detail below.

### 3.10.2.1 Effect of the percentage of silica particles and humic acid sodium salt (HA)

The adsorption performance of sorbent depends on the amount of silica and humic acid. Therefore, the content of these composition presences on Si-HA-Alg particles should be studied. The amount of alginate was fixed at 2 (% w/v) while the content of silica and humic acid salt varied from 0-2 (% w/v). The sorbent preparation in this section was detailed in **Table 3.11**.

**Table 3.11** The composition of silica gel and humic acid on alginate sorbent study

Adsorbent	Alginate (g)	Silica gel (g)	Humic acid (g)
Alg	0.4000 ± 0.0010	-	-
Si1%-Alg		0.2000 ± 0.0010	-
Si2%-Alg		0.4000 ± 0.0010	-
HA1%-Alg		-	0.2000 ± 0.0010
HA2%-Alg		-	0.4000 ± 0.0010
Si1%-HA1%-Alg		0.2000 ± 0.0010	0.2000 ± 0.0010
Si2%-HA2%-Alg		0.4000 ± 0.0010	0.4000 ± 0.0010
Si1%-HA2%-Alg		0.2000 ± 0.0010	0.4000 ± 0.0010
Si2%-HA1%-Alg		0.4000 ± 0.0010	0.2000 ± 0.0010

### 3.10.2.2 Percentage of alginate study

Due to the problem of humic acid leaching while performing the adsorption process, the amount of alginate should be investigated. The content of silica gel and humic acid was fixed at 1 (% w/v) when the amount of alginate varied from 1-4 (% w/v). The detail of adsorbent preparation was shown in **Table 3.12**.

**Table 3.12** The alginate sorbent preparation for alginate content study

Adsorbent	Alginate (g)	Silica gel (g)	Humic acid (g)
Si1%-HA1%-Alg1%	0.2000 ± 0.0010	0.2000 ± 0.0010	0.2000 ± 0.0010
Si1%-HA1%-Alg2%	0.4000 ± 0.0010		
Si1%-HA1%-Alg4%	0.8000 ± 0.0010		

The leaching of humic acid was also tested by measuring the absorbance of carbonyl groups on their structure at 300 nm.

### 3.11 The preliminary test for paraquat adsorption by NPC-PBZ-m

To estimate the possibility of NPC-PBZ-m sorbent for paraquat adsorption, many parameters affecting the adsorption performance including the KOH activation step, the washing step after activation, and agitation direction (adsorption step) were considered.

#### 3.11.1 The effect of KOH activation, DI washing step after activation and agitation direction on paraquat adsorption on NPC-PBZ-m

Three steps of the process including activation step, DI washing step after activation and the effect of agitation direction on adsorption efficiency were studied. The different pathways of adsorption methods were illustrated as shown in **Figure 3.7**



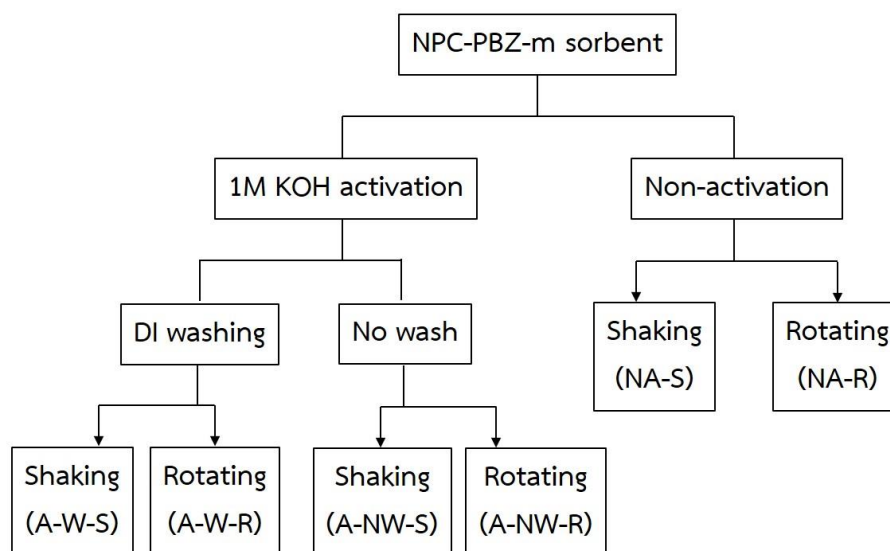


**Figure 3.7** The experimental design to investigate 3 factors: activation, washing and agitation direction, on the paraquat adsorption efficiency. (A): activation, (W): washing step, (S) orbital shaker (x-y direction), and (R) rotating shaker, (NA): no activation, and (NW): no washing step.

A  $0.050 \pm 0.001$  mg of NPC-PBZ-m was activated by using 1 M of KOH solution or DI water for 1 hour in 50 mL of polypropylene tube. Then, either KOH solution or DI water was discarded from NPC-PBZ-m material. After the activation step, the requirement of DI washing step was tested before adding a 50 mL of  $2 \mu\text{g/mL}$  of paraquat solution into the tube. In this study, the activated NPC-PBZ-m was washed with DI-water until neutral pH to eliminate the free hydroxide ion (using pH meter to check the pH). Next, the adsorption process was performed in two shaking directions which are rotating ( $360^\circ$ ) at 30 rpm/min and X-Y direction for 1 hour.

After the adsorption process was done for each studied factor, the filtrate solution was measured by UV-Visible spectrophotometer at 257 nm. The paraquat adsorption performance was estimated by calculating a percentage of adsorption.

### 3.11.2 The stability of paraquat in KOH activation

Even though the KOH solution was discarded from the NPC-PBZ-m sorbent before adding the paraquat solution. To ensure the paraquat compound does not

degrade in basic condition, the 2 µg/mL of paraquat solution was prepared in 1 M KOH and kept at ambient temperature. Then, the prepared solution was tested with blue free radical reaction after 1, 2, and 24 hours by testing with glucose 1 M, 150 µL. The signal paraquat of blue free radical was pursued at 604 nm.

### 3.11.3 The study of solvent for paraquat desorption

After a  $0.050 \pm 0.001$  mg of NPC-PBZ-m was activated by 1M KOH, 50 mL of 2 µg/mL paraquat solution was added into an extraction tube. The rotating adsorption was performed under 30 rpm/min for 1 hour. Then, an NPC-PBZ-m material was washed with DI water before adding the desorbing solvents. 0.1, 0.5 and 1 M of hydrochloric acid (HCl) was tested. The mixture of HCl acid and methanol at 70:30 (% v/v) was also tested by varying the concentration of HCl (HCl-MeOH). The paraquat concentration in the desorbing solvents was monitored by measuring the absorbance at 257 nm.

### 3.12 The optimization of paraquat blue free radical reaction for colorimetric method

Due to the reaction occurring in basic media, the optimum parameters which are a reducing agent and concentration of sodium hydroxide was also studied. Many chemical reagents such as ascorbic acid, sodium borohydride, and sodium dithionite were used as a reducing agent for paraquat reduction [33-35]. However, these reagents have some limitations in terms of stability and are harmful to use. Therefore, reducing sugar, as glucose, was adopted to reduce the paraquat since it is low cost, and non-toxic chemical substance. A 1.5 mL of 1 and 5 µg/mL paraquat solutions was prepared in 1 M HCl-MeOH (70:30). The suitable concentration of glucose and sodium hydroxide concentration were studied. The absorbance intensity of paraquat blue free radical was pursued at 5 minutes of reaction time by measuring absorbance at 604 nm.

### 3.12.1 The concentration and volume of glucose

To get the suitable conditions, the concentrations of glucose were studied in the range of 0.1-3 M while the volume was fixed at 200  $\mu\text{L}$ . After obtaining the suitable concentration, the volumes of glucose varied from 50-300  $\mu\text{L}$  were studied. The volume of 5 M NaOH concentration was fixed at and 250  $\mu\text{L}$ .

### 3.12.2 The concentration and volume of NaOH

The sodium hydroxide concentration varied from 0.1-10 M was optimized. Moreover, the volume of optimized sodium hydroxide solution was also investigated. The glucose concentration and volume were fixed at 1 M and 150  $\mu\text{L}$ , respectively.

### 3.12.3 The suitable of reaction time

To obtain a suitable reaction time for blue color development, 1.5 mL of 0.5, 1, and 3  $\mu\text{g}/\text{mL}$  of paraquat solutions was separately performed the reaction under an optimum condition without heating temperature required.

### 3.12.4 Limit of detection (LOD) and limit of quantitation (LOQ) for paraquat blue free radical reaction

The reagent blank of 1 M HCl-MeOH (70:30) was performed by adding 0.15 mL of 1 M glucose and 0.25 mL of 5 M NaOH and measured the signal at 600 nm for 9 replicates. LOD and LOQ of the method were calculated by using average signal of reagent blank and standard deviation of signal blank. The working range was also considered based on LOQ value.

### 3.13 Optimization conditions for paraquat-NPC-PBZ-m batch adsorption study

To obtain the suitable condition for paraquat adsorption, many parameters such as KOH concentration for activation step, and 1 M HCl-MeOH (70:30) volume was assessed. A  $0.050 \pm 0.001$  mg of NPC-PBZ-m and 50 mL of 2  $\mu\text{g}/\text{mL}$  paraquat solution was fixed in this section, while the NaOH concentration and volume of 1 M HCl:MeOH (70:30, % v/v) were varied. The studied KOH concentration range was 0.1-1 M with fixed volume of 50 mL. For the desorption study, every 2 mL of HCl:MeOH was collected.

The paraquat concentration in the desorbing solvent was then determined using UV-Vis at 604 nm using the linear equation which was obtained in **section 3.12.4**. The step of experiment in this section was shown **Figure 3.8**.

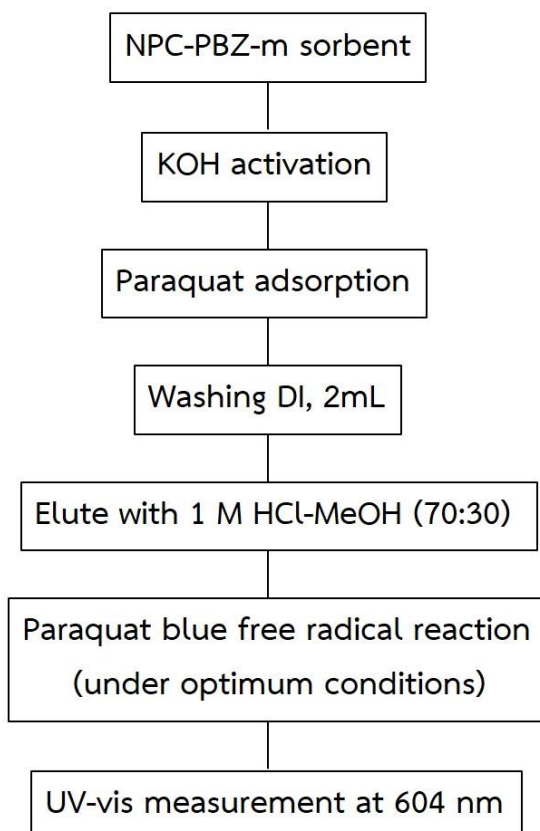


**Figure 3.8** The experimental step for paraquat determination by using paraquat blue free radical reaction.

### 3.14 The performance of NPC-PBZ-m for paraquat determination

The performance of the proposed method was tested by using paraquat solution with varied concentration from 0.05-1  $\mu\text{g/mL}$ . The adsorption and paraquat blue free radical process were performed under the optimum conditions. The elution concentration of paraquat was calculated by using a linear equation which was obtained in **section 3.12.4**. Moreover, the linear relationship between initial concentration and the concentration in the mixture solvent (HCl:MeOH) was investigated in this section. Firstly,  $0.050 \pm 0.001$  mg of NPC-PBZ-m was activated by

using 50 mL of 0.1 M KOH. Next, the solution of KOH was discarded and 50 mL of paraquat solution with varied concentration from 0.05-1 mL was added to the reaction tube for 1 hour. Then, the paraquat on NPC-PBZ-m was desorbed by using 2 mL of 1 M HCl-MeOH (70:30, % v/v). Finally, 1.5 mL of the desorbing solvent was added with 150  $\mu$ L of 1 M glucose solutions and 250  $\mu$ L of 5 M sodium hydroxide. The reaction was settled for 5 minutes to let the color development completely followed by measuring with UV-Vis at 604 nm.

### **3.15 The suggestion of this proposed method to enhance the efficiency for paraquat detection**

To enhance the performance of NPC-PBZ-m for paraquat adsorption, the parameters which are the weight of NPC-PBZ-m and the volume of KOH for activation step that might be affect the paraquat adsorption capacity. Therefore, these two variables were selected to assess the presumption.

#### **3.15.1 Weight of NPC-PBZ-m study**

A 0.050 and 0.100 mg of NPC-PBZ-m were adopted to compare the efficiency for paraquat adsorption. 50 mL of 0.5  $\mu$ g/mL of paraquat solution was added in the extraction tube after the NPC-PBZ-m activation step using 0.1 M KOH at the fixed ratio of 1:1 (mg/mL). The desorbing solvent was tested with paraquat blue free radical reaction by measuring the absorbance intensity at 604 nm.

#### **3.15.2 The ratio of NPC-PBZ-m weight to KOH volume (mg/mL) study**

The NPC-PBZ-m weight was fixed at 0.100 mg. Three volumes of 1M KOH which are 50, 100, and 150 mL were used to activate the sorbent with the ratio of NPC-PBZ-m weight per volume of KOH were 1:0.5, 1:1, and 1:2, respectively. After that, 50 mL of 0.5  $\mu$ g/mL of paraquat solution was filled in the reaction tube and the adsorption-desorption process was performed under the optimum conditions. The desorption solvent was reacted with glucose and NaOH to form paraquat blue free radical. The absorbance intensity was pursued by measuring absorbance at 604 nm.

## CHAPTER IV

### RESULTS AND DISCUSSION

In our study, the method for atrazine determination in water samples was developed. Due to the concentration level of atrazine presence in environmental water was very low, the pre-concentration units are required. Moreover, the colorimetric pre-screening for atrazine analysis was also developed based on Konig's reaction in this study. Nanoporous carbon derived melamine based polybenzoxazine or NPC-PBZ-m was packed into an empty cartridge column to use as a pre-concentration unit. After eluting the atrazine compound out of the NPC-PBZ-m column, the solution was measured by two techniques which are HPLC-UV and colorimetric method (Konig's reaction). This chapter is divided into four main parts. In the first part, many techniques were used for characterizations of NPC-PBZ-m sorbent are reported. In the second part, the optimal conditions of pre-concentration procedure of atrazine using NPC-PBZ-m pre-concentration unit were investigated. In the third part, an atrazine colorimetric detection based on Konig's reaction was also developed and the suitable parameters were optimized in this section. Finally, the proposed method was applied to determine atrazine compounds in environmental water samples.

#### 4.1 Characterization of nanoporous carbon derived from melamine based polybenzoxazine (NPC-PBZ-m) sorbent

Due to the synthesis of NPC-PBZ-m composed of three steps as described in **section 3.3**. In this part, the characterization was observed on two materials which are melamine based polybenzoxazine (PBZ-m) and carbon nanoporous melamine based polybenzoxazine (NPC-PBZ-m). First, the success of PBZ-m synthesis was confirmed by using FTIR techniques. After that, PBZ-m was pyrolyzed to create NPC-PBZ-m material. The surface properties and surface morphology of NPC-PBZ-m were investigated by using various techniques are described as follow

#### 4.1.1 Melamine based polybenzoxazine (PBZ-m) characterization

To synthesize PBZ-m material, an opaque melamine based benzoxazine organogel was polymerized under temperature programmed conditions. The previous research explains the mechanism of benzoxazine polymerization occurring via the opening of the oxazine ring structure and creating the Mannich base bridge instead. This phenomenon is called ring-opening polymerization [59]. The proposed reaction of melamine based polybenzoxazine or PBZ-m synthesis is shown in **Figure 4.1**. To confirm the success of PBZ-m synthesis, the functional group of benzoxazine structure was pursued by using FTIR-KBr pellet technique.

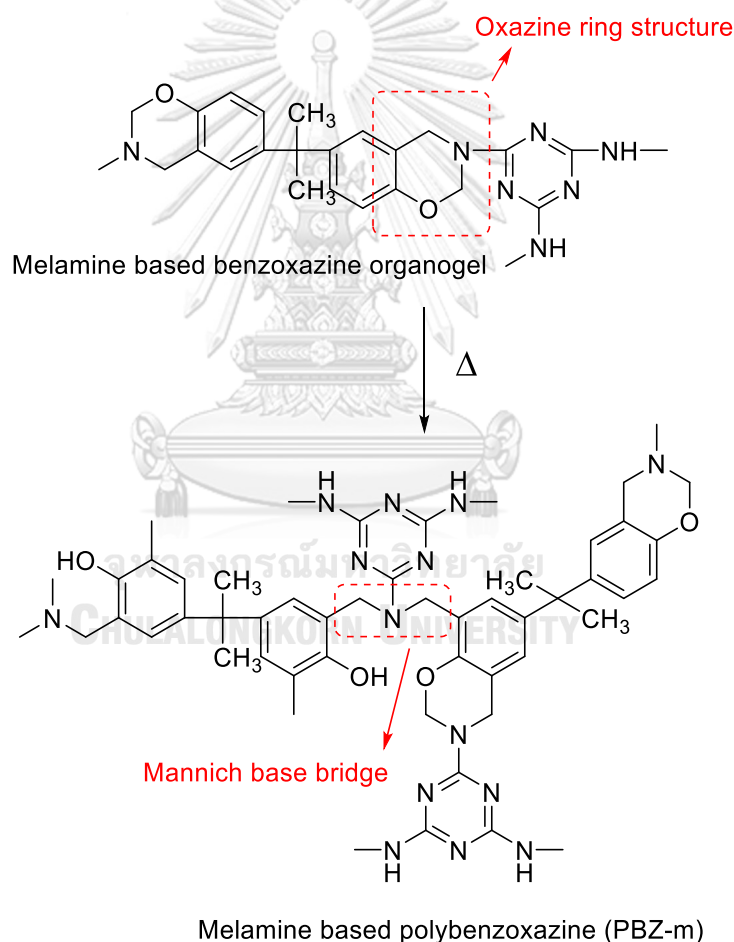


**Figure 4.1** The oxazine ring and Mannich base bridge structures.

To reveal the oxazine-ring opening polymerization of melamine based benzoxazine organogel, asymmetric stretching of C-N-C ( $1173\text{ cm}^{-1}$ ), C-O-C ( $1249\text{ cm}^{-1}$ ) and  $\text{CH}_2$  wagging ( $1360\text{ cm}^{-1}$ ) belong to oxazine structure were illustrated in **Figure 4.2**.

Furthermore, the out-of-plane bending vibrations of C-H and tri-substituted benzene ring were also noticed at 980 and 1507  $\text{cm}^{-1}$ , respectively [58,59]. As the results, the successful synthesis of melamine based polybenzoxazine (PBZ-m) can be confirmed as the intensity of C-N-C and C-O-C characteristic peak at 1173 and 1249  $\text{cm}^{-1}$  decreased after curing process due to ring-opening polymerization of benzoxazine organogel.

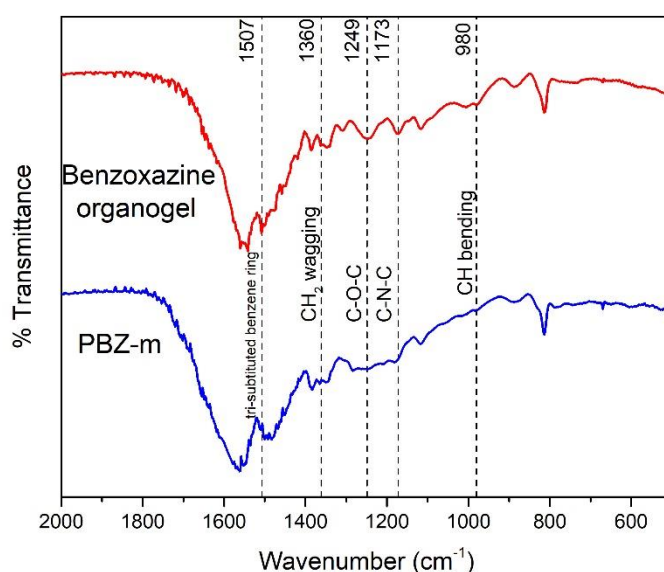


**Figure 4.2** FTIR spectra of Melamine based benzoxazine organogel and melamine based polybenzoxazine (PBZ-m).

#### 4.1.2 The textural properties of nanoporous carbon derived from melamine based polybenzoxazine (NPC-PBZ-m)

After ring-opening polymerization via temperature curing, the melamine based polybenzoxazine (PBZ-m) was pyrolyzed under  $\text{N}_2$  atmosphere at 800  $^{\circ}\text{C}$ . The pore characteristics of NPC-PBZ-m was investigated using the Autosorb 1-MP analyzer at -196  $^{\circ}\text{C}$ . The  $\text{N}_2$  adsorption-desorption isotherms of NPC-PBZ-m is shown in **Figure 4.3A**. As IUPAC classified, the adsorption isotherm of NPC-PBZ-m sorbent exhibits type IV which can indicate as a mesoporous material. Moreover, a H1 hysteresis loop also presents that referred to a narrow distribution of uniform pores [32,61].



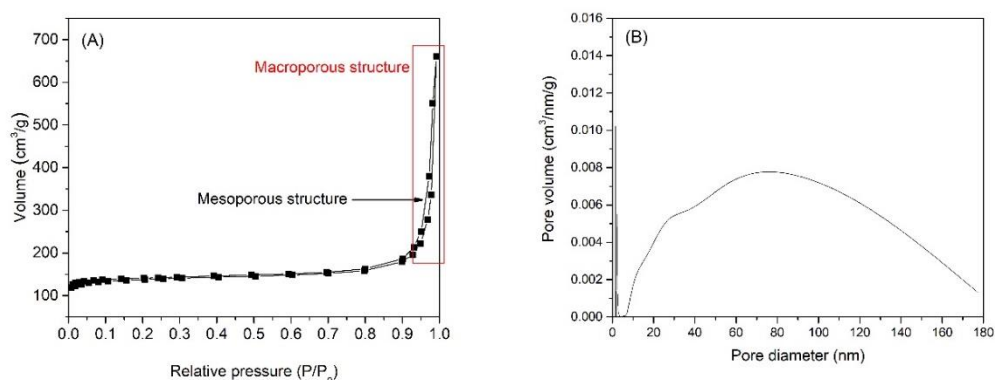


**Figure 4.3**  $N_2$  adsorption-desorption isotherms (A) and pore size distributions (B) of NPC-PBZ-m.

Moreover, the NPC-PBZ-m sorbent also contained a macroporous structure as the result in **Figure 4.3B** showed that the adsorption characteristic was steeply increased at high relative pressure ( $P/P_0 > 0.9$ ). The textural properties of NPC-PBZ-m are listed in **Table 4.1**.

**Table 4.1** Textural properties of NPC-PBZ-m

<sup>a</sup> $S_{bet}$ ( $m^2/g$ )	<sup>b</sup> $S_{micro}$ ( $m^2/g$ )	<sup>c</sup> $S_{meso}$ ( $m^2/g$ )	<sup>d</sup> $V_{total}$ ( $cm^3/g$ )	<sup>b</sup> $V_{micro}$ ( $cm^3/g$ )	<sup>c</sup> $V_{meso}$ ( $cm^3/g$ )	Average pore diameter (nm)
419	169	191	1.02	0.09	0.87	9.75

<sup>a</sup> Obtained from multi point BET method.

<sup>b</sup> Obtained from  $t$ -plot method.

<sup>c</sup> Obtained from BJH method.

<sup>d</sup> Obtained from total pore volume calculated from nitrogen adsorption at  $P/P_0 = 0.992$ .

#### 4.1.3 The functionality of nitrogen- and carbon-containing on nanoporous carbon derived from melamine based polybenzoxazine (NPC-PBZ-m)

To obtain the possible structure of N-active species on NPC-PBZ-m sorbent, XPS N1s narrow scan spectra was used to investigate the nitrogen functionalities existence. **Figure 4.4A** Illustrated the deconvolution of XPS spectra into five main

peaks which compose of pyridine-N (398.2 eV), secondary-N (399.3 eV), pyrrolic or pyridone-N (400.8 eV), quaternary-N (402.1 eV) and oxide-N (403.5 eV) [31,98,99]. Moreover, the deconvoluted XPS C1s narrow scan spectra (**Figure 4.4B**) showed four main peaks that consist of C-C (284.6 eV), C-N (286.0 eV), C=N (287.5 eV) and C=O (289.3 eV) [100]. As a result, it can imply that NPC-PBZ-m contains a high percentage of pyridine-N, pyridone-N and C-C bond ( $sp^2$ ) on their structure, serving as the active sites for atrazine adsorption. The probable structure of NPC-PBZ-m sorbent was expressed in **Figure 4.4C**. Furthermore, oxide-N and C=O groups are probably generated by the oxidation of the material since the exposure to ambient air after carbonization [98].

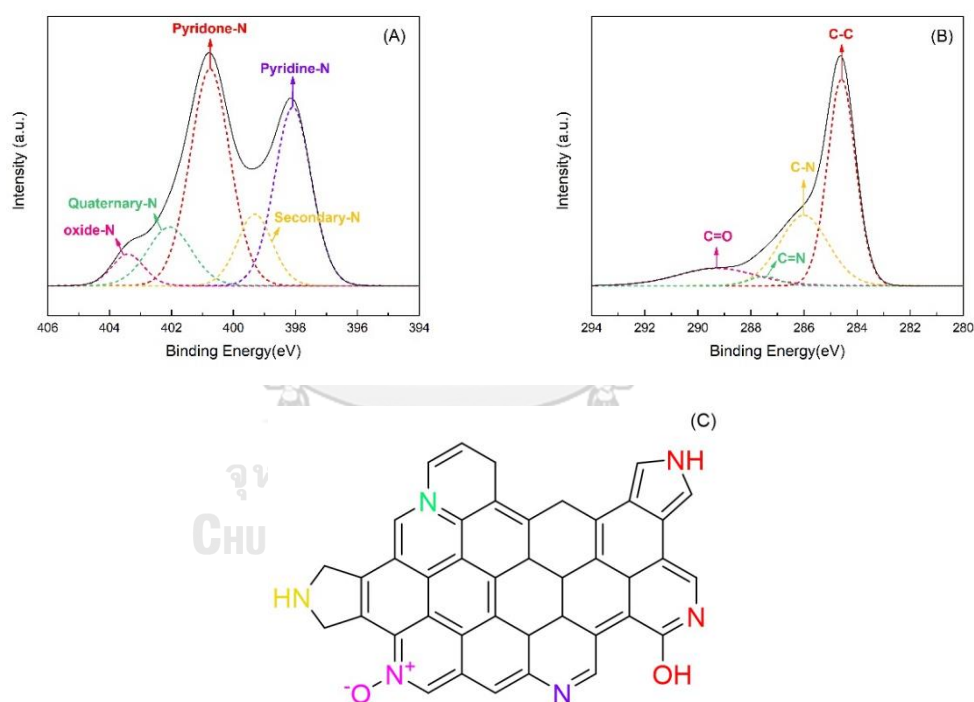


**Figure 4.4** XPS narrow scan spectra of N1s (A) and C1s (B) and proposed structure of NPC-PBZ-m (C).

#### 4.1.4 The surface morphology of nanoporous carbon derived from melamine based polybenzoxazine (NPC-PBZ-m)

Field emission scanning electron microscope was conducted to observe the surface morphology of NPC-PBZ-m sorbent. **Figure 4.5A and B** showed that the PBZ-

m and NPC-PBZ-m are composed of numerous tiny clusters connecting which can generate pore networks and contribute 3D interconnected structure, respectively. The appearance can be explained by phase separation phenomena between benzoxazine monomers and the suitable solvent system. Due to an easy miscibility of melamine-based benzoxazine monomers in ethanol/water solvent, the formation of benzoxazine particles during the sol-gel process is slowly growing. It generates many small primary clusters connecting together during the phase separation process [32,61]. Moreover, in case of NPC-PBZ-m, the rougher surface was obtained after carbonization based on non-carbon elements eliminated and organized crystallographic formation of carbon [101].

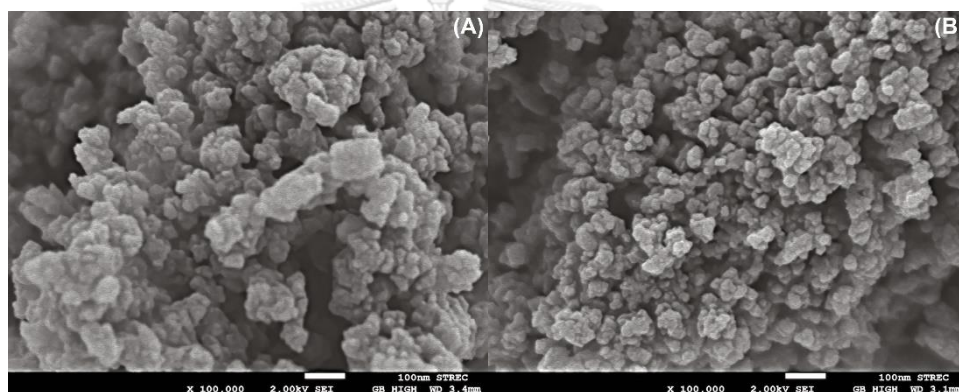


**Figure 4.5** SEM micrographs of PBZ-m (A) and NPC-PBZ-m (B) at 100,000X magnification.

#### 4.2 Optimization parameters affecting on NPC-PBZ-m pre-concentration efficiency

In the work, NPC-PBZ-m sorbent was packed in a SPE empty cartridge column to use as pre-concentration column. The adsorption and elution steps are performed by using a syringe pump. To estimate the suitable condition with real matrix systems, an agricultural water is applied in this section. The water was collected from a rice field in Lopburi province which ensured no atrazine usage. Many variables affecting adsorption-elution efficiency were evaluated by measuring the peak area of the atrazine amount in the elution fraction using HPLC-UV technique to obtain the optimal conditions.

#### 4.2.1 Effect of pH on atrazine-NPC-PBZ-m adsorption

Generally, the pH range of the surface water samples is around 6.5-8.5. However, in some areas the pH might be below 5 or above 9. Therefore, the studied pH of 3, 7 and 9 were selected in the study. As shown in **Figure 4.6**, there is no difference in the adsorption efficiency among the studied pH values. The calculation of adsorption efficiency was described in **section 3.10.2**.

At the studied pHs higher than  $pK_a$  of atrazine (2.2) [29], atrazine was in the non-protonated form in the studied range. Therefore, the interactions occurring between atrazine and the adsorbents might be the  $\pi$ - $\pi$  interaction and Van der Waals interaction which are pH independent. It can imply that the adsorption interaction between atrazine and NPC-PBZ-m does not depend on pH. Therefore, the water sample was measured without step for pH adjustment.

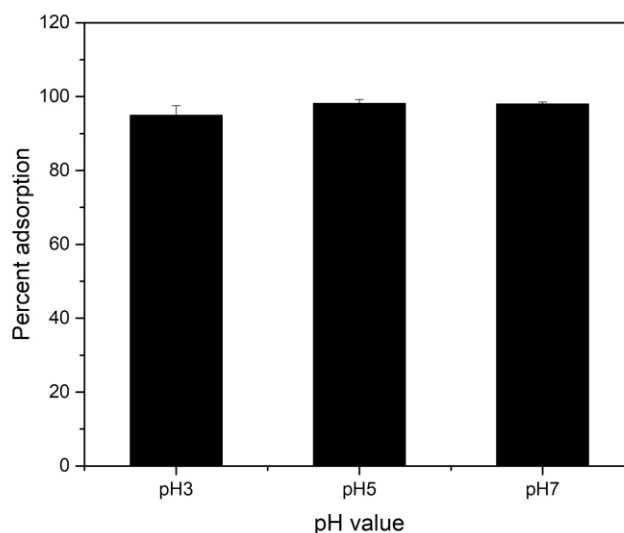


**Figure 4.6** Effect of pH on atrazine-NPC-PBZ-m batch adsorption.

#### 4.2.2 Effect of NPC-PBZ-m particle size

The particle size of the irregular shape of NPC-PBZ-m should be controlled to achieve the best adsorption performance. Therefore, the material was prepared using a household blender and test sieves. In this section, 300 mg of two NPC-PBZ-m particle sizes which are 0.44-0.57 mm (No. 30-40 mesh) and 0.25-0.44 mm (No. 40-60 mesh) were

packed into an empty cartridge column. A 300 mL of atrazine solution (25 µg/L) passes through the column and every 1 mL of elution fraction was collected for 10 fractions. From **Figure 4.7**, the result showed that a higher peak area of atrazine is obtained from the smaller particle size (0.25-0.44 nm) for all the elution fractions. It can imply that the packing characteristics of small particles are denser. Therefore, it can improve the chance of atrazine diffusion and adsorption towards NPC-PBZ-m sorbent.

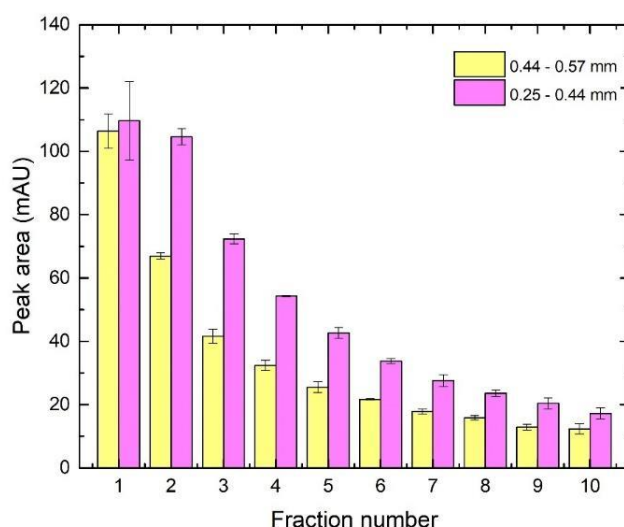


**Figure 4.7** Effect of NPC-PBZ-m particle size.

#### 4.2.3 Effect of NPC-PBZ-m weight

Due to the weight of adsorbent plays an important role on the adsorption performance as reported in previous studies [74,77]. In this study, 100-400 mg of NPC-PBZ-m particle size between range 0.25-0.44 nm was packed into an empty cartridge column. 300 mL of 25 µg/L atrazine water sample flow through the NPC-PBZ-m pre-concentration column and elutes with 1 mL of methanol. The result shown in **Figure 4.8** demonstrated that the highest atrazine amount was obtained when the column was packed with 200 mg of NPC-PBZ-m. However, increasing the NPC-PBZ-m weight from 200 to 400 mg, atrazine concentration decreased. This observation can be explained by adsorption-re-adsorption phenomenon of atrazine could occur because

the NPC-PBZ-m material has a lot of active sites. Hence, 200 mg of NPC-PBZ-m was chosen as the optimal NPC-PBZ-m amount for further studies.

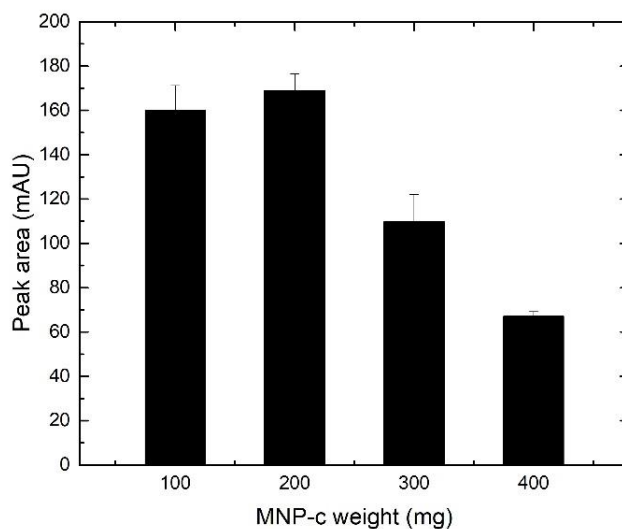


Figure 4.8 Effect of NPC-PBZ-m weight.

#### 4.2.4 Effect of sample flow rate

The influence of flow rate on the pre-concentration efficiency of the NPC-PBZ-m column was examined by varying flow rate between 5-12 mL/min. From **Figure 4.9**, the result estimated the impact of adsorption flow rate on the pre-concentration of atrazine for 10 and 25  $\mu\text{g/L}$  of atrazine solutions. There is no different trend that could be observed. Although using the lowest flow rate (5 mL/min) has demonstrated the highest pre-concentrated atrazine amount, which might be due to the more contact time between NPC-PBZ-m adsorbents and atrazine itself, the operation time was too long. In contrast, when the flow rate is as high as 12 mL/min, the content of atrazine in the eluent was lowest. This might be the result of the inadequate contact time between atrazine and NPC-PBZ-m sorbent. Therefore, a flow rate of 10 mL/min was chosen for atrazine pre-concentration.

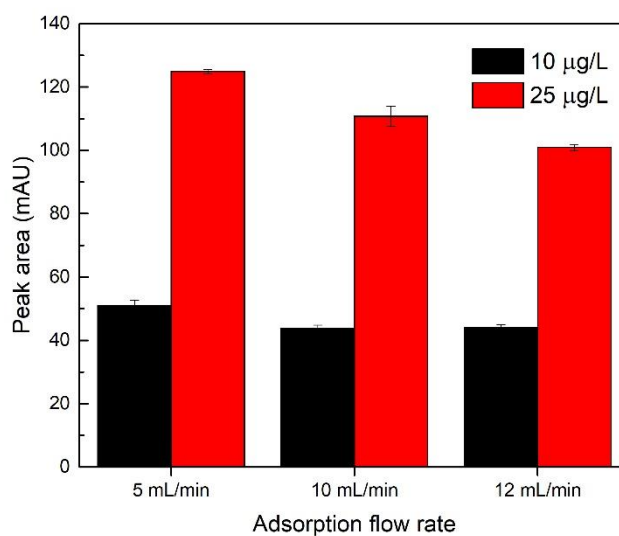
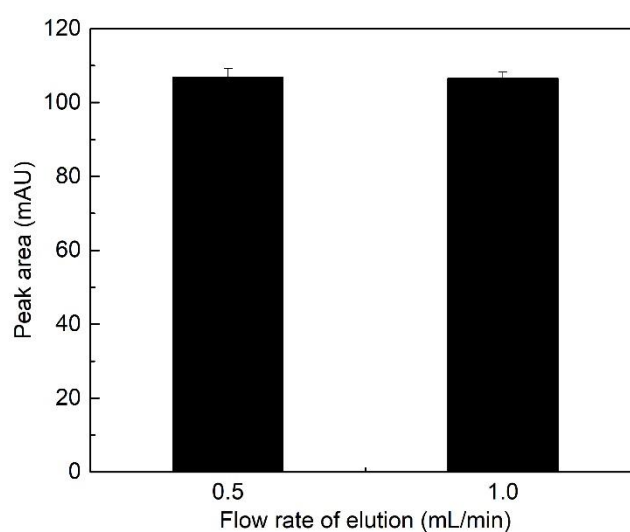


Figure 4.9 Effect of sample flow rate.

#### 4.2.5 Effect of eluent volume (methanol) and elution flow rate

Since the volume of methanol can affect the atrazine pre-concentration efficiency, the suitable methanol volume was investigated. A 300 mL of 25 µg/L of atrazine spiked in water sample was loaded into a pre-concentration column followed by eluting using methanol at 1 mL/min. The studied range was 3-5 mL. A 3 mL of methanol was selected based on many factors including the obtained concentration, the volume needed for the further analysis.

The effect of flow rate on atrazine desorption was studied. The flow rate of methanol was examined at 0.5 and 1 mL/min while the volume was fixed at 3 mL. The flow rates of methanol had no obvious impact on the atrazine desorption. Therefore, the flow rate of methanol at 1 mL/min was adopted in this proposed method. The results showed in **Figure 4.10**.



**Figure 4.10** Effect of elution flow rate.

To conclude the optimal conditions for pre-concentration procedure, the suitable values of all parameters are listed in **Table 4.2**. Furthermore, this condition was conducted to investigate the effect of other pesticides interference and NPC-PBZ-m sorbent reusability in further study.

**Table 4.2** The optimum conditions of NPC-PBZ-m pre-concentration procedure

Parameters	Optimum values
Particle size of NPC-PBZ-m	0.25-0.44 nm (Mesh No. 40-60)
Weight of NPC-PBZ-m	200 mg
Sample flow rate	10 mL/min
Elution flow rate	1 mL/min
Elution volume	3 mL



#### 4.2.6 Reusability of NPC-PBZ-m pre-concentration column

From the economic point of view, the reusability of NPC-PBZ-m column has to be evaluated. A 30  $\mu\text{g/L}$  atrazine in water sample was loaded into the NPC-PBZ-m column and performed under the optimal conditions as indicated in **Table 4.2**. The result was estimated by calculating a percent relative difference of peak area between the first cycle and other cycles. A percent relative difference is set at 10% as the maximum acceptable value.

From **Figure 4.11**, our results demonstrated that the NPC-PBZ-m column can be applied for atrazine pre-concentration in a real matrix sample over 8 cycles of adsorption-desorption process without any significant loss.

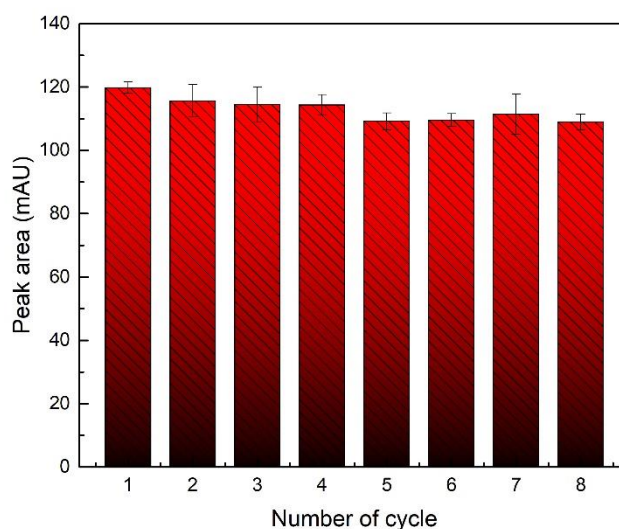


**Figure 4.11** Reusability of NPC-PBZ-m column based on optimum conditions.

#### 4.3 Selectivity of HPLC-UV analysis

This proposed method was applied to detect atrazine in water samples which have differences in matrix substances. Therefore, the selectivity of the HPLC-UV method was evaluated by comparing the chromatograms obtained from the standard, spiked blank samples with those obtained from the blank samples.

The results showed that atrazine standard solution has retention time of  $3.5 \pm 0.1$  minutes (Figure 4.12). Therefore, the chromatogram of other samples should not have any peak at 3.5 minutes which can cause interference with the signal of atrazine.

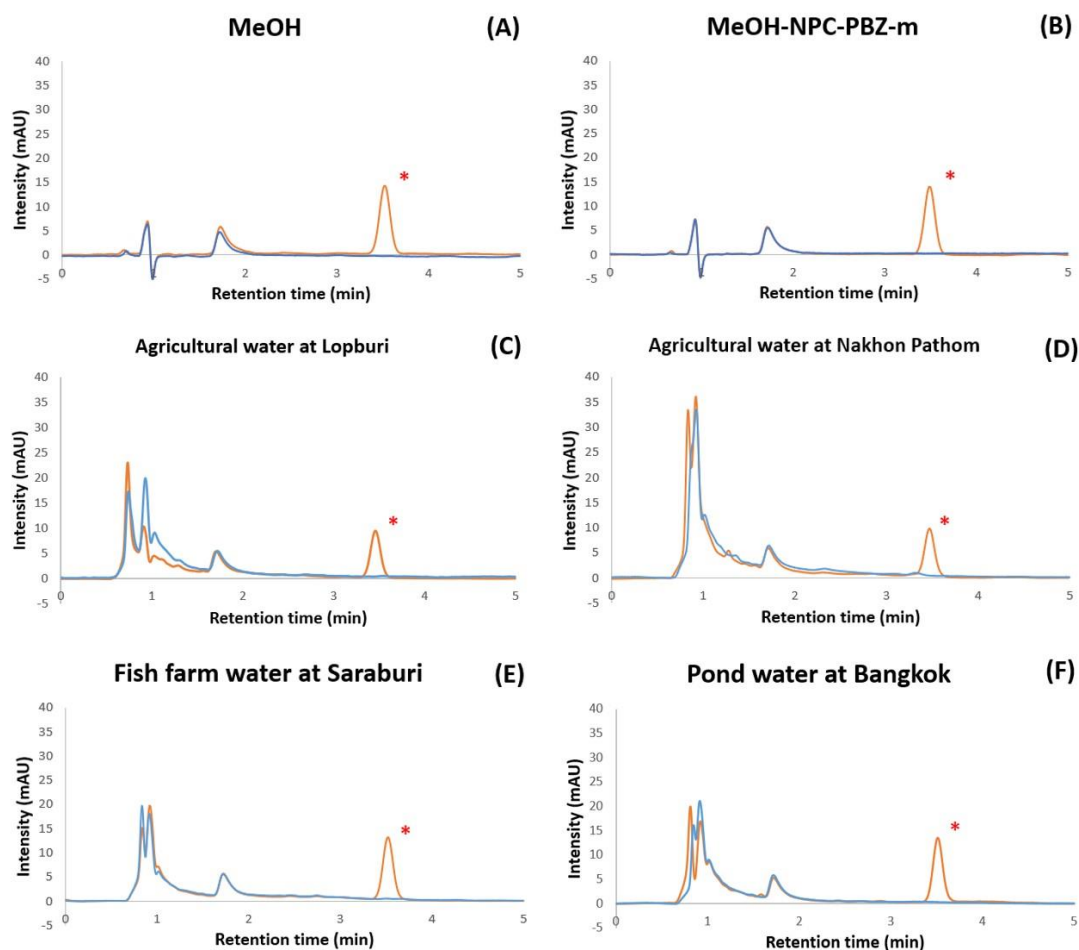


**Figure 4.12** Chromatogram of atrazine spiked in various solutions: MeOH (A), MeOH-NPC-PBZ-m (B), Lopburi (C) and Nakhon Pathom (D), fish farm water (E), and pond water (F). Blue line : non-spiked solvent or water samples; orange line : spiked solvent or water samples.

The result showed that there is no matrix from water samples interfering with the atrazine peak. Therefore, the concentration of atrazine after pre-concentration can be determined using HPLC-UV analysis system.

Because the concentration after pre-concentration need to be quantified, the matrix effect on the quantitation was investigated. A series of standard solution 0.1-5

$\mu\text{g/mL}$ , as the range of expected value of atrazine concentration, were prepared in MeOH, MeOH after passing the NPC-PBZ-m column, and MeOH sample blank solvent. From **Table 4.3**, the slope ratios of MeOH-NPC-PBZ-m versus MeOH solvent and of MeOH-sample blank versus MeOH were in range of 0.8-1.2 [102] indicating that there is no effect of matrix on any types of the calibration curves using HPLC-UV analysis system. Moreover, the difference of two calibration curves was also assessed using paired t-test. It can imply that an external calibration curve can be prepared using MeOH for atrazine determination without any interference from the matrix. Moreover, an enrichment factor of the proposed method can be evaluated using the obtained of linear equation.

**Table 4.3** The effect of matrix from NPC-PBZ-m and sample blank on an external calibration curve preparation

Solvent systems	Linear equation <sup>a</sup>	R <sup>2</sup>	Slope ratios (matrix/solvent)	Paired t-Test <sup>b</sup>
MeOH	$y = 114.84x + 0.4293$	0.9981	-	-
MeOH-NPC-PBZ-m	$y = 111.05x + 3.4317$	0.9990	0.97	1.375
MeOH-sample blank	$y = 120.70x + 0.7405$	0.9987	1.05	-2.293

<sup>a</sup> The concentration of atrazine standard solutions ranges from 0.1-5  $\mu\text{g/mL}$

<sup>b</sup> The comparison of calibration curve in MeOH, MeOH-NPC-PBZ-m, and MeOH-sample blank using t-stat at 95% of confident level = 2.365

#### 4.4 Enrichment factor

In order to find enrichment factor, HPLC-UV analysis method measuring the concentration after pre-concentration was firstly validated.

The IDL and LOQ were calculated from the peak area of 12 replicates of sample blank solvent (0  $\mu\text{g/mL}$  atrazine spiked). The performance of HPLC-UV for measuring atrazine after pre-concentration was reported at IDL and LOQ were 1.97 and 14.38

$\mu\text{g/L}$ , respectively. 5-30  $\mu\text{g/L}$  of atrazine in agricultural water samples were pre-concentrated under the optimum conditions. As previously demonstrated, the external calibration curve could be used to identify the atrazine concentration in the eluent. The initial concentration and the concentration after pre-concentrated were plotted in x-axis and y-axis, respectively. From **Figure 4.13**, our result showed that the relationship was linearity and enrichment factor can be calculated from the slope. The proposed method gave an average enrichment factor of 35.1.

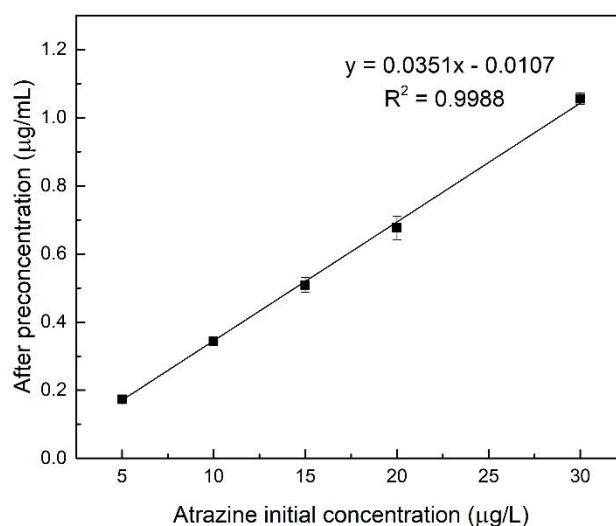


**Figure 4.13** Linear relationship of atrazine concentration before and after pre-concentration.

#### 4.5 The precision and interferences of NPC-PBZ-m column for atrazine adsorption

##### 4.5.1 Repeatability ( $\text{RSD}_r$ ) and reproducibility ( $\text{RSD}_R$ ) of pre-concentration procedure

The  $\% \text{RSD}_r$  and  $\% \text{RSD}_R$  were studied by loading a 300 mL of 30  $\mu\text{g/L}$  of atrazine into NPC-PBZ-m pre-concentration column with the same column for repeatability test ( $n = 8$ ) and separate column for reproducibility test ( $n = 3$ ). After pre-concentration, the amount of atrazine in the elution fraction was determined by using HPLC-UV and the atrazine concentration in the eluent was calculated using the equation:  $y = 114.84x$

+ 0.4293. The %RSD<sub>r</sub> and %RSD<sub>R</sub> from the proposed method were obtained as 3.82 and 4.41, respectively. The results are accepted for Association of Official Chemists, AOAC (%RSD<sub>r</sub> < 15 and %RSD<sub>R</sub> < 22). Moreover, from the result of reproducibility, it can be concluded that each NPC-PBZ-m column delivers similar pre-concentration performance.

#### 4.5.2 Effect of other pesticides on atrazine adsorption on NPC-PBZ-m pre-concentration column

Due to the usage of atrazine with other pesticides in agricultural productions [95,96], the environmental water sample can be contaminated with various pesticides species. The presence of other pesticides compounds could interfere with the adsorption efficiency of atrazine on the NPC-PBZ-m pre-concentration column. Therefore, the performance of NPC-PBZ-m column on atrazine adsorption when other pesticides contained in water samples was evaluated under the optimal conditions (**Table 4.2**). In this section, the concentration level of atrazine at 15 µg/L was tested. The mixture standard solution between atrazine and other pesticides were prepared in agricultural water at the ratio of 1:100 and 1:500 over atrazine concentration. The result was assessed by comparing the concentration of atrazine in each solution. The percent relative error is acceptable at lower than 5%.

**Table 4.4** Effect of pesticides on atrazine adsorption of NPC-PBZ-m column

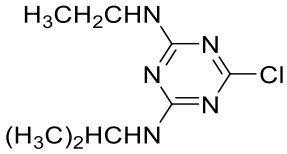
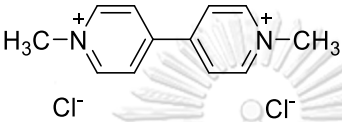
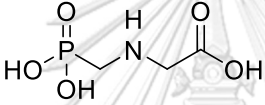
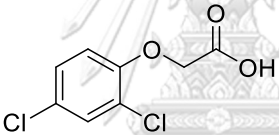
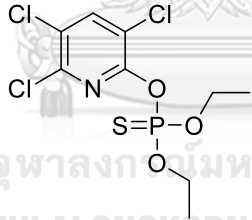
Pesticides	Concentration Ratio Pesticides x/atrazine (conc. of the pesticides, $\mu\text{g/mL}$ )	Concentration Of atrazine ( $\mu\text{g/mL}$ ) $\pm$ standard deviation <sup>a</sup>	%relative error
Atrazine	-	0.546 $\pm$ 0.008	-
Paraquat	500 (7.5)	0.566 $\pm$ 0.027	3.61
Glyphosate	500 (7.5)	0.542 $\pm$ 0.015	-0.75
2,4-D	100 (1.5)	0.572 $\pm$ 0.030	4.75
Chlorpyrifos	100 (1.5)	0.564 $\pm$ 0.022	3.26

<sup>a</sup> The peak area of atrazine (15  $\mu\text{g/L}$ ) after pre-concentration step calculated by using an external calibration curve:  $y = 114.84x + 0.4293$ .

As the percent relative error was set at 5% as the maximum allowance value, our results indicated that paraquat and glyphosate can coexist at the higher concentration level comparing to 2,4-D and chlorpyrifos (**Table 4.4**). These can be explained by the structure of NPC-PBZ-m material as shown in **Figure 4.4C**. The NPC-PBZ-m sorbent has graphitic C-C ( $\text{sp}^2$ ) and nitrogen substituted aromatic rings as pyridine-N and pyridone-N structures. These characteristics possess a better affinity for non-polar compounds via  $\pi$ - $\pi$  stacking and Van der Waals force [29,82]. Therefore, the compound which has aromatic structure similar to atrazine, 2,4-D and chlorpyrifos, can be adsorbed by NPC-PBZ-m sorbent. Moreover, these compounds exhibit the hydrophobic properties indicating by  $\log P_{ow}$ , while glyphosate and paraquat are hydrophilic. For this reason, the weaker interactions between these herbicides with NPC-PBZ-m might be formed. The structure and  $\log P_{ow}$  value of these compounds was shown in **Table 4.5**.

It can imply that the developed NPC-PBZ-m pre-concentration unit can be applied for atrazine determination in real water samples.

**Table 4.5** The structure and log Pow of other pesticides

Pesticides	Structure	Log Pow	Ref.
Atrazine	 <chem>CCNc1nc(Cl)n(CN)c1</chem>	2.61	[103]
Paraquat	 <chem>C[N+]1=CC=CC=C1C2=CC=CC=C2[N+]3=CC=CC=C3C</chem>	-4.50	[104]
Glyphosate	 <chem>OC(=O)CNCP(=O)(O)O</chem>	-3.22	[105]
2,4-D	 <chem>CC(=O)Oc1cc(Cl)cc(Cl)c1</chem>	2.80	[104]
Chlorpyrifos	 <chem>CCOP(=S)(OCC)Oc1nc(Cl)c(Cl)c(Cl)n1</chem>	4.7-5.3	[106]

#### 4.6 Optimization parameters affecting on atrazine-colorimetric detection

After atrazine was pre-concentrated by NPC-PBZ-m sorbent, the elution fraction was also determined by UV-Vis. The colorimetric method is developed based on Konig's reaction from previous work [39]. The reaction is divided into three steps which are quaternary pyridinium halide (step 1), glutaconic dialdehyde (step 2), and polymethine dye compound (step 3) formations, respectively. Therefore, many reagents that are used in every step are required to investigate for suitable conditions. In this section, to clarify the results, the study of an optimized parameter is separated followed by the step of reaction from step 1 to 3.

#### 4.6.1 Investigation of pyridine and conc. HCl volume (step 1)

The previous work reported that the suitable condition of the step 1 reaction has to be in a sufficiently acid medium [85]. In acid conditions, the proton from HCl can protonate the nitrogen substituted position at benzene ring of atrazine and pi-electron can be delocalized. Meanwhile, the lone pair of nitrogen in pyridine will attach on the carbon atom next to chlorine atom which induces the chlorine atom cleavage as  $\text{Cl}^-$  ion. The proposed reaction regarding the nucleophilic aromatic substitution was shown in **Figure 4.14**. This mechanism is also reported in previous works [107,108].

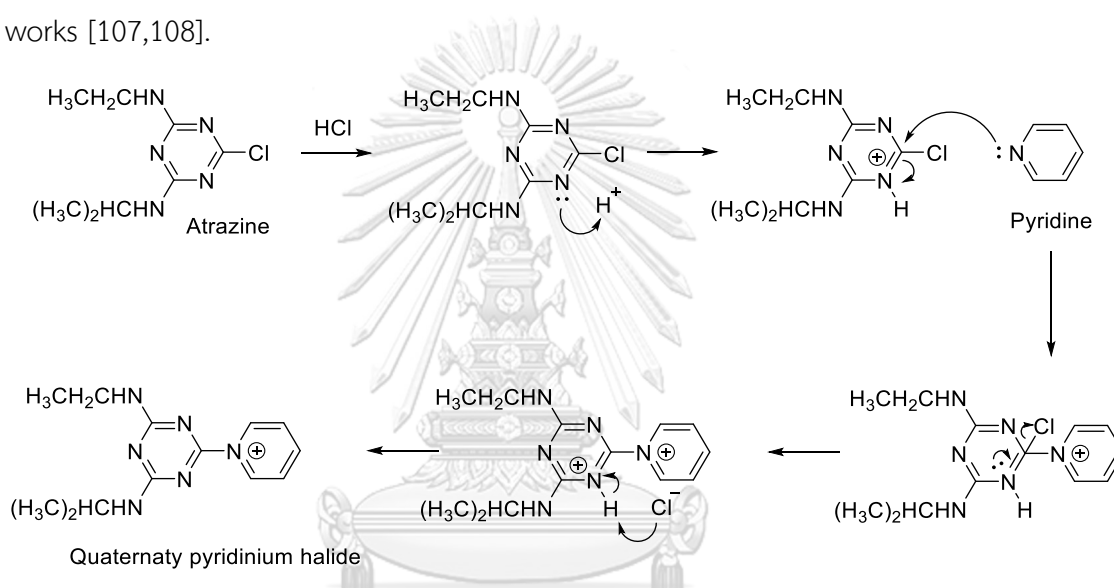


**Figure 4.14** The proposed reaction mechanism of König's reaction (step 1).

Unfortunately, the quaternary pyridinium halide compound is colorless. Therefore, the volume of pyridine and conc. HCl were investigated by measuring the absorbance signal of polymethine dye compound (step3) at 487 nm. To create a dye product, the experiment was adapted from previous work [39] that used 0.1 mL of 10 (% v/v) aniline.

##### 4.6.1.1 Effect of pyridine volume

To avoid the dilution effect, neat pyridine was used. A 0.5 mL of atrazine solution, 1 and 5  $\mu\text{g}/\text{mL}$ , was separately tested with a varied volume of pyridine from 0.2-0.5 mL. From our result in **Figure 4.15A** demonstrated that at 1  $\mu\text{g}/\text{mL}$  of atrazine test, an equal absorbance intensity was obtained although the amount of pyridine



increased. In case of 5  $\mu\text{g}/\text{mL}$  of atrazine study, the intensity of absorbance decreased when pyridine volume increased to 0.5 mL. It may be caused by the increase in the viscosity of the mixture solution restricting the rate of reaction. Therefore, the suitable pyridine volume was 0.2 mL.

#### 4.6.1.2 Effect of conc. HCl volume

The volume of conc. HCl varied from 0-0.15 mL while the volume of pyridine was fixed at 0.2 mL. **Figure 4.15B** demonstrated that the highest absorbance was obtained when the volume of conc. HCl was 0.1 mL. Therefore, 0.2 and 0.1 mL of pyridine and conc. HCl were used for further studies.

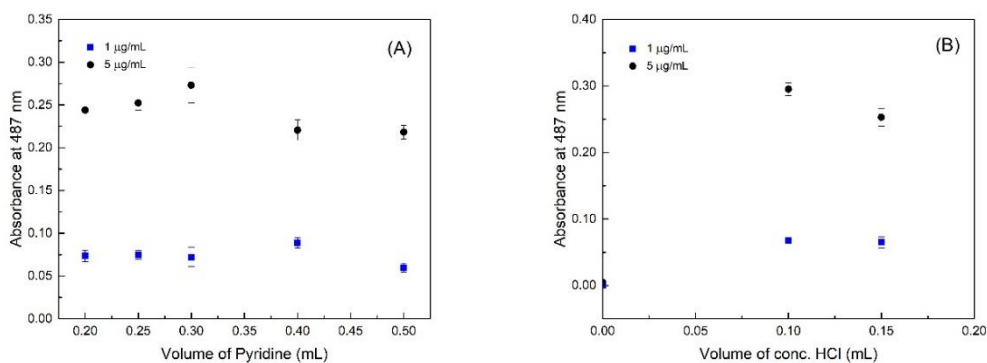


**Figure 4.15** Effect of pyridine volume (A) and conc. HCl volume (B) in step 1.

#### 4.6.2 Effect of temperature, heating time, and sodium hydroxide (NaOH) concentration (step 2)

Based on the orange-red polymethine compound are occurred via the coupling reaction of glutaconic dialdehyde and *p*-Anisidine. Therefore, many parameters such as temperature, heating time, and NaOH concentration that can affect the glutaconic dialdehyde formation (step 2) were investigated. The suitable variable is pursued by measuring the absorbance signal of glutaconic dialdehyde at 437 nm using UV-Visible spectrophotometer [109]. A 0.5 mL of atrazine solution, 1 and 5  $\mu\text{g}/\text{mL}$ , was added with 0.2 mL of pyridine and 0.15 mL of conc. HCl. The solution was adopted for investigation in this section.

#### 4.6.2.1 Effect of reaction temperature

In previous work, the effect of temperature on glutaconic dialdehyde was reported [36]. Therefore, the temperature was studied ranging from 35 to 70 °C. From our result, the maximum intensity of glutaconic dialdehyde was obtained when the temperature was only 40 °C while the previous work requires a boiling condition to generate a glutaconic dialdehyde product [36,38,39,85]. Therefore, the reaction temperature was chosen at 40 °C. The result was shown in **Figure 4.16A**.

#### 4.6.2.2 Effect of heating time

The suitable time for heating reaction was also studied. The result indicated that the highest signal of glutaconic dialdehyde product received when heating time increased to 20 min. After that, the same level of signal was obtained when increasing the heating time from 20 to 60 min as shown in **Figure 4.16B**. So, the suitable heating time was 20 min.

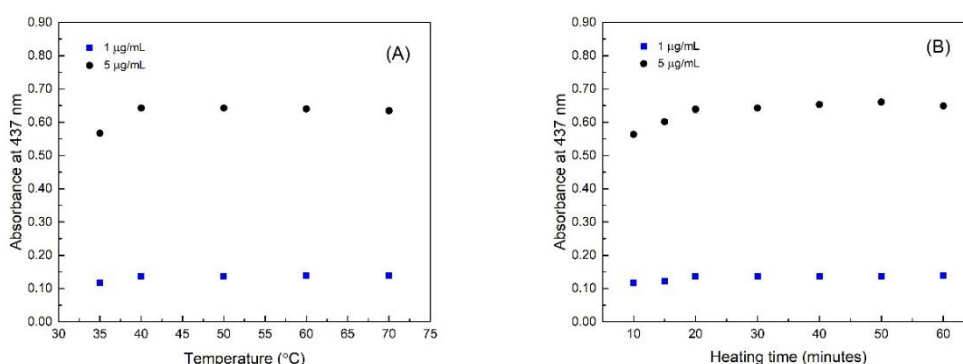


**Figure 4.16** Effect of reaction temperature (A) and heating time (B).

#### 4.6.2.3 Effect of NaOH concentration

After a quaternary pyridinium halide was obtained, this compound further reacts with NaOH to create carbinol base and glutaconic dialdehyde as described in **Figure 3.4**. Therefore, the NaOH concentration was investigated varying from 2 – 8 M while the volume was fixed at 0.5 mL. The result in **Figure 4.17** showed that the absorbance increases with concentration of NaOH. It means that more

glutaconic aldehyde was obtained. Unfortunately, the precipitation occurred at the next step when using the concentration of NaOH over 5 M.

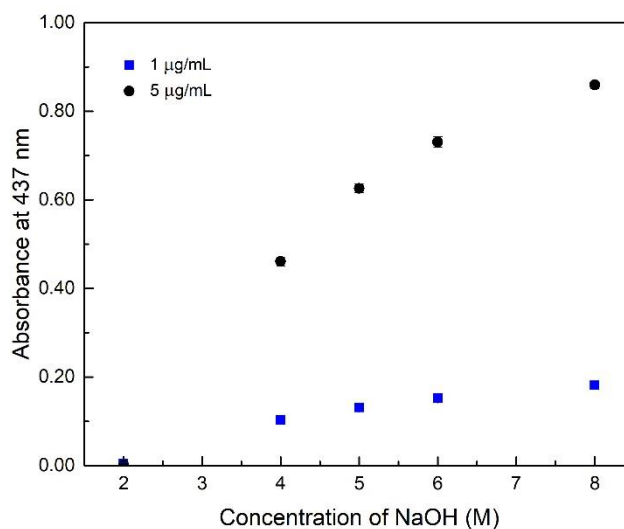


**Figure 4.17** Effect of NaOH concentration.

From our results, the optimized temperature and heating time were 40 °C and 20 min while the suitable concentration of NaOH was 5 M. Moreover, the proposed reaction mechanism in step 2 was shown in **Figure 4.18**. As the carbon atom beside  $N^+$  position in a quaternary pyridinium halide structure was attacked with hydroxide ion ( $OH^-$ ) from NaOH. Then, the carbinol base was formed. Due to highly amount of  $OH^-$  in reaction, the carbinol base reacts with another  $OH^-$  to cleave the aromatic ring until the glutaconic dialdehyde was obtained.

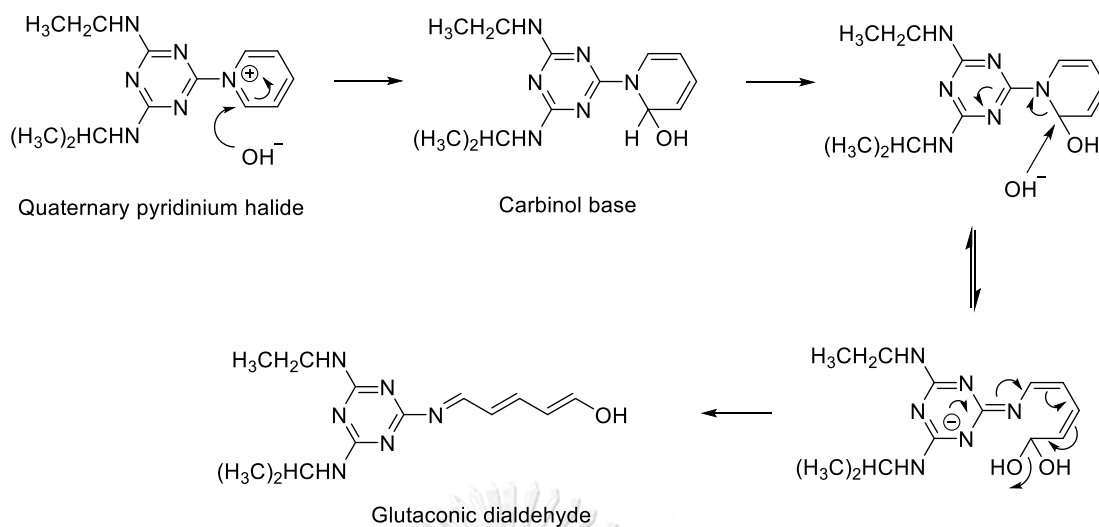


**Figure 4.18** The proposed reaction mechanism of König's reaction (step 2).

#### 4.6.3 Preliminary study of various coupling reagents

Due to the glutamic dialdehyde compound being unstable, the coupling steps are required. Many reagents were used to create the stable polymethine dye compound. Polymethine compounds can absorb light in visible regions from 400 - 800 nm depending on their structures. Many coupling reagents have been applied for coupling reactions with atrazine in the König's reaction final step. The coupling agent such as aniline, sulfanilic acid and 4-aminophenol were tested in this section. Moreover, the coupling reaction was performed under acidic medium which was reported in previous studies [36,40]. Therefore, conc. HCl was chosen as pH adjusting solvent. The suitable concentration of reagents and volume of conc. HCl (step 3) were investigated using atrazine concentration levels of 1 and 5  $\mu\text{g}/\text{mL}$  after glutamic dialdehyde formation under optimized condition. The maximum wavelength for aniline, sulfanilic acid, and 4-aminophenol were 487, 460, and 467 nm, respectively. Moreover, the response of a color changing with atrazine concentration in each reagent was also considered.

##### 4.6.3.1 Aniline

The suitable volume of conc. HCl was studied at atrazine 1  $\mu\text{g}/\text{mL}$ . 0.255-0.80 mL of conc. HCl volume was studied with aniline concentration fixed at 10 (%v/v). While the obtained volume of conc. HCl was chosen to study the aniline

concentration. From our results in **Figure 4.19A** showed that the signal was increased when the volume of conc. HCl increased to 0.3 mL and no more significant intensity was obtained when using higher volume of acid. Therefore, 0.3 mL of conc. HCl was chosen. Then, aniline concentration was also optimized. The suitable of aniline concentration was selected at 8 (% w/v) as shown in **Figure 4.19B**.

#### 4.6.3.2 Sulfanilic acid

The volume of conc. HCl varied from 0.2-0.5 mL when sulfanilic concentration was fixed at 0.3 (% w/v). While, the concentration of sulfanilic acid was investigated under the suitable volume of conc. HCl. The results showed in **Figure 4.19C and D** which 0.35 mL of conc. HCl and 0.5 mL of 0.6 (% w/v) sulfanilic acid were reported as the optimum conditions.

#### 4.6.3.3 4-aminophenol

A varied conc. HCl from 0.15-0.4 mL was tested with concentration of 4-aminophenol was fixed at 0.2 mL of 0.7 (% w/v). The result indicated that the absorbance intensity increased when increasing a volume of conc. HCl to 0.2 mL after that the signal was dropped as shown in **Figure 4.19E**. Therefore, 0.2 mL of conc. HCl was used to estimate the suitable concentration 4-aminophenol. The result shown in **Figure 4.19F**, 0.5 (% w/v) of 4-aminophenol 0.2 mL was chosen for the suitable value.

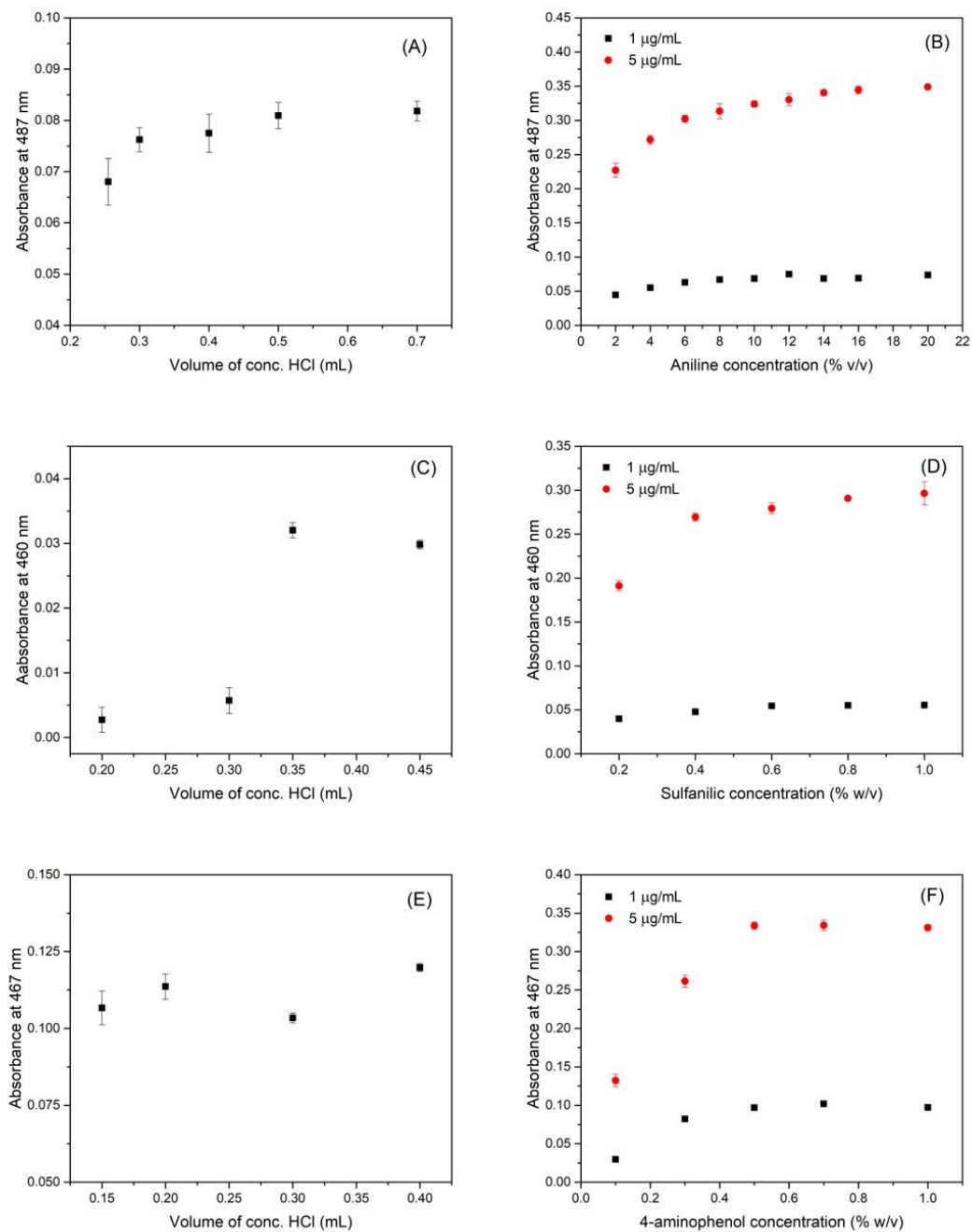


**Figure 4.19** The study of volume of conc. HCl for aniline (A), concentration of aniline (B), volume of conc. HCl for sulfanilic acid (C), concentration of sulfanilic acid (D), volume of conc. HCl for 4-aminophenol (E), concentration of 4-aminophenol (F).

However, the polymethine dye compounds obtained from these coupling reagents do not show very distinct and intense color. Moreover, they show

the similar maximum wavelength between 460-487 nm. The UV-Vis spectra of polymethine compounds were shown in **Figure 4.20A**, when 5  $\mu\text{g/mL}$  of atrazine was used. Moreover, the color of polymethine compound of each coupling agent were also illustrated in **Figure 4.20B**. The yellow solution was obtained even though the difference of coupling reagents were used. However, the changes in yellow color intensity are quite difficult to distinguish by naked-eye.

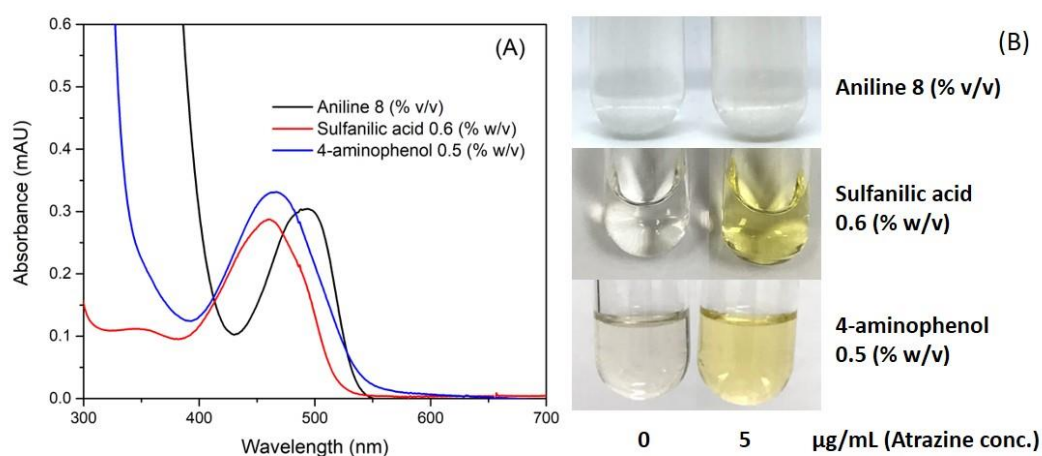


**Figure 4.20** UV-Vis spectra (A) and solution color of polymethine compounds coupling with aniline, sulfanilic acid, and 4-aminophenol (B).

In this study, the color of polymethine compound was expected to provide a longer maximum wavelength. Therefore, the coupling reagents should have electron donating groups on the structure which electron delocalized can occur. A new coupling reagent, *p*-Anisidine, was selected because their structure has methoxy groups that are an electron donor. Moreover, this reagent can be dissolved in MeOH which is used as eluent in the pre-concentration step.

#### 4.6.4 Optimization of *p*-Anisidine as the coupling reagent (step 3)

In this work, *p*-Anisidine was chosen because it has many advantages such as easy to find, low cost, and can be dissolved in MeOH which is a solvent system of colorimetric method. At this step, the glutamic dialdehyde was coupled with *p*-

Anisidine under the suitable pH of solutions. The proposed mechanism of this step was shown in **Figure 4.21**.

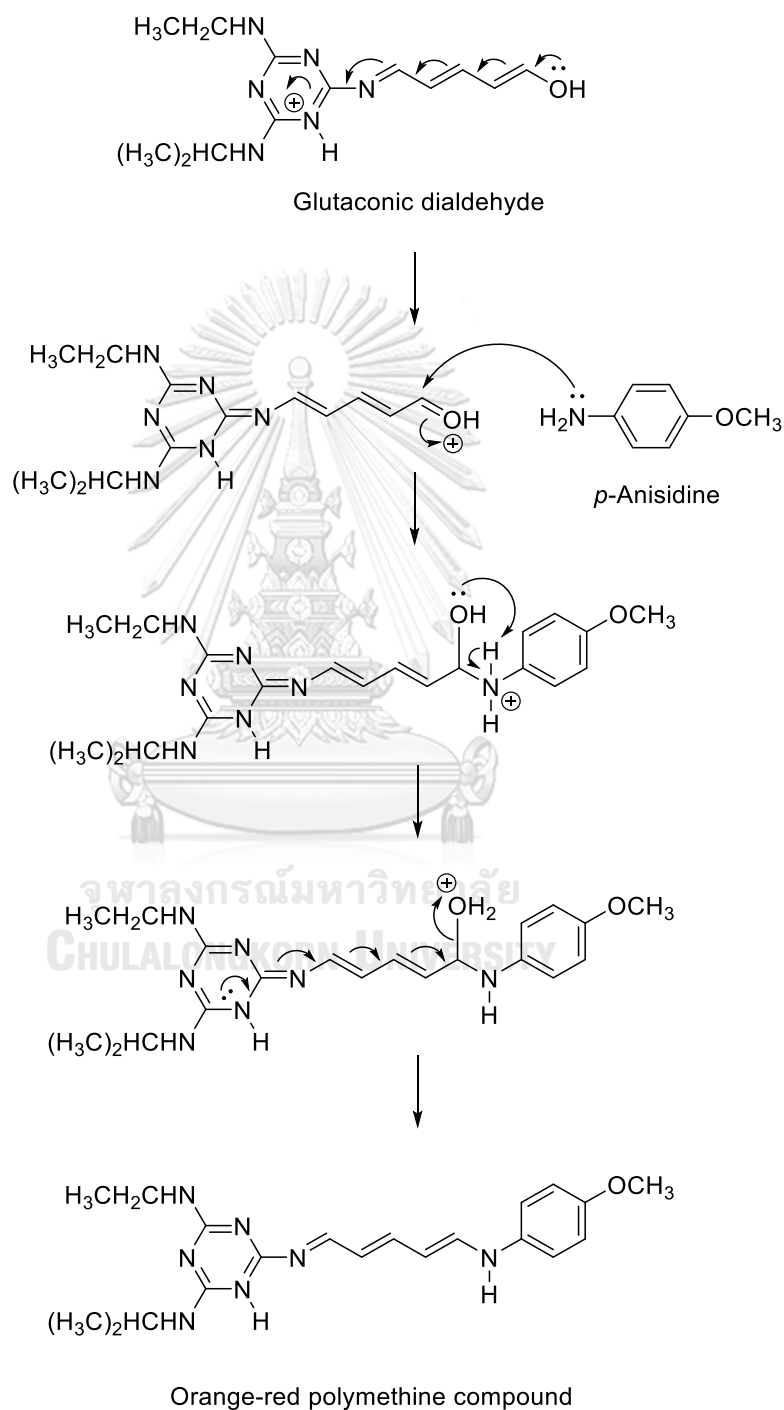


**Figure 4.21** The proposed reaction mechanism of Konig's reaction (step 3).



#### 4.6.4.1 Volume of conc. HCl for coupling step

Before the coupling step, the pH of glutaconic dialdehyde had to be adjusted. To eliminate the effect of dilution, the volume of reagent needs to be minimized. The 0.125, 0.15 and 0.2 mL of conc. HCl were used in this study. It can be clearly seen that the highest amount of polymethine compound produced when 0.15 mL of conc. HCl was used. However, the decrease in the dye production was observed especially when 5  $\mu\text{g}/\text{mL}$  of atrazine was used (**Figure 4.22A**). It may be because the pH of the reaction ( $\text{pH} = 4.99$ ) is below the  $\text{pK}_a$  of *p*-Anisidine ( $\text{pK}_a = 5.29$ ) resulting in that the N atom of *p*-Anisidine was protonated [110]. So, the *p*-Anisidine could not couple with glutaconic dialdehyde compound causing less amount of polymethine compound.

#### 4.6.4.2 Effect of *p*-Anisidine concentration

Due to the amount of coupling reagent affecting the color intensity of the polymethine compound, the suitable *p*-Anisidine concentration had to be investigated. The level of concentration was varied from 2-15 (% w/v). In **Figure 4.22B**, the result demonstrated that when the concentration of coupling reagent increased, the increase in the color intensity of the product was clearly seen especially at 5  $\mu\text{g}/\text{mL}$  of atrazine. On the other hand, there is no significant impact on the final product formation for 1  $\mu\text{g}/\text{mL}$  of atrazine. However, the excess amount of *p*-Anisidine interfered with the color of reagent blank showing pale-yellow color. Therefore, 6 (% w/v) of *p*-Anisidine was chosen and it is adequate for complete color development.

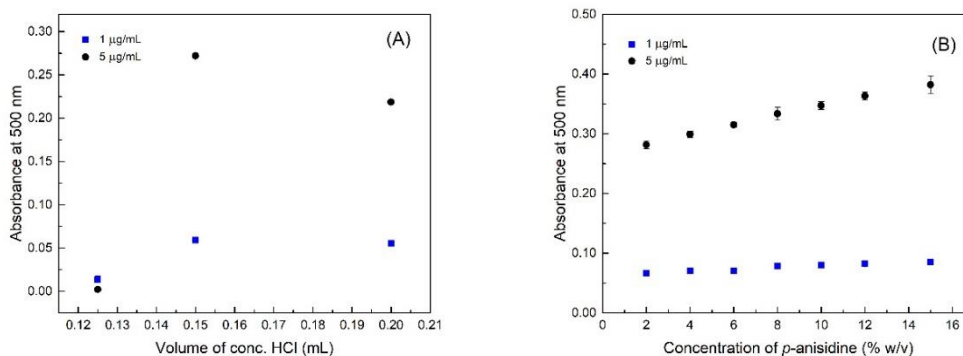


**Figure 4.22** Effect of conc. HCl volume (A) and p-Anisidine concentration (B) on orange-red polymethine compound formation.

#### 4.6.4.3 Effect of reaction time on orange-red polymethine compound formation

To access the proper reaction time for the stable color development of orange-red polymethine compounds, the reaction time varied from 1-60 minutes. After 0.25 mL of 6% (w/v) of p-Anisidine was added to the solution. The color development was pursued by measuring the absorbance at 500 nm with UV-Visible spectrophotometer. From **Figure 4.23**, the result indicated that the absorbance intensity ranges from 1 to 20 minutes increased rather rapidly. After that, the signal slowly increases after 20 minutes onwards for all of atrazine concentration (0.5-2 µg/mL). Therefore, the reaction time at 20 min was chosen in this work.

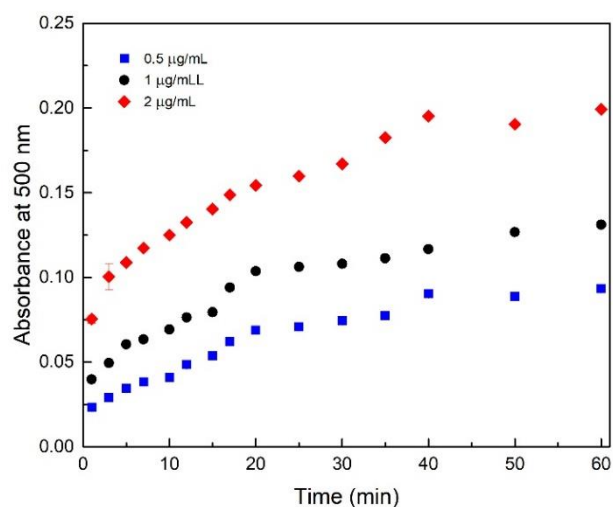


**Figure 4.23** Effect of reaction time on orange-red polymethine compound formation.

From our results, the optimum conditions of colorimetric method of atrazine are listed in **Table 4.6**.

**Table 4.6** The optimum conditions of colorimetric method based on Konig's reaction

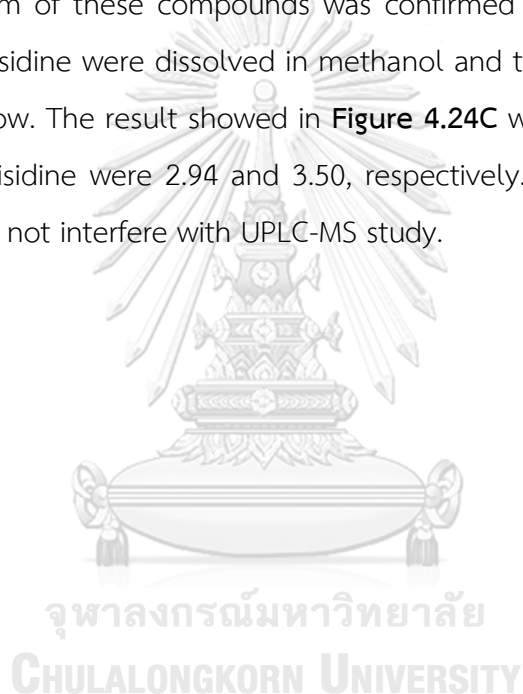
Parameters	Optimum values
Volume of pyridine	0.2 mL
Volume of conc. HCl <sup>a</sup>	0.1 mL
Temperature	40 °C
Heating time	20 mins
NaOH concentration	5 M, 0.5 mL
Volume of conc.HCl <sup>b</sup>	0.15 mL
<i>p</i> -Anisidine	6 (% w/v), 0.25 mL
Reaction time	20 mins

<sup>a</sup> The volume of conc. HCl for quaternary pyridinium halide formation (step 1)

<sup>b</sup> The volume of conc. HCl for coupling reaction (step 3)

#### 4.6.5 Characterization of an orange-red polymethine compound

To confirm the reaction occurred, 5, 25, and 50  $\mu\text{g/mL}$  of atrazine standard solution and reaction were injected to HPLC-UV. From our result in **Figure 4.24A and B** showed retention time of an orange red methane compound (8.23 min) has lower than atrazine compound (6.00 min). It may cause the polymethine compound to be easier protonated by acid in the mobile phase than atrazine which has  $pK_a$  around 1.7 [42]. Therefore, atrazine compounds are more retained by the C18 column than polymethine compounds which have positive charge on their structure. Moreover, the peak chromatogram of these compounds was confirmed by the UV spectrum. The pyridine and *p*-Anisidine were dissolved in methanol and the log  $P_{ow}$  value of these compounds was low. The result showed in **Figure 4.24C** which the retention time of pyridine and *p*-Anisidine were 2.94 and 3.50, respectively. This can ensure that the peak reagent does not interfere with UPLC-MS study.



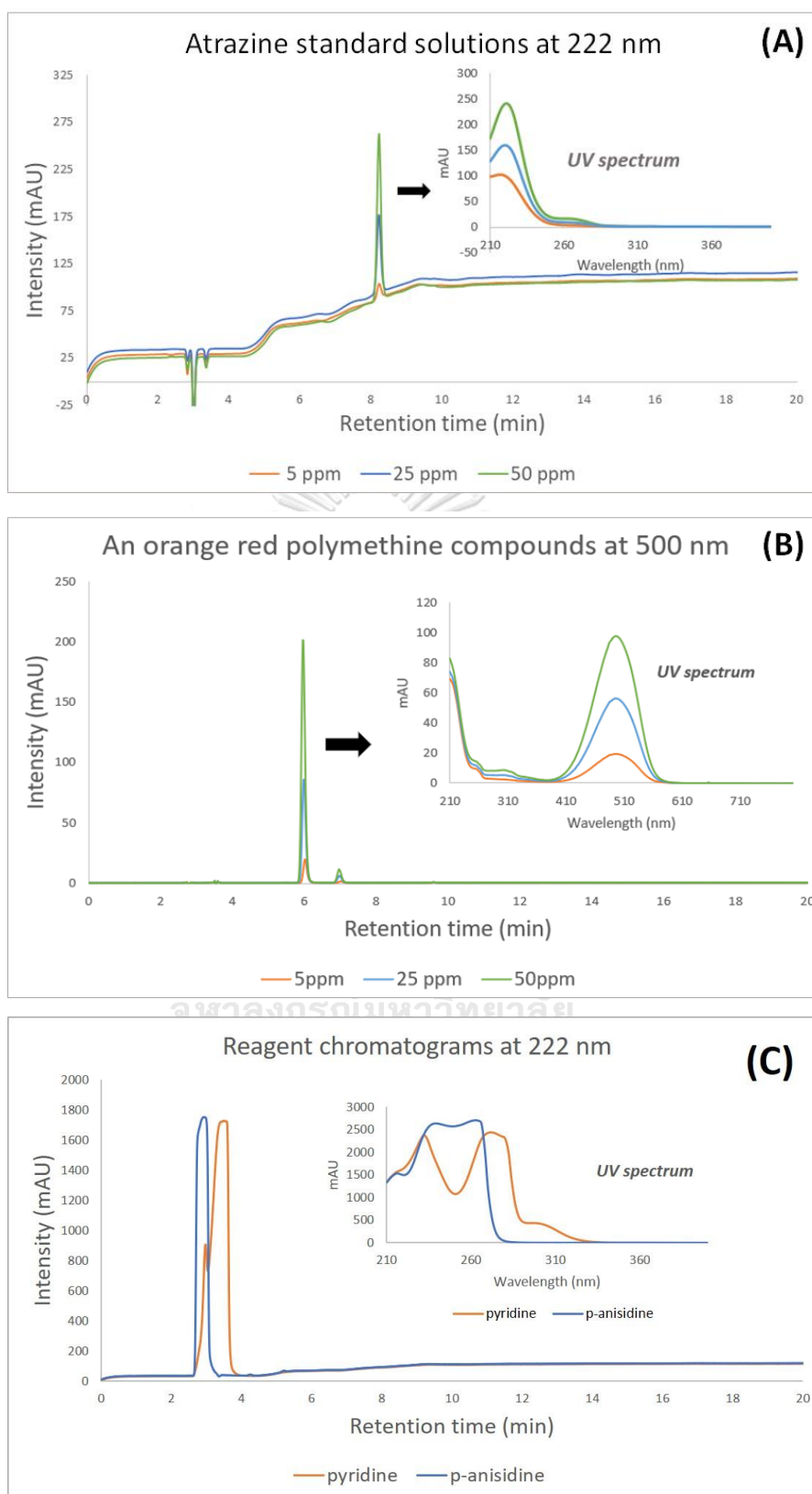


**Figure 4.24** The peak chromatograms of atrazine standard solution (A), orange-red polymethine compound (B), and pyridine and p-Anisidine reagents (C).

The weight of an orange red polymethine compound (**Figure.4.21**) was calculated as 381.23. Due to UPLC-MS performed in electrospray ionization which the structure was protonated with proton ( $H^+$ ). The total ion chromatogram (TIC) and extracted ion chromatogram of atrazine (EIC) were evaluated. The results in **Figure 4.25A** showed that atrazine has a retention time at 11.27 min. Because UPLC-MS and HPLC-UV use the same column and similar conditions, it can predict the retention time of a polymethine compound via the result from HPLC-UV determination. Therefore, the retention time of polymethine dye should be less than 11.27 min. One ( $M+H^+$ ) and two hydrogen atoms ( $M+2H^+$ ) protonation were investigated. However, no peak appeared at this condition unless the EIC chromatogram illustrated a peak at 7.91 and 9.13 minutes of three protons protonated on a polymethine structure. The mass per charge ratio was 128.08 ( $M+3H^+$ ). The peak order of UPLC-MS and HPLC-UV was similar as shown in **Figure 4.25B**. This result showed the same peak order agreed with HPLC-UV. Therefore, a possibility of an orange-red polymethine compound was being shown in **Figure 4.21**.

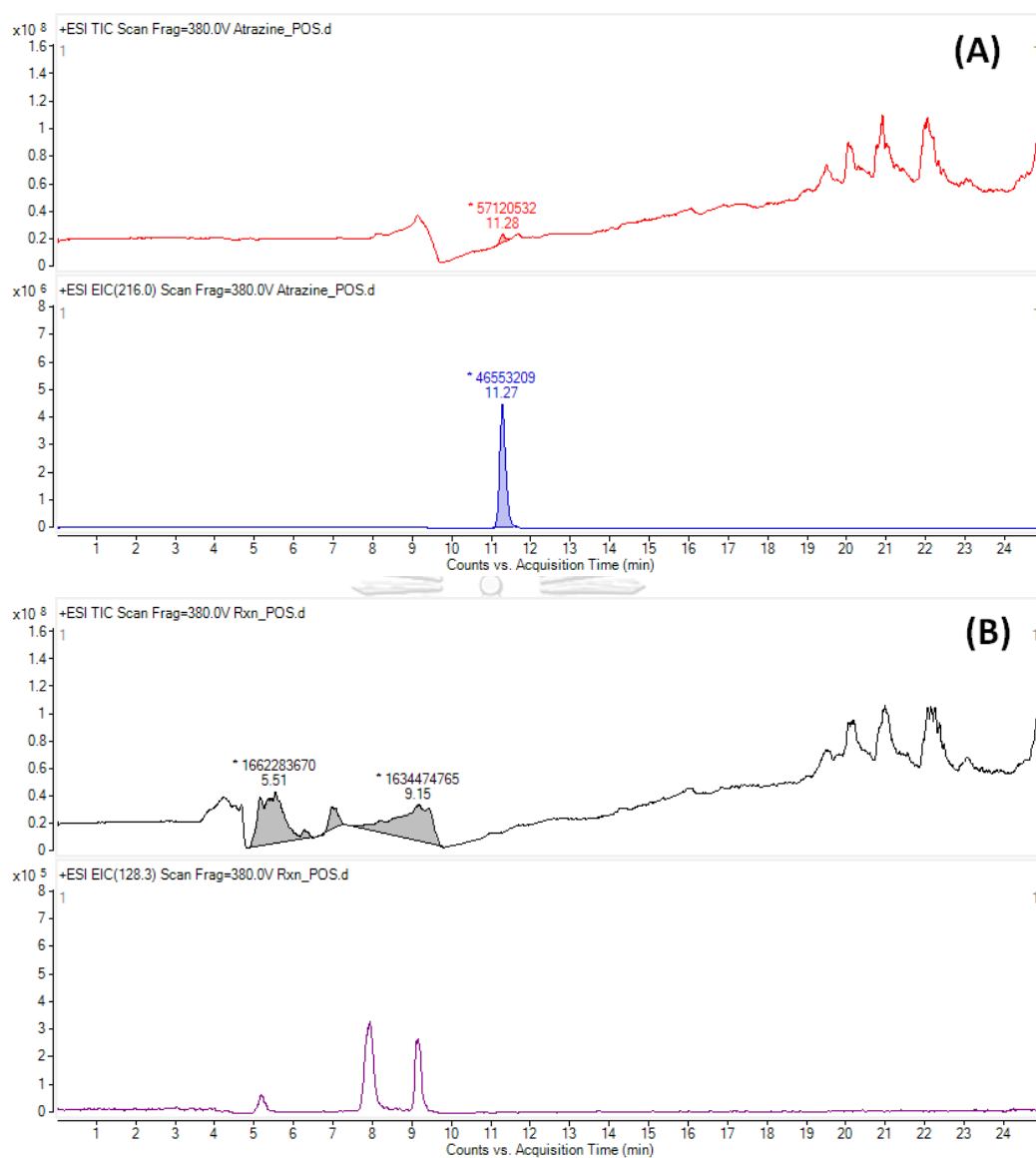


Figure 4.25 TIC and EIC of Atrazine (A) and orange-red polymethine compound (B).

#### 4.6.6 The analytical performance of atrazine via the Konig's reaction using *p*-Anisidine as coupling reagent

The analytical performance of the proposed colorimetric method was investigated including matrix effect, linearity, limit of detection, and limit of quantitation.

The validity of the colorimetric method had to be assessed. The optimum condition of colorimetric method (Table 4.6) were used to test a method performance for atrazine analysis. A 0.5 mL of atrazine standard solutions (0.1 – 5  $\mu\text{g/mL}$ ) in

methanol solvent was prepared as described in **section 3.5.2.2**. These solutions were used to evaluate the validity of the proposed method. The response of the polymethine dye compound was measured by UV-Vis.

#### 4.6.6.1 Matrix effect

The effect of NPC-PBZ-m matrix on colorimetric analysis was also estimated by comparing the slope of external calibration curves which were prepared in MeOH and MeOH-NPC-PBZ-m solvents. The absorbance intensity of orange-red polymethine compounds at 500 nm was plotted with atrazine concentration range from 0-5  $\mu\text{g/mL}$ . The results indicated that a slope ratio in MeOH and MeOH-NPC-PBZ-m solvent systems was in range of 0.8-1.2 and its closeness was confirmed by paired t-test. From the data in **Table 4.7**, it can imply that an external calibration curve can be used for quantitative determination using methanol (MeOH) as a solvent which the matrix from NPC-PBZ-m sorbent has no effect on UV-Vis method detection.

**Table 4.7** Matrix effect of NPC-PBZ-m sorbent on calibration curve of colorimetric method

Solvent systems	Linear equation <sup>a</sup>	R <sup>2</sup>	Slope ratios (matrix/solvent)	Paired t-Test <sup>b</sup>
MeOH	$y = 0.0531x + 0.0007$	0.9982	-	-
MeOH-NPC-PBZ-m	$y = 0.0545x - 0.0020$	0.9968	1.03	0.033

<sup>a</sup> The concentration of atrazine standard solutions ranges from 0-5  $\mu\text{g/mL}$

<sup>b</sup> The comparison of calibration curve in MeOH and MeOH-NPC-PBZ-m using t-stat at 95% of confident level = 2.365

#### 4.6.6.2 Dynamic range, Instrument detection limit (IDL), limit of quantitation (LOQ) for UV-Vis measurement

The calibration curve was plotted from 0 to 1  $\mu\text{g/mL}$  atrazine against the signal of orange-red polymethine compound. The IDL and LOQ were calculated using standard deviation of linear regression line and slope of the external calibration



curve preparing in methanol solvent. The IDL and LOQ were 0.044 and 0.144  $\mu\text{g/mL}$ , respectively.

From our result in **section 4.6.6.1**, the dynamic range in the proposed method was reported from 0.5-5  $\mu\text{g/mL}$  which linear regression equation and a correlation coefficient ( $R^2$ ) were  $y = 0.0538x - 0.0020$  and 0.9977, respectively. From our result, the linear equation and color chart for atrazine detection could also be observed by naked eye as shown in **Figure 4.26**.

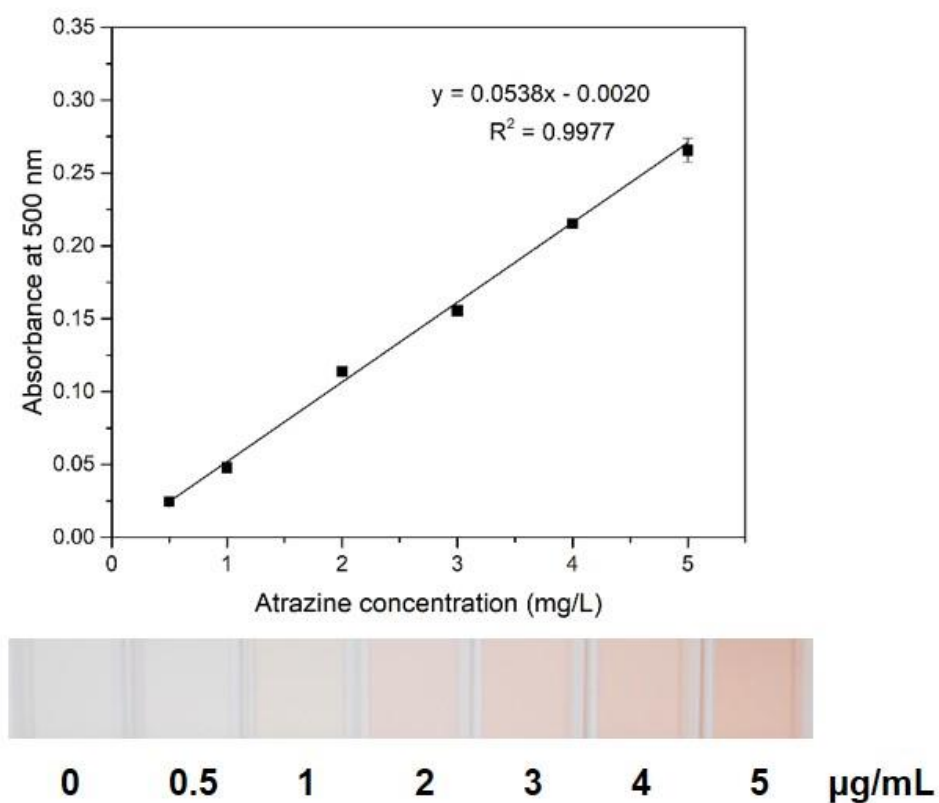


**Figure 4.26** The linear relationship between atrazine concentration and the absorbance intensity of polymethine compound at 500 nm and the color chart for atrazine determination.

#### 4.6.6.3 Effect of other pesticides on UV-Vis method (Konig's reaction)

From our results in **section 4.5.2**, it can be concluded that other pesticides do not interfere with the adsorption of atrazine on NPC-PBZ-m sorbent. However, the presence of other herbicides affecting colorimetric measurement should be evaluated. Because the elution fraction will be measured by this proposed method, the concentration of atrazine was fixed at 1  $\mu\text{g/mL}$  as it is the expected concentration level after the pre-concentration step. The solution preparation was described in **section 3.5.5.2**. The absorbance of the orange-red polymethine compound was measured by UV-Visible spectrophotometer at 500 nm. The result was assessed by comparing the concentration of atrazine (A) and others (AP, AG, AD, and AC). The percent relative error is acceptable at lower than 5%.

**Table 4.8** Effect of other pesticides on UV-Vis method determination based on Konig's reaction

Pesticide standard solution <sup>a</sup>	Concentration ratio of X/A level ( $\mu\text{g/mL}$ )	Concentration ( $\mu\text{g/mL}$ ) $\pm$ standard deviation <sup>b</sup>	%relative error
A	-	0.9514 $\pm$ 0.0257	-
AP	10	1.0448 $\pm$ 0.0130	9.8
AG	50	0.9478 $\pm$ 0.0421	-0.38
AD	100	0.9932 $\pm$ 0.0427	4.39
AC	100	0.9244 $\pm$ 0.0429	-2.84

<sup>a</sup> Atrazine, paraquat, glyphosate, and 2,4-D chlorpyrifos were denoted as A, P, G, D, and C

<sup>b</sup> AX is the mixture of atrazine with the other pesticides (X)

The results in **Table 4.8** showed that 2,4-D, and chlorpyrifos could interfere less comparing to glyphosate and paraquat. The color of orange-red

polymethine dyes obtained from AD and AC samples delivered the same color intensity as the atrazine solution for all studied ratios (**Figure 4.27**). In the case of AD, even though the paraquat concentration was downed to 10  $\mu\text{g/mL}$ , a %relative error is still high.

Therefore, it can be concluded that even if the concentration of 2,4-D, and chlorpyrifos are higher than atrazine up to 100 times, the colorimetric detection was not interfered. While the concentration of paraquat needs to be lower than atrazine concentration for more than 10 times.

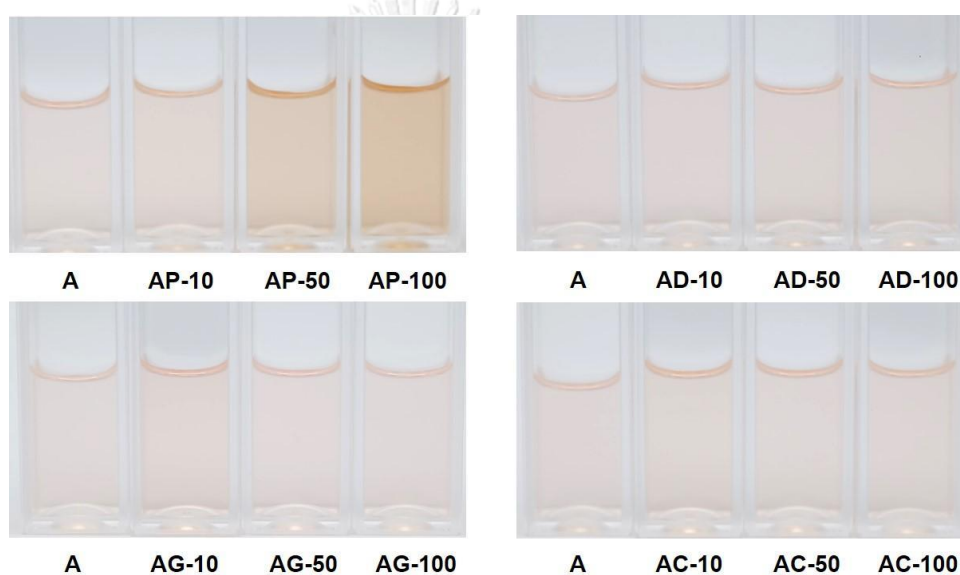


**Figure 4.27** Effect of other pesticides on the color of polymethine compound development: atrazine (A); paraquat (P); glyphosate (G); 2,4-D (D); chlorpyrifos (C). AX is the mixture of atrazine with the other pesticides (X). The absorbance of orange-red polymethine compound performed at 1  $\mu\text{g/mL}$  of atrazine.

#### 4.7 Quantitative analysis

In this work, the colorimetric method will be validated against the HPLC-UV analysis method. The validation of the developed method was evaluated under the optimum extraction and detection conditions. Linear working range, correlation coefficients, method detection limit (MDL), limit of quantitation (MDQ), matrix effect, accuracy and precision were estimated. An agricultural water sample (Lopburi province, Thailand) spiked with atrazine concentration from 5-30  $\mu\text{g/L}$  were performed with

optimum conditions for both HPLC and Konig's reaction (N=3). The method limit of detection (MDL) and method quantitation limit (MQL) were estimated as follows:

$$\text{MDL} = \frac{3\text{SD}}{\text{Slope}} \dots\dots\dots(4.1)$$

$$\text{MQL} = 3.3 * \text{MDL} \dots\dots\dots(4.2)$$

Slope : the slope of calibration

SD : the standard deviation of linear regression line

The obtained calibration curves were linear over the range of 5–30 µg/L with the satisfactory correlation coefficient ( $R^2 \geq 0.99$ ) with the method detection limits below 3 µg/L for both analysis methods as shown in **Table 4.9**.

**Table 4.9** Analytical performance of the HPLC-UV and UV-Vis

Analysis methods	Calibration curve	R <sup>2</sup>	Working range	MDL (µg/L) / MQL (µg/L)
HPLC-UV	y = 4.0357x - 0.8049	0.9988	5 – 30 µg/L	1.05 / 3.45
UV-Vis	y = 0.0016x + 0.001	0.9979	10 – 30 µg/L	2.26 / 7.46

CHULALONGKORN UNIVERSITY

The accuracy and precision of the developed method was performed under optimum conditions by spiking in an agricultural water sample collected from Lopburi province, Thailand with atrazine at the concentration level of 5, 10, 15 and 20 µg/L (n = 3). From **Table 4.10**, the accuracy and precision for both HPLC-UV and UV-Vis were acceptable based on AOAC implying that the developed methods have good sensitivity and reproducibility for the analysis of atrazine.

**Table 4.10** Mean recoveries of atrazine for both HPLC-UV and UV-Vis

Analysis method	Recovery percentage, (%RSD)			
	5 µg/L	10 µg/L	15 µg/L	20 µg/L
HPLC-UV	105 (8.1)	101 (3.8)	99 (6.2)	98 (6.7)
UV-Vis	< MQL	107 (14.7)	100 (1.0)	101 (4.7)

#### 4.7.1 Interferences in the performance of the developed method

The result in **Table 4.11** indicated the glyphosate provided the highest limit of concentration ratio at 500 times (7.5 ppm) while chlorpyrifos and 2,4-D gave the limit at 100 times (1.5 ppm) over atrazine concentration. Unfortunately, the color of the orange-red polymethine compound was interfered when the initial concentration of paraquat in water sample was 1.5 µg/mL. From the result, it could be concluded that paraquat will be co-elute with methanol. The observed color was shown in **Figure 4.28**.

**Table 4.11** Effect of other pesticides on atrazine determination

Pesticides	Concentration Ratio Pesticides x/atrazine (conc. of the pesticides, $\mu\text{g/mL}$ )	Concentration Of atrazine ( $\mu\text{g/mL}$ ) $\pm$ standard deviation <sup>a</sup>	%relative error
Atrazine (A)	-	$0.801 \pm 0.078$	-
Glyphosate (AG)	500 (7.5)	$0.789 \pm 0.089$	-1.50
Chlorpyrifos (AC)	100 (1.5)	$0.794 \pm 0.108$	-1.01
2,4-D (AD)	100 (1.5)	$0.778 \pm 0.150$	-2.88
Paraquat (AP)	<100 (1.5)	$0.946 \pm 0.228$	18.1

<sup>a</sup> The concentration of orange-red dye compound after the pre-concentration step of  $15 \mu\text{g/L}$  atrazine

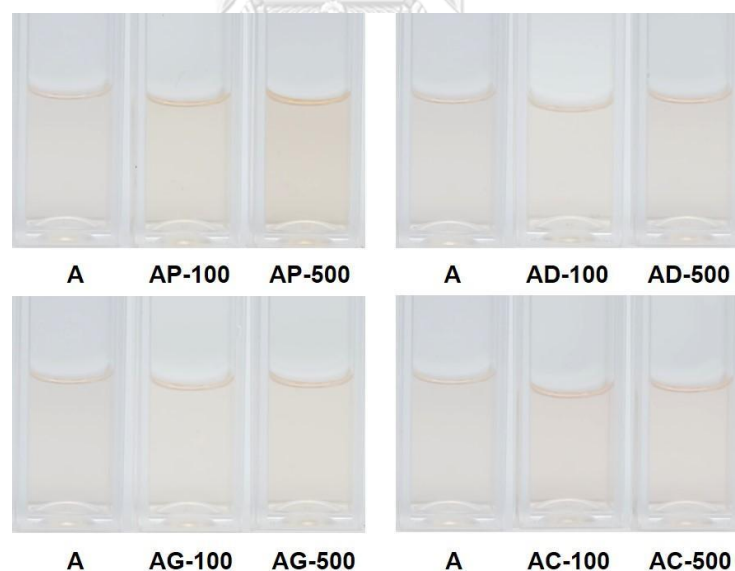


**Figure 4.28** Effect of other pesticides on the colorimetric analysis. Atrazine (A); paraquat (P); glyphosate (G); 2,4-D (D); chlorpyrifos (C). AX is the mixture of atrazine with the other pesticides (X).

#### 4.7.2 Matrix-match calibration curves on HPLC-UV measurement

As addressed before, the matrix could have an impact on the developed methods. Therefore, the matrix-matched calibration curves were constructed using both HPLC-UV and colorimetric methods for atrazine determination. Three different sources of water samples were assessed by using matrix-matched calibration curves. A 0-30 µg/L of atrazine was spiked in three water samples which are agricultural waters (Lopburi and Ratchaburi province) and pond water (Bangkok). After the pre-concentration step, the linear curves of all water samples were plotted and the slopes were evaluated. **Table 4.12** showed a slope ratio of other samples to Lopburi water sample was in an acceptable range (0.8-1.2). Therefore, a pre-concentration method combined with HPLC-UV determination can be applied for detection of atrazine in agricultural water samples without effect from matrix substance.

**Table 4.12** Matrix-matched calibration curve of water samples on HPLC-UV determination

Water samples	Linear equation <sup>a</sup>	R <sup>2</sup>	MDL/MQL (µg/L)	Slope ratios
Lopburi agricultural	$y = 4.0080x - 0.2322$	0.9992	1.05/3.45	-
Nakhon Pathom agricultural	$y = 3.6174x + 7.423$	0.9984	1.43/4.73	0.90
Pond	$y = 4.8125x + 3.8406$	0.9963	2.22/7.33	1.20

<sup>a</sup> The concentration of spiked atrazine standard solutions ranges from 0-30 µg/L

For colorimetric analysis, three matrix-matched calibration curves were also constructed. The slope of linear relationship obtained from pond water and Ratchaburi agricultural water were compared with Lopburi water samples. **From Table 4.12**, the atrazine analysis should not suffer from the different sample matrix collected from the

different agricultural areas. However, the result has demonstrated that the developed colorimetric method could not be used to determine the atrazine content in surface water samples from Pond. This can be explained by the matrix of samples that can interfere with the process of atrazine adsorption on NPC-PBZ-m sorbent. In other words, the water sample with lower matrix substance (Pond water) can give a better atrazine extraction efficiency. Therefore, the higher amount of atrazine in the elution fraction was obtained and led to provide a higher sensitivity for colorimetric detection.

**Table 4.13** Matrix-matched calibration curves of water samples on UV-Vis determination

Water samples	Linear equation <sup>a</sup>	R <sup>2</sup>	MDL/MQL (µg/L)	Slope ratios
Lopburi agricultural	$y = 0.0015x + 0.0034$	0.9961	2.26/7.46	-
Nakhon Pathom agricultural	$y = 0.0016x + 0.0051$	0.9938	2.87/9.48	1.07
Pond	$y = 0.0021x + 0.0036$	0.9988	1.27/4.20	1.40

<sup>a</sup> The concentration of spiked atrazine standard solutions ranges from 0 – 30 µg/L

#### 4.8 Application to environmental water samples for atrazine determination

Under the optimum condition for pre-concentration and colorimetric method were investigated, the proposed method was applied to analyze the atrazine in real water samples. The accuracy and precision of method was also reported in this section.

Three environmental water samples, surface waters collected from a rice field in Nakhon Pathom Province, a fish farm in Saraburi and a Pond were collected and filtered with CA membrane to remove the suspended organic matters. After that, the atrazine standard solution was spiked into the water samples. The developed methods were performed under the optimum conditions (n = 3) as detailed in **Table 4.2 and 4.6.**



From **Table 4.14**, the HPLC-UV method was successfully applied for atrazine analysis in water samples with the satisfactory recoveries (98-126%) with the RSD below 6.3%. Therefore, the NPC-PBZ-m column analyzed with HPLC analysis at 222 nm could be used to analyze atrazine in various surface water samples from agricultural and aquaculture areas and a pond with a good accuracy and precision.

However, the colorimetric analysis method has its own limitations. The sample matrix has an impact on the performance of the UV-Vis method. From **Table 4.14**, it can be concluded that the proposed method can be used to determine atrazine concentrations in surface water samples collected from agricultural and aquaculture areas.

**Table 4.14** The recovery and precision in water samples determined by proposed methods

Water samples	Spiked level (µg/L)	HPLC-UV <sup>a</sup>			UV-Vis <sup>b</sup>			T-test <sup>c</sup>
		Found (µg/L)	%Recovery	%RSD	Found (µg/L)	%Recovery	%RSD	
Nakhon	0	< MQL	-	-	< MQL	-	-	-
Pathom agricultural	10.0	11.5	115	6.3	13.7	137	7.5	-2.503
	20.0	19.6	98	3.3	22.3	104	5.6	-2.413
Fish farm	0	< MQL	-	-	< MQL	-	-	-
	8.00	8.58	107	5.0	< MQL	-	-	-
	25.0	25.9	104	3.6	26.1	105	5.0	0.577
Pond	0	N.D.	-	-	N.D.	-	-	-
	10.0	12.4	124	1.0	14.7	147	5.4	-4.364
	20.0	25.2	126	2.0	28.1	140	1.8	- 12.751

<sup>a</sup> Concentration was calculated by Lopburi agricultural water's equation  $y = 4.0357x - 0.8049$

<sup>b</sup> Concentration was calculated by Lopburi agricultural water's equation  $y = 0.0016x + 0.0010$

<sup>c</sup> Comparison of concentration in HPLC-UV and UV-Vis method using t-stat at 95% of confident level = 4.302

Moreover, the performances of both methods applying for water samples from agricultural and fish farm areas were compared using a paired t-test. Upon a paired t-test, the differences in these two proposed analysis methods were not found for agricultural and fish farm water samples. Therefore, the low-cost colorimetric analysis method to determine trace-level of atrazine in agricultural water was developed in this study.



For paraquat determination, the adsorbent for paraquat determination was designed to provide a good adsorption with low back pressure. Since the paraquat has positive charge on their structure, the composition of adsorbent should have a negative charge presence on their surface. Three chemical substances which are sodium alginate, humic acid, and silica gel were reported to adsorb paraquat via electrostatic interaction. Therefore, the enlarged Si-HA-Alg material design was prepared and performed the batch-adsorption preliminary test before switching to use in column flow unit.

#### 4.9 The preparation of silica-humic acid entrapped calcium alginate hydrogel (Si-HA-Alg)

To form a solid gel bead, sodium alginate can be crosslinked with a common agent as calcium chloride ( $\text{CaCl}_2$ ). In this work, the proposed method was designed to apply this material for batch adsorption of paraquat. The Si-HA-Alg beads were prepared by using agar mold 0.8 (% w/v) containing 0.8 M of  $\text{CaCl}_2$  solution. The adsorption performance was assessed by comparing the absorbance signal between paraquat standard and filtrate as described in **section 3.10.2** that the filtrate reacted with glucose and NaOH reagent to form a paraquat blue free radical as shown in **Figure 2.14**. The absorbance intensity was measured at 600 nm using UV-Vis.

##### 4.9.1 Effect of the percentage of silica particles and humic acid sodium salt (HA)

To investigate the suitable Si-HA-Alg beads component, the amount of alginate content was fixed at 2 (% w/v) while the content of either silica or humic acid varied from 0-2 (% w/v). The sorbent preparation was described in **section 3.10.2.1**. The weights of the prepared bead varied between 0.0300-0.0900 g depending on the composition. From **Figure 4.29**, our results showed that when the sorbent contains either silica or humic acid, the percentage of adsorption is lower than the sorbent that contains both of components. Moreover, the lowest of percentage adsorption was obtained when the adsorbent contains only alginate composition. The Si1%-HA1%-Alg and Si1%-HA2%-Alg sorbents provided the similar adsorption performance. However,

the higher content of humic acid can enhance the leaching effect from humic acid content. Therefore, the suitable composition of Si-HA-Alg bead was 1 (% w/v) for both silica and humic acid salt contents.

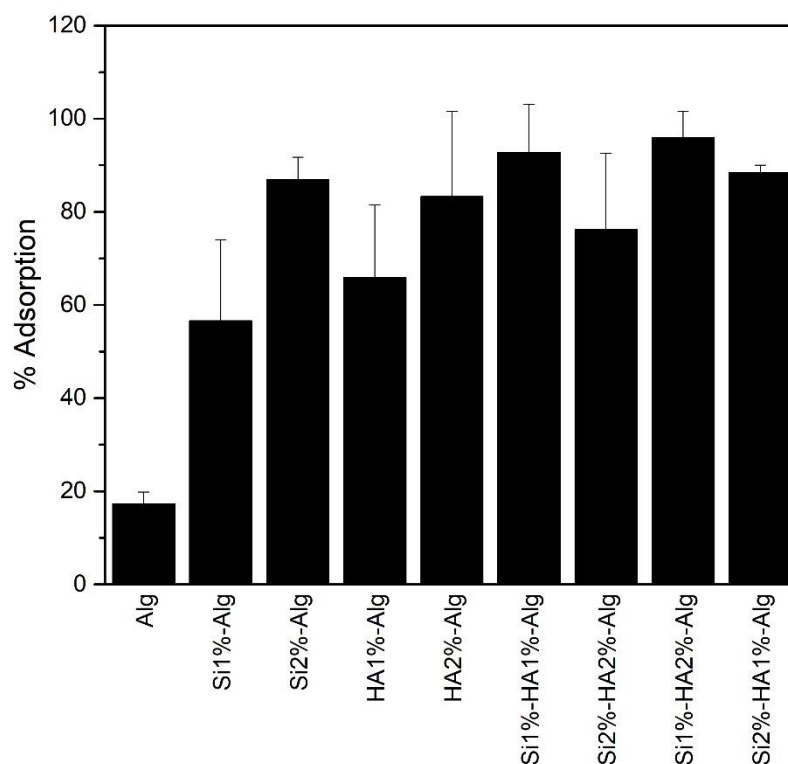


**Figure 4.29** The different amount of silica (Si) (0-2 % w/v) and humic acid (HA) (0-2 % w/v) contained in alginate bead (Alg) affecting paraquat adsorption efficiency. The concentration of alginate (Alg) was fixed at 2 (% w/v).

#### 4.9.2 Percentage of alginate study

Due to the leaching effect of humic acid from previous results, the concentration of alginate should be investigated. In this section, the content of silica and humic acid were fixed at 1 (% w/v) while the concentrations of alginate varied from 1-4 (% w/v) were studied. After Si-HA-Alg beads preparation, the adsorption step was performed. The filtrate solution was collected when the paraquat solution was adsorbed for 1 hour. The volume of mixture solution of silica, humic acid, and alginate was fixed at 1 mL for one piece of sorbent bead preparation. Therefore, the weights of a Si-HA-Alg bead varied between 0.0300-0.0500 g depending on the composition.

The adsorption percentage was indicated in **Figure 4.30A**. The decrease of adsorption performance was obtained when increasing alginate contents from 1-4 (% w/v). This can be implied that the higher content of alginate composition could make it more difficult for paraquat penetration into alginate beads. Therefore, the decrease in the adsorption performance was obtained. Moreover, the leaching effect of humic acid was also evaluated by monitoring the absorbance at 300 nm [111]. The Si-HA-Alg beads with varied content of alginate were soaked in DI water for 1 and 12 hours. The result showed in **Figure 4.30B**, when the amount of alginate increased, the signal of the leaching humic acid decreased. This phenomenon can be assumed that the amount of alginate affects the leaching of humic acid from in Si-HA-Alg beads.

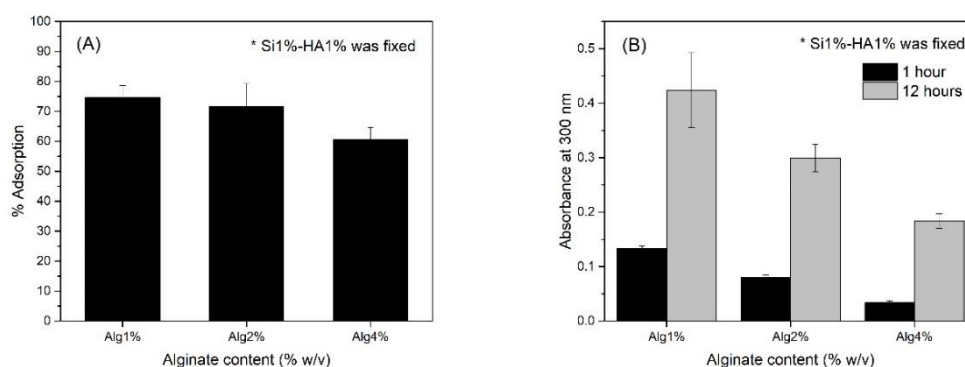


**Figure 4.30** Alginate content affecting on paraquat adsorption (A) and humic acid leaching (B).

From our results, it can be concluded that Si-HA-Alg materials have some limitations which can affect the adsorption performance. The varying of Si-HA-Alg weight leads to the proposed method having poor repeatability. Moreover, the leaching effect from humic acid causes the material cannot be reused and this phenomenon may interfere with the colorimetric detection in further steps.

Based on our finding in the atrazine adsorption, paraquat can be adsorbed on NPC-PBZ as well. It might be because the structure of NPC-PBZ-m contains a lot of aromatic compounds which could be expected to interact with paraquat via  $\pi$ - $\pi$  or Van der Waals interactions. Based on XPS spectrum (**Figure 4.4**) showed the characteristic

of binding oxide-N and C=O energy at 403.5 eV and 289.3 eV, respectively. These structures could interact towards a positive charge of the paraquat molecule. Therefore, the possibility of paraquat adsorption on NPC-PBZ-m material was tested by performing the batch adsorption experiment. To enhance the paraquat adsorption via coulombic interactions, the activation step is required to generate negative charges on the surface.

Due to paraquat having positive charge on their structure, the activation step of NPC-PBZ-m should be required. In 2017, Safitri *et al.* [112] studied the effect of KOH activating agents on a rice-husk based carbon sorbent for chromium (Cr) metal adsorption. The step of KOH activation was performed by only contacting the sorbent to varied concentrations of KOH at ambient temperature for 1.5 hours. Then, washing the material until constant pH was obtained followed by dried in an oven for 1 hour at 105 °C before usage. Therefore, only the step of immersing NPC-PBZ-m into KOH solution at room temperature was tested to estimate the performance of NPC-PBZ-m for paraquat adsorption.

Meanwhile, Nuilerd *et al.* [113] reported that the increase in the specific surface area and -OH functional groups on the carbon surface were observed from using KOH as activating agent.

#### 4.10 The effect of KOH activation, DI washing step after activation and agitation direction on paraquat adsorption on NPC-PBZ-m

To compare the paraquat adsorption efficiency in each condition, the detail of the designed experiment was described in **section 3.11.1**. The suitable adsorption step based on three parameters which are activation step, DI-washing step requirement after KOH activation, and agitation direction on adsorption were pursued by measuring the filtrate solutions with UV-Vis at 257 nm. After that, the adsorption percentage of each condition was calculated as described in **section 3.10.2.1**.

Our result in **Figure 4.31** showed that the KOH activation step provides a higher percentage of adsorption for both of agitation directions (rotating and x-y) which are represented in red lines (a1 and a2), though the washing step was applied. It might be explained that the hydroxide ion can activate the NPC-PBZ-m surface and enhance the adsorption of paraquat via coulombic interactions or dipole-dipole interactions. Furthermore, the effect of DI-washing step shown in the green line (b1 and b2) demonstrated that the DI washing step can remove the hydroxide groups from the surface causing a lower adsorption efficiency. From this information, it can be concluded that NPC-PBZ-m should be activated with KOH solution without DI-washing step requirement before the paraquat adsorption was performed.

To study the agitation direction on adsorption, the blue line (c) indicated the rotating adsorption gave a higher adsorption efficiency than the adsorption done in x-y direction. It may be caused by the probability of paraquat contact with NPC-PBZ-m sorbent could be enhanced when the rotating adsorption was performed. Therefore, the A-NW-R pathway, which means the KOH activation without step of DI washing and rotating adsorption, is the optimum condition for paraquat adsorption method.



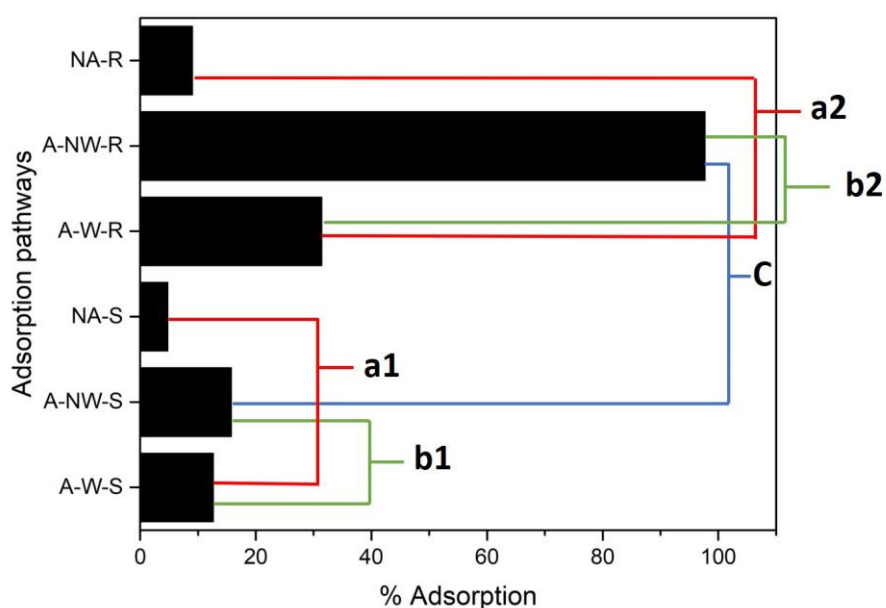


**Figure 4.31** The effects of three factors on the paraquat adsorption efficiency investigation. (A): activation, (W): washing step, (S) shaking adsorption (x-y direction), and (R) rotating adsorption, (NA): no activation, and (NW): no washing step.

#### 4.11 The stability of paraquat in KOH activation

To ensure the decrease of absorbance intensity in filtrate occurring from paraquat adsorption phenomena, 2  $\mu\text{g}/\text{mL}$  of paraquat was prepared in 1 M KOH solution. Then, the prepared solution was tested with blue free radical reaction when time passed for 1, 2, and 24 hours. The paraquat blue free radical intensities are relatively constant over 2 hours. This indicates that the decrease in the paraquat content in the filtrate was caused by the adsorption.

#### 4.12 The study of desorption solvent for paraquat determination

The interaction between NPC-PBZ-m sorbent and paraquat was might have occurred via electrostatic interaction or  $\pi$ - $\pi$  stacking. Many types of desorption solvent such as sodium chloride (NaCl), calcium chloride ( $\text{CaCl}_2$ ) solution and ammonium



chloride ( $\text{NH}_4\text{Cl}$ ) were tested. However, no signal of paraquat in the solvent was obtained.

In 2010, Zhou *et al* [114] applied the mixture solvent between HCl 1 M and methanol at volume ratio was 70:30 for desorption paraquat and diquat after the pre-concentration using  $\text{N}_2$  doped  $\text{TiO}_2$  nanotubes as solid sorbent. Therefore, these mixture solvents were adopted to test the performance for paraquat desorption.

Two desorption solvents, 0.1-1 M of hydrochloric solution and the mixture solution of HCl-MeOH (70:30) solutions were studied by measuring the absorbance at 257 nm. The result showed that the mixture solvent of HCl-MeOH (70:30) gave higher desorption efficiency than hydrochloric solution alone as can be seen from **Figure 4.32**. It can be implied that the interaction of paraquat adsorption may not only occur via electrostatic interaction but also  $\pi$ - $\pi$  interaction. Therefore, the mixture solution of 1 M HCl-MeOH (70:30, % v/v) was used as a desorption solvent.

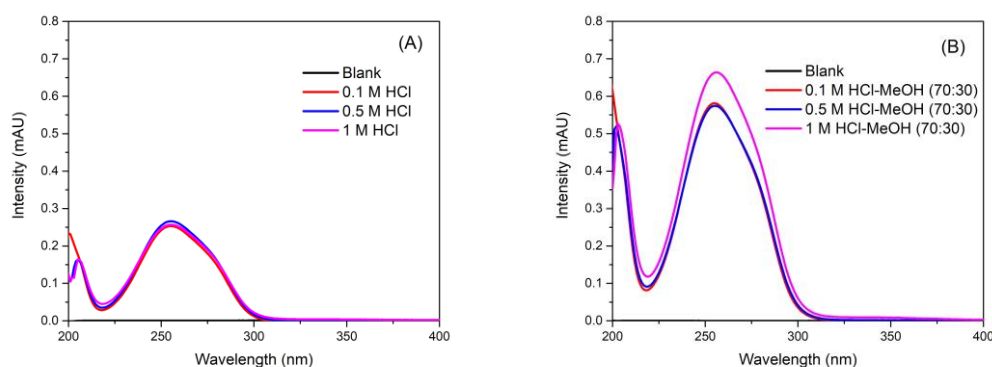


**Figure 4.32** Effect of HCl solution (A) and mixture of HCl-MeOH at ratio 70:30 (B) on paraquat desorption.

#### 4.13 The optimization of paraquat blue free radical reaction for colorimetric method

The previous result demonstrated that the 70:30 (% v/v) of 1 M HCl:MeOH was suitable to desorb paraquat. Therefore, the paraquat blue free radical needs to be developed in this media solvent. Due to the color reaction occurring in the alkaline

medium [73], the affecting parameters including reducing agent and concentration of NaOH were also optimized.

#### 4.13.1 The concentration and volume of glucose study

In this work, glucose was used as a reducing agent for paraquat reduction. A concentration and volume of glucose varied from 0.1-3 M and 50-300  $\mu\text{L}$  were tested, respectively. **Figure 4.33A and B** indicated that 150  $\mu\text{L}$  of 1 M glucose solutions was an optimum volume which was chosen for further studies.

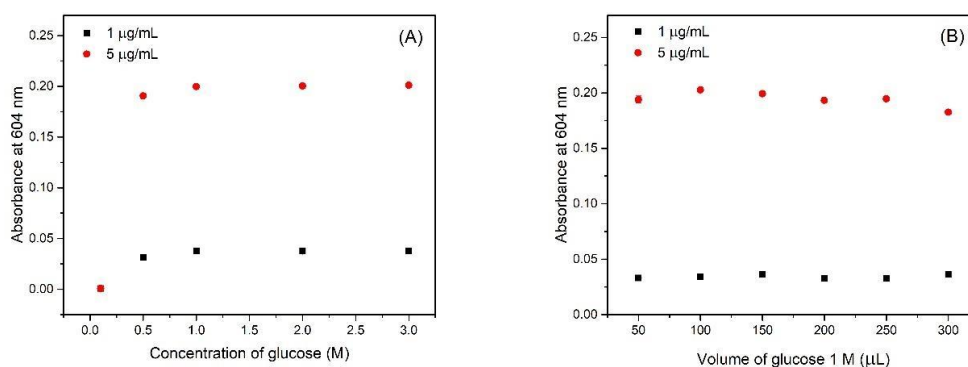


**Figure 4.33** Glucose concentration (A) and volume of glucose 1 M (B) on paraquat blue free radical reaction.

#### 4.13.2 The concentration and volume of NaOH study

A 1.5 mL of 1 and 5  $\mu\text{g/mL}$  paraquat solutions performed the reaction by using a suitable condition for glucose as described in **section 4.13.1**. From our studies, the results in **Figure 4.34A and B** indicated that 250  $\mu\text{L}$  of 5 M sodium hydroxide was an optimized condition for paraquat blue free radical reaction.

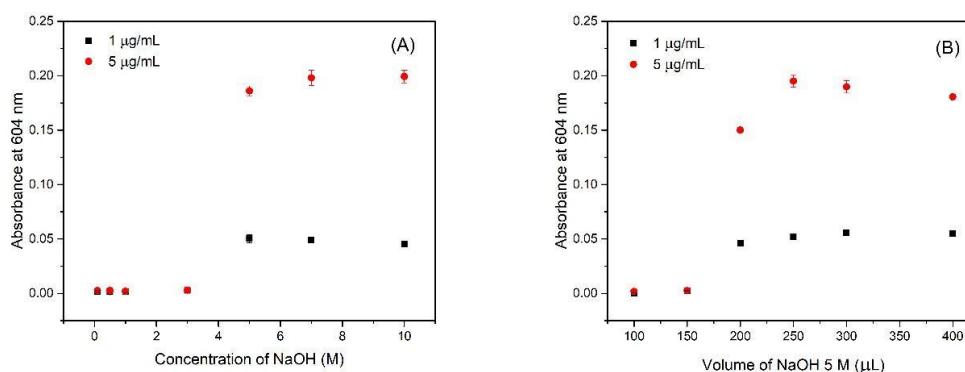


**Figure 4.34** NaOH concentration (A) and volume of NaOH 5 M (B) on paraquat blue free radical reaction.

#### 4.13.3 The suitable of reaction time

The reaction times of the developed analysis method were studied. To let the color of reaction be developed completely, 0.5, 1, and 3 µg/mL of paraquat solution were performed in the reaction under an optimized condition as described in **section 4.13.1 and 4.13.2**. The reaction times were varied from 0-30 minutes. The results showed that a stable of blue free radical absorbance intensity was obtained within 5 minutes as shown in **Figure 4.35**. Moreover, the reaction can occur without any heating temperature applied.

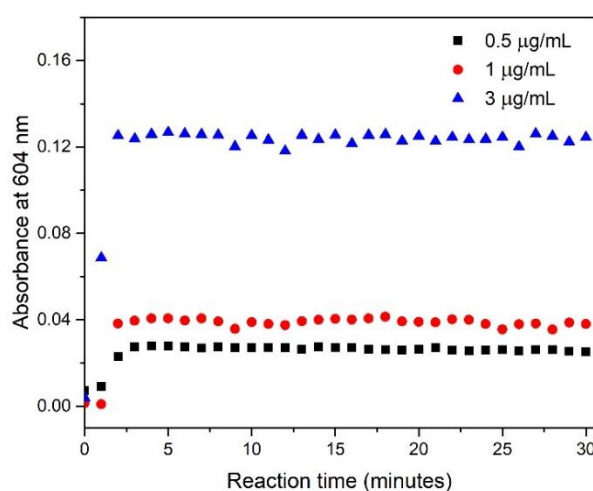


**Figure 4.35** The effect of reaction time on paraquat blue free radical determination.

#### 4.13.4 Instrument detection limit (IDL) and limit of quantitation (LOQ) for paraquat blue free radical reaction

The calibration curve was plotted from 0-5 µg/mL of paraquat solution against the signal of paraquat blue free radical. The IDL and LOQ were investigated by measuring signals of reagent blank which performed the reaction under optimum conditions. The obtained IDL and LOQ values from UV-Vis measurement at 604 nm were 0.098 and 0.495 µg/mL, respectively. The working range of paraquat quantitation was reported to be 0.5-5 µg/mL which linear equation and correlation coefficient ( $R^2$ ) were  $y = 0.0378x + 0.0117$  and 0.9979, respectively.

#### 4.14 Optimization conditions for paraquat-NPC-PBZ-m batch adsorption

The proposed method was developed for paraquat detection via paraquat blue free radical reaction. Therefore, various parameters including KOH concentration for activation step, ratio of NPC-PBZ-c weight and KOH volume, and 1 M HCl-MeOH (70:30) volume which can affect both of paraquat adsorption and desorption steps were also investigated. The paraquat content in the desorbing solvent solution was performed by the paraquat blue free radical reaction under the optimum condition and measured by UV-Vis at 604 nm.

##### 4.14.1 Effect of KOH concentration on activation step

In this study, the NPC-PBZ-c was activated with the various concentrations of KOH ranging from 0.1-1 M for 1 hour before adding 50 mL of 2 µg/mL paraquat solution for adsorption. The desorption step was performed by using a vortex with 2 mL of 1M HCl: MeOH (70:30). The suitable concentration of KOH was investigated by measuring the paraquat concentration after the desorption step. The concentration of paraquat was calculated using an external calibration curve as shown in **section 4.13.4**. The result showed that the adsorbed paraquat increased with the concentration of NaOH up to 0.3 M. However, the intensity of paraquat blue free radical when KOH concentration ranging from 0.1-0.3 M was insignificant. Therefore, 0.1 M of KOH solution was used as activating agents for NPC-PBZ-m in the activation step as the result is shown in **Figure 4.36**.

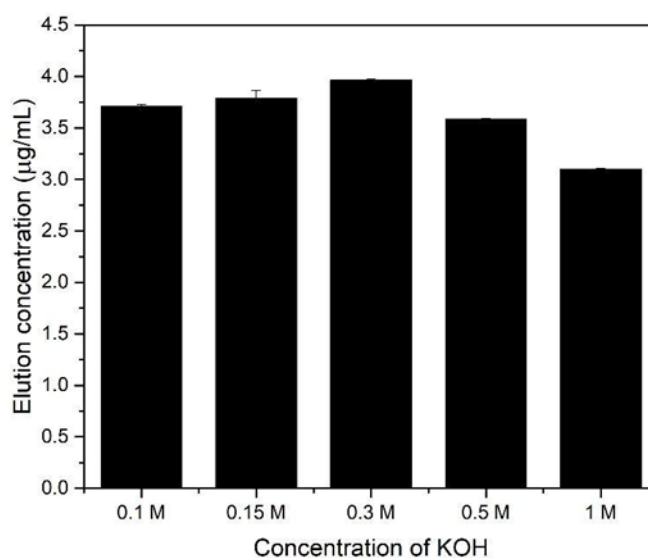


**Figure 4.36** Effect of KOH concentration on activation step on paraquat adsorption.

#### 4.14.2 Study of the volume of desorbing solvent on the paraquat determination

The volume of 1M HCl: MeOH (70:30) can affect the desorption efficiency. The 2 mL of paraquat solution was needed to conduct the colorimetric method. Therefore, every 2 mL of HCl:MeOH was collected for 5 fractions. The results shown in **Figure 4.37** indicating that the highest amount of paraquat was obtained since the first fraction, and the amount of paraquat decreased with the further desorption fractions from 2-5 (< LOD). Therefore, the optimized volume of HCl 1M: MeOH (70: 30) was found to be 2 mL.

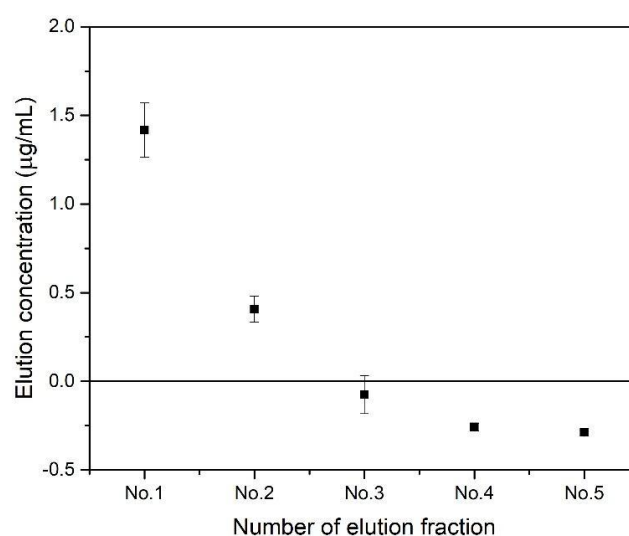


**Figure 4.37** Number of desorption fraction study on paraquat desorption.

#### 4.15 The performance of proposed method for paraquat detection

The adsorption and desorption processes were performed under the optimum conditions followed by the colorimetric detection via paraquat blue free radical reaction using 50 mL of 0.05-1 µg/mL of paraquat solution. The relationship between the signal of paraquat blue free radical against the concentration of paraquat was observed as shown in **Figure 4.38**. Although the performance of the proposed method is not low enough compared to the many reported methods, this developed method can be improved to achieve the desired target as an example given below.

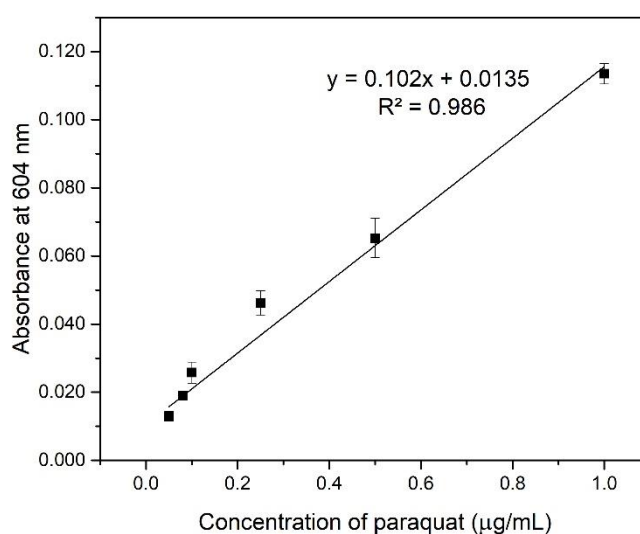


**Figure 4.38** Correlation curve between paraquat concentration against absorbance signal of blue radical at 600 nm.

#### 4.16 The suggestion of this proposed method to enhance the efficiency for paraquat detection

The adsorption efficiency of paraquat on NPC-PBZ-m might be improved when increased the amount of sorbent or volume of 0.1 M KOH. Therefore, the alteration of paraquat blue free radical intensity was investigated when the amount of NPC-PBZ-m or volume of activating agent changed.

##### 4.16.1 Effect of NPC-PBZ-m weight on paraquat adsorption

A 50 mL of 0.5 µg/mL paraquat solution was prepared and adsorbed by either 0.050 and 0.100 mg of NPC-PBZ-m. The adsorption and desorption processes were conducted under the optimum conditions. Then, the paraquat content in the desorbing solvent was measured by UV-Visible spectrophotometer. The extraction efficiency can be increased with increasing the weight of the NPC-PBZ-m (**Figure 4.39A**). As can be seen that the increase in the NPC-PBZ-m dosage, the possibility of paraquat contact to the sorbent also increased in the batch process.

#### 4.16.2 The ratio of NPC-PBZ-m weight to KOH volume (mg/mL) affecting on paraquat adsorption

Three ratios of NPC-PBZ-m weight to 0.1 M KOH volume, which are 1:0.5, 1:1, and 1:2, were studied. From the previous results, the weight of sorbent and paraquat solution was fixed at 0.100 g and 50 mL of 0.5  $\mu\text{g/mL}$ , respectively. After adsorption step, the paraquat was desorbed by using 2 mL of 1 M HCl-MeOH (70:30). Then, paraquat blue free radical was performed under the optimum conditions. The results shown in **Figure 4.39B**. The intensity of paraquat blue free radical increased with the increase in the KOH volume (mL) from 50 to 100 mL as the ratio were 1:0.5 and 1:1, respectively. However, the same absorbance value was still obtained even the volume of KOH solution higher than NPC-PBZ-m weight (at the ratio of 1:2). Therefore, it can be concluded that the suitable ratio of NPC-PBZ-m weight to the volume of 0.1 M of KOH solution was 1:1.

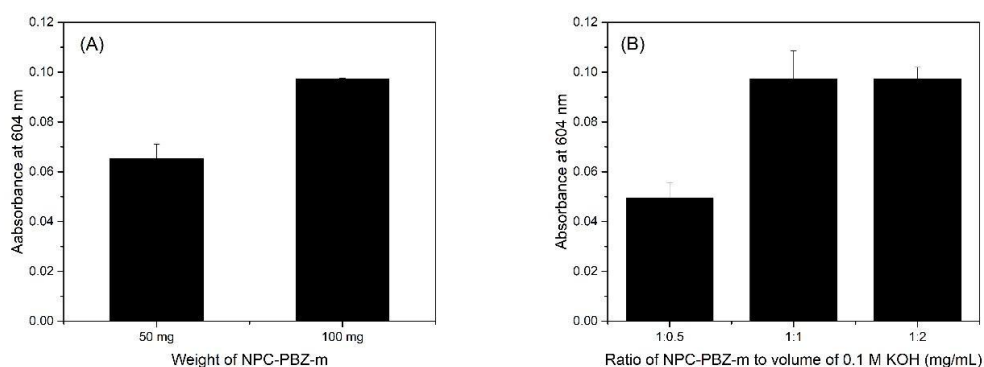


**Figure 4.39** Effect of NPC-PBZ-m weight (A) and ratio of NPC-PBZ-m weight to 0.1 M KOH volume (B) on paraquat adsorption.



## CHAPTER V

### CONCLUSION

#### 5.1 Conclusion

The nanoporous carbon derived from melamine based polybenzoxazine (NPC-PBZ-m) was prepared to use as atrazine sorbent. The success of NPC-PBZ-m synthesis was confirmed by FTIR technique. Moreover, the porous structure, surface area, and surface functional group were characterized by FE-SEM, BET, and XPS techniques, respectively. The results showed that NPC-PBZ-m sorbent has an average pore diameter of 9.75 nm that can act as nanoporous material which contains a mesoporous structure according to IUPAC classification. Therefore, NPC-PBZ-m sorbent shows the great permeability material which can be adopted to pre-concentrate atrazine by using only a syringe pump. Moreover, the presence of pyridine-N, pyridone-N, and C-C bond ( $sp^2$ ), as the main type of N- and C- atoms, on their surface can be implied that these functional groups serving as binding sites for atrazine occurring via  $\pi$ - $\pi$  interaction or Van der Waals force. Various parameters that can affect atrazine pre-concentration including NPC-PBZ-m particle size, weight of sorbent, adsorption-elution flow rate, and elution volume were also optimized. In addition, the effects of other pesticides interference that are widely used with atrazine were also studied. The figure of merit in HPLC-UV measurement showed method detection limit (MDL) and method quantitation limit (MQL) at 1.05  $\mu\text{g/L}$  and 3.45  $\mu\text{g/L}$ , respectively.

Furthermore, the colorimetric method was also developed based on König's reaction for atrazine determination. Various parameters affecting the sensitivity of polymethine compound such as concentration and volume of reagent, heating temperature and time, as well as response time were also investigated. A new coupling reaction, *p*-Anisidine, reacts with atrazine to give an orange-red polymethine compound which has a maximum wavelength at 500 nm. To study the interference species, other pesticides, glyphosate, 2,4-D, and chlorpyrifos, do not interfere with the color response when they are present in the solution. However, in the harsh acidic or

basic media, the color solution of paraquat expresses more tense orange-yellow color. The figure of merit in UV-Visible spectrophotometer showed method detection limit (MDL) and method quantitation limit (MQL) at 2.26  $\mu\text{g/L}$  and 7.46  $\mu\text{g/L}$ , respectively. Moreover, the color of polymethine compound can be distinguished by naked eye detection when the concentration of atrazine ranges from 1-5  $\mu\text{g/mL}$ .

For paraquat analysis, silica-humic acid entrapped calcium alginate hydrogel (Si-HA-Alg) was prepared to use as paraquat sorbent. The agar- mold contained  $\text{CaCl}_2$  was adopted to prepare the alginate cylinder. The suitable composition of silica gel and humic acid sodium salt was 1 (% w/v) while the content of alginate can affect the humic acid leaching phenomenon. Moreover, the weight of sorbent is quietly difficult to control causing the effect of repeatability of method. As the information, NPC-PBZ-m was adopted to assess the possibility for paraquat adsorption. The preliminary test showed paraquat can be adsorbed by NPC-PBZ-m and the desorption process can be performed using 1 M HCl-MeOH (70:30) as a desorbing solvent. Moreover, the collected desorbing solvent was also tested with the paraquat blue free radical reaction by measuring at 604 nm using UV-Visible spectrophotometer. The performance of method was reported from 0.05-1  $\mu\text{g/mL}$  with correlation coefficient at 0.986.

## 5.2 Suggestion of future work

The NPC-PBZ-m material showed a possibility for paraquat adsorption. The suggestion for the future work is to improve the detection limit and various water sample could be employed to test the feasibility of the adsorbent.

## REFERENCES

1. Socio-economic context and role of agriculture, country fact sheet on food and agriculture policy trends. (2018). from Food and agriculture organization of the United Nations. <http://www.fao.org/3/i8683EN/i8683en.pdf>
2. Agricultural statistics of Thailand 2018. (2018). from Office of Agricultural Economics.
3. Tomková, H., Sokolová, R., Opletal, T., Kučerová, P., Kučera, L., Součková, J., Skopalová, J., & Barták, P., Electrochemical sensor based on phospholipid modified glassy carbon electrode - determination of paraquat. *J. Electroanal. Chem.* **2018**, *821*, 33-39.
4. Phewnil, O.-A., Tungkananurak, N., Panichsakpatana, S., & Pitiyont, B., Phytotoxicity of atrazine herbicide to fresh water macrophyte duckweed (*Lemna perpusilla* Torr.) in Thailand. *Environ. Nat. Resour. J.* **2012**, *10*, 16-27.
5. Rinsky, J. L., Hopenhayn, C., Golla, V., Browning, S., & Bush, H. M., Atrazine exposure in public drinking water and preterm birth. **2012**, *127*, 72-80.
6. รายงานสรุปวัตถุอันตรายที่มีการนำเข้าสูงสุด 10 อันดับแรก ปี 2562. Retrieved 17 November 2020  
[http://www.doa.go.th/ard/wp-content/uploads/2020/02/HASTAT62\\_03.pdf](http://www.doa.go.th/ard/wp-content/uploads/2020/02/HASTAT62_03.pdf)
7. Dinis-Oliveira, R. J., Remiao, F., Carmo, H., Duarte, J. A., Navarro, A. S., Bastos, M. L., & Carvalho, F., Paraquat exposure as an etiological factor of Parkinson's disease. *Neurotoxicology* **2006**, *27*, 1110-1122.
8. Jablonowski, N. D., Schaffer, A., & Burauel, P., Still present after all these years: persistence plus potential toxicity raise questions about the use of atrazine. *Environ. Sci. Pollut. Res.* **2011**, *18*, 328-331.
9. Basini, G., Bianchi, F., Bussolati, S., Baioni, L., Ramoni, R., Grolli, S., Conti, V., Bianchi, F., & Grasselli, F., Atrazine disrupts steroidogenesis, VEGF and NO production in swine granulosa cells. *Ecotoxicol. Environ. Saf.* **2012**, *85*, 59-63.

10. Yang, Y., Cao, H., Peng, P., & Bo, H., Degradation and transformation of atrazine under catalyzed ozonation process with TiO<sub>2</sub> as catalyst. *J. Hazard. Mater.* **2014**, 279, 444-451.
11. Bethsass, J., & Colangelo, A., European Union bans atrazine, while the United States negotiates continued use. **2006**, 12, 260-267.
12. Chuntib, P., & Jakmune, J., Simple flow injection colorimetric system for determination of paraquat in natural water. *Talanta* **2015**, 144, 432-438.
13. Groundwater quality standards (Thailand). Retrieved 17 November 2020, from Water Environment Partnership in Asia: WEPA [http://www.wepa-db.net/policies/law/thailand/std\\_groundwater.htm](http://www.wepa-db.net/policies/law/thailand/std_groundwater.htm)
14. Amondham, W., Parkpian, P., Polprasert, C., DeLaune, R. D., & Jugsujinda, A., Paraquat adsorption, degradation, and remobilization in tropical soils of Thailand. *J. Environ. Sci. Health B* **2006**, 41, 485-507.
15. Panuwet, P., Siriwong, W., Prapamontol, T., Ryan, P. B., Fiedler, N., Robson, M. G., & Barr, D. B., Agricultural pesticide management in Thailand: situation and population health risk. *Environ Sci Policy* **2012**, 17, 72-81.
16. แนวทางการแก้ปัญหาสารเคมีกำจัดศัตรูพืชตลอดห่วงโซ่การผลิตในพื้นที่ต้นน้ำ ระบบนิเวศ และประชาชนในพื้นที่. Retrieved 17 November 2020 [http://www.thaipan.org/sites/default/files/file/pesticide\\_doc27.pdf](http://www.thaipan.org/sites/default/files/file/pesticide_doc27.pdf)
17. Phewnil, O.-A., Tungkananurak, N., Panichsakpatana, S., Pitiyont, B., Siripat, N., & Watanabe, H., The residues of atrazine herbicide in stream water and stream sediment in Huay Kapo watershed, Phetchabun Province, Thailand. *Environ. Nat. Resour. J.* **2012**, 10, 42-52.
18. Taguchi, V. Y., Jenkins, S. W. D., Crozier, P. W., & Wang, D. T., Determination of diquat and paraquat in water by liquid chromatography (electrospray ionization) mass spectrometry. *J. Am. Soc. Mass Spectrom.* **1998**, 9, 830-839.
19. Ou, S., Wang, Y., Chen, X.-B., Chen, J., & Chen, L., Determination of paraquat in environmental water by ionic liquid-based liquid phase extraction with direct injection for hplc. *J. Anal. Chem.* **2018**, 73, 862-868.
20. Cameiro, M. C., Puignou, L., & Galceran, M. T., Comparison of capillary electrophoresis and reversed-phase ion-pair high-performance liquid

- chromatography for the determination of paraquat , diquat and difenzoquat. *J. Chromatogr. A* **1994**, *669*, 217-224.
21. Nasir, T., Herzog, G., Hebrant, M., Despas, C., Liu, L., & Walcarius, A., Mesoporous silica thin films for improved electrochemical detection of paraquat. *ACS Sens.* **2018**, *3*, 484-493.
  22. Graziano, N., Mcguire, M. J., Roberson, A., Adams, C., Jiang, H., & Blute, N., 2004 National atrazine occurrence, monitoring program using the abraxia ELISA method. *Environ. Sci. Technol.* **2006**, *40*, 1163-1171.
  23. Ma, W. T., Cai, Z., & Jiang, G. B., Determination of atrazine, deethylatrazine and simazine in water at parts-per-trillion levels using solid-phase extraction and gas chromatography/ion trap mass spectrometry. *Rapid Commun. Mass Spectrom.* **2003**, *17*, 2707-2712.
  24. Trajkovska, V., Petrovska-Jovanovic, S., & Cvetkovski, M., Development and optimization of a method for the determination of simazine, atrazine and propazine using solid-phase extraction and hplc/gc. *J. Serbian Chem. Soc.* **2001**, *66*, 199-204.
  25. Brigante, M., Zanini, G., & Avena, M., Effect of humic acids on the adsorption of paraquat by goethite. *J. Hazard. Mater.* **2010**, *184*, 241-247.
  26. Ruiz, M., Barron-Zambrano, J., Rodilla, V., Szygula, A., & Sastre, A. M. (2008). *Paraquat sorption on calcium alginate gel beads*. Paper presented at the 4th WSEAS/IASME international conference on Dynamical systems and control.
  27. Brigante, M., & Schulz, P. C., Adsorption of paraquat on mesoporous silica modified with titania: effects of pH, ionic strength and temperature. *J. Colloid Interface Sci.* **2011**, *363*, 355-361.
  28. Leovac, A. S., Vasyukova, E., Ivančev-Tumbas, I. I., Uhl, W., Kragulj, M. M., Tričković, J. S., Kerkez, Đ. V., & Dalmacija, B. D., Sorption of atrazine, alachlor and trifluralin from water onto different geosorbents. *RSC Adv.* **2015**, *5*, 8122-8133.
  29. Lladó, J., Lao-Luque, C., Ruiz, B., Fuente, E., Solé-Sardans, M., & Dorado, A. D., Role of activated carbon properties in atrazine and paracetamol adsorption equilibrium and kinetics. *Process Saf Environ Prot* **2015**, *95*, 51-59.

30. Chen, G. C., Shan, X. Q., Zhou, Y. Q., Shen, X. E., Huang, H. L., & Khan, S. U., Adsorption kinetics, isotherms and thermodynamics of atrazine on surface oxidized multiwalled carbon nanotubes. *J. Hazard. Mater.* **2009**, *169*, 912-918.
31. Manmuanpom, N., Thubsuang, U., Dubas, S. T., Wongkasemjit, S., & Chaisuwan, T., Enhanced CO<sub>2</sub> capturing over ultra-microporous carbon with nitrogen-active species prepared using one-step carbonization of polybenzoxazine for a sustainable environment. *J. Environ. Manage.* **2018**, *223*, 779-786.
32. Rattanopas, O., Naewrittikul, W., & Chaisuwan, T., The nanoporous carbon derived from melamine based polybenzoxazine and NaCl templating. *Key Eng. Mater.* **2018**, *779*, 129-136.
33. Shivhare, P., & Gupta, V. K., Spectrophotometric method for the determination of paraquat in water, grain and plant materials. *Analyst* **1991**, *116*, 391-393.
34. Rai, M. K., Das, J. V., & Gupta, V. K., A sensitive determination of paraquat by spectrophotometry. *Talanta* **1997**, *45*, 343-348.
35. Kuan, C. M., Lin, S. T., Yen, T. H., Wang, Y. L., & Cheng, C. M., Paper-based diagnostic devices for clinical paraquat poisoning diagnosis. *Biomicrofluidics* **2016**, *10*, 034118.
36. Kesari, R., & Gupta, V. K., A simple method for the spectrophotometric determination of atrazine using p-aminoacetophenone and its application in environmental and biological samples. *Talanta* **1998**, *47*, 1085-1092.
37. Martins, E. C., Melo Vde, F., & Abate, G., Evaluation of flow injection analysis method with spectrophotometric detection for the determination of atrazine in soil extracts. *J. Environ. Sci. Health B* **2016**, *51*, 609-615.
38. Tamrakar, U., Mathew, S. B., Gupta, V. K., & Pillai, A. K., Determination of atrazine in environmental and biological samples using solid phase extraction and spectrophotometry. *J. Anal. Chem.* **2009**, *64*, 386-389.
39. Shah, J., Rasul Jan, M., & Ara, B., Spectrophotometric method for determination of atrazine and its application to commercial formulations and real samples. *Int J Environ Anal Chem* **2008**, *88*, 1077-1085.

40. Tiwari, N., Asthana, A., & Upadhyay, K., A sensitive spectrophotometric determination of atrazine in micellar medium and its application in environmental samples. *Res. Chem. Intermed.* **2013**, *39*, 2867-2879.
41. Bus, J. S., & Gibson, J. E., Paraquat: model for oxidant-initiated toxicity. *Environ. Health Perspect.* **1984**, *55*, 37-46.
42. Cheremisinoff, N. P., & Rosenfeld, P. E. (2011). Atrazine. In *Handbook of pollution prevention and cleaner production: best practices in the agrochemical industry* (pp. 215-231): William Andrew (publisher).
43. Eisler, R. (1990). Paraquat hazards to fish, wildlife, and invertebrates: a synoptic review. from U.S. Fish and Wildlife Service Patuxent Wildlife Research Center Laurel.
44. Ishida, H. (2011). Overview and historical background of polybenzoxazine research. In *Handbook of Benzoxazine Resins* (pp. 3-81).
45. Rucigaj, A., Alic, B., Krajnc, M., & Sebenik, U., Curing of bisphenol A-aniline based benzoxazine using phenolic, amino and mercapto accelerators. *EXPRESS Polym. Lett.* **2015**, *9*, 647-657.
46. Kim, H. J., Brunovska, Z., & Ishida, H., Synthesis and thermal characterization of polybenzoxazines based on acetylene-functional monomers. *Polymer* **1999**, *40*, 6565-6573.
47. Lorjai, P., Chaisuwan, T., & Wongkasemjit, S., Porous structure of polybenzoxazine-based organic aerogel prepared by sol-gel process and their carbon aerogels. *J. Sol-Gel Sci. Technol.* **2009**, *52*, 56-64.
48. Holly, F. W., & Cope, A. C., Condensation products of aldehydes and ketones with o-Aminobenzyl alcohol and o-Hydroxybenzylamine. *J. Am. Chem. Soc.* **1944**, *66*, 1875-1879.
49. Burke, W. J., 3,4-Dihydro-1,3,2H-Benzoxazines. reaction of p-substituted phenols with N,N-Dimethylolamines. *J. Am. Chem. Soc.* **1949**, *71*, 609-612.
50. Zhang, Q., Yang, P., Deng, Y., Zhang, C., Zhu, R., & Gu, Y., Effect of phenol on the synthesis of benzoxazine. *RSC Adv.* **2015**, *5*, 103203-103209.

51. Chirachanchai, S., Phongtamrug, S., Laobuthee, A., & Tashiro, K. (2011). Mono-Substituted Phenol-Based Benzoxazines. In *Handbook of Benzoxazine Resins* (pp. 111-126).
52. Ning, X., & Ishida, H., Phenolic materials via ring- opening polymerization of benzoxazines: effect of molecular structure on mechanical and dynamic mechanical properties. *J. Polym. Sci. B Polym. Phys.* **1994**, *32*, 921-927.
53. Wang, Y.-X., & Ishida, H., Cationic ring-opening polymerization of benzoxazines. *Polymer* **1999**, *42*, 4563-4570.
54. Arslan, M., Kiskan, B., & Yagci, Y., Ring-opening polymerization of 1,3-Benzoxazines via borane catalyst. *Polymers* **2018**, *10*, 239.
55. Riess, G., Schwob, J. M., & Guth, G. Ring opening polymerization of benzoxazines - a new route to phenolic resins. In *Advances in polymer synthesis* (Vol. 31, pp. 27-49).
56. Chutayothin, P., & Ishida, H., Cationic ring-opening polymerization of 1,3-Benzoxazines: mechanistic study using model compounds. *Macromolecules* **2010**, *43*, 4562-4572.
57. Dunkers, J., & Ishida, H., Reaction of benzoxazine-based phenolic resins with strong and weak carboxylic acids and phenols as catalysts. *J Polym Sci A Polym Chem* **1999**, *37*, 1913-1921.
58. Shi, J., Zheng, X., Xie, L., Cao, F., Wu, Y., & Liu, W., Film-forming characteristics and thermal stability of low viscosity benzoxazines derived from melamine. *Eur. Polym. J.* **2013**, *49*, 4054-4061.
59. Chaisuwan, T., Komalwanich, T., Luangsukrerk, S., & Wongkasemjit, S., Removal of heavy metals from model wastewater by using polybenzoxazine aerogel. *Desalination* **2010**, *256*, 108-114.
60. Landau, M. V., Sol-Gel process. 119-160.
61. Thubsuang, U., Ishida, H., Wongkasemjit, S., & Chaisuwan, T., Self-formation of 3D interconnected macroporous carbon xerogels derived from polybenzoxazine by selective solvent during the sol-gel process. *J. Mater. Sci.* **2014**, *49*, 4946-4961.



62. Hassan, A. F., Abdel-Mohsen, A. M., & Fouda, M. M., Comparative study of calcium alginate, activated carbon, and their composite beads on methylene blue adsorption. *Carbohydr. Polym.* **2014**, *102*, 192-198.
63. Salisu, A., Sanagi, M. M., Abu Naim, A., Wan Ibrahim, W. A., & Abd Karim, K. J., Removal of lead ions from aqueous solutions using sodium alginate-graft-poly(methyl methacrylate) beads. *Desalination Water Treat.* **2016**, *57*, 15353-15361.
64. Montanucci, P., Terenzi, S., Santi, C., Pennoni, I., Bini, V., Pescara, T., Basta, G., & Calafiore, R., Insights in behavior of variably formulated alginate-based microcapsules for cell transplantation. *BioMed Res. Int.* **2015**, 965804-965813.
65. Senesi, N., Binding mechanisms of pesticides to soil humic substances. *Sci. Total Environ.* **1992**, 63-76.
66. Islam, K. M. S., Schuhmacher, A., & Gropp, J. M., Humic acid substances in animal agriculture. *Pak J Nutr* **2005**, *4*, 126-134.
67. Kara, H., Ayyildiz, H. F., & Topkafa, M., Use of aminopropyl silica-immobilized humic acid for Cu(II) ions removal from aqueous solution by using a continuously monitored solid phase extraction technique in a column arrangement. *Colloids Surf. A Physicochem. Eng. Asp.* **2008**, *312*, 62-72.
68. Melo, B. A. G. d., Motta, F. L., & Santana, M. H. A., Humic acids: Structural properties and multiple functionalities for novel technological developments. *Mater. Sci. Eng. C* **2016**, *62*, 967-974.
69. Crespilho, F. N., Zucolotto, V., Siqueira, J. R., Constantino, C. J. L., Nart, F. C., & Oliveira, O. N., Immobilization of humic acid in nanostructured layer-by-layer films for sensing applications. *Environ. Sci. Technol.* **2005**, *39*, 5385-5389.
70. Tatikolov, A. S., Polymethine dyes as spectral-fluorescent probes for biomacromolecules. *J. Photochem. Photobiol. C* **2012**, *13*, 55-90.
71. Polymethine Dyes. In: Van Nostrand's Scientific Encyclopedia.
72. I.Tolmachev, A., & YA.II'Chenko, R. POLYMETHINE DYES. In: Kirk-Othmer Encyclopedia of Chemical Technology.

73. Yuen, S. H., Bagness, J. E., & Myles, D., Spectrophotometric determination of diquat and paraquat in aqueous herbicide formulations. *Analyst* **1967**, *92*, 375-381.
74. Katsumata, H., Kaneco, S., Suzuki, T., & Ohta, K., Determination of atrazine and simazine in water samples by high-performance liquid chromatography after preconcentration with heat-treated diatomaceous earth. *Anal. Chim. Acta* **2006**, *577*, 214-219.
75. Zhao, F., Wang, S., She, Y., Zhang, C., Zheng, L., Jin, M., Shao, H., Jin, F., Du, X., & Wang, J., Subcritical water extraction combined with molecular imprinting technology for sample preparation in the detection of triazine herbicides. *J. Chromatogr. A* **2017**, *1515*, 17-22.
76. Kueseng, P., Nisoa, M., & Sontimuang, C., Rapid preparation of molecularly imprinted polymers by custom-made microwave heating for analysis of atrazine in water. *J. Sep. Sci.* **2018**, *41*, 2783-2789.
77. Mohammadi, F., Esrafil, A., Kermani, M., Farzadkia, M., Gholami, M., & Behbahani, M., Application of amino modified mesostructured cellular foam as an efficient mesoporous sorbent for dispersive solid-phase extraction of atrazine from environmental water samples. *Microchem. J.* **2019**, *146*, 753-762.
78. Zhang, H., Yuan, Y., Sun, Y., Niu, C., Qiao, F., & Yan, H., An ionic liquid-magnetic graphene composite for magnet dispersive solid-phase extraction of triazine herbicides in surface water followed by high performance liquid chromatography. *Analyst* **2018**, *143*, 175-181.
79. Yue, Z., & Economy, J., Nanoparticle and nanoporous carbon adsorbents for removal of trace organic contaminants from water. *J Nanopart Res* **2005**, *7*, 477-487.
80. Zhou, Q., Xiao, J., Wang, W., Liu, G., Shi, Q., & Wang, J., Determination of atrazine and simazine in environmental water samples using multiwalled carbon nanotubes as the adsorbents for preconcentration prior to high performance liquid chromatography with diode array detector. *Talanta* **2006**, *68*, 1309-1315.
81. Tang, W.-W., Zeng, G.-M., Gong, J.-L., Liu, Y., Wang, X.-Y., Liu, Y.-Y., Liu, Z.-F., Chen, L., Zhang, X.-R., & Tu, D.-Z., Simultaneous adsorption of atrazine and Cu (II) from

- wastewater by magnetic multi-walled carbon nanotube. *Chem. Eng. J.* **2012**, *211-212*, 470-478.
82. Lupul, I., Yperman, J., Carleer, R., & Gryglewicz, G., Adsorption of atrazine on hemp stem-based activated carbons with different surface chemistry. *Adsorption (Boston)* **2015**, *21*, 489-498.
83. Yang, B. Y., Cao, Y., Qi, F. F., Li, X. Q., & Xu, Q., Atrazine adsorption removal with nylon6/polypyrrole core-shell nanofibers mat: possible mechanism and characteristics. *Nanoscale Res. Lett.* **2015**, *10*, 207.
84. Siangproh, W., Somboonsuk, T., Chailapakul, O., & Songsrirote, K., Novel colorimetric assay for paraquat detection on-silica bead using negatively charged silver nanoparticles. *Talanta* **2017**, *174*, 448-453.
85. Radke, R. O., Armstrong, D. E., & Chesters, G., Herbicide colorimetric procedures, evaluation of pyridine-alkali colorimetric method for determination of atrazine. *J. Agric. Food Chem.* **1966**, *14*, 70-73.
86. Freeman, W. H. (2010). APPENDIX H Standard Reduction Potentials.
87. Chou, Y. H., Yu, J. H., Liang, Y. M., Wang, P. J., Li, C. W., & Chen, S. S., Recovery of Cu(II) by chemical reduction using sodium dithionite: effect of pH and ligands. *Water Sci. Technol.* **2015**, *72*, 2089-2094.
88. Bodner Research Web, Electro chemical reactions, The standard-state half-cell potential for the oxidation of glucose. Retrieved 17 November 2020 <http://chemed.chem.purdue.edu/genchem/topicreview/bp/ch20/electro.php>
89. Kesari, R., Rai, M., & Gupta, V. K., A sensitive spectrophotometric method for the determination of paraquat in food and biological samples. *J. AOAC Int.* **1997**, *80*, 388-391.
90. Brunauer, S., Emmett, P. H., & Teller, E., Adsorption of gases in multimolecular layers. *J. Am. Chem. Soc.* **1938**, *60*, 309-319.
91. Joyner, L. G., Barrett, E. P., & Skold, R., The determination of pore volume and area distributions in porous substances. II. Comparison between nitrogen isotherm and mercury porosimeter methods. *J. Am. Chem. Soc.* **1951**, *73*, 3155-3158.
92. Lippens, B. C., & Boer, J. H. D., Studies on pore systems in catalysts V. The t method. *J. Catal.* **1965**, *4*, 319-323.

93. Xu, S., Lu, H., & Chen, L., Double water compatible molecularly imprinted polymers applied as solid-phase extraction sorbent for selective preconcentration and determination of triazines in complicated water samples. *J. Chromatogr. A* **2014**, *1350*, 23-29.
94. Yogendrarajah, P., Van Poucke, C., De Meulenaer, B., & De Saeger, S., Development and validation of a QuEChERS based liquid chromatography tandem mass spectrometry method for the determination of multiple mycotoxins in spices. *J. Chromatogr. A* **2013**, *1297*, 1-11.
95. Regehr, D. L., & Norwood, C. A. (2008). Benefits of triazine herbicides in ecofallow. In *Environmental Science* (pp. 175-183).
96. DeLorenzo, M. E., & Serrano, L., Individual and mixture toxicity of three pesticides; atrazine, chlorpyrifos, and chlorothalonil to the marine phytoplankton species *Dunaliella tertiolecta*. *J. Environ. Sci. Health B* **2003**, *38*, 529-538.
97. Ndi Nsami, J., & Ketcha Mbadcam, J., The adsorption efficiency of chemically prepared activated carbon from cola nut shells by on methylene blue. *J. Chem.* **2013**, 1-7.
98. Liu, Z., Du, Z., Song, H., Wang, C., Subhan, F., Xing, W., & Yan, Z., The fabrication of porous N-doped carbon from widely available urea formaldehyde resin for carbon dioxide adsorption. *J. Colloid Interface Sci.* **2014**, *416*, 124-132.
99. Chambrion, P., Suzuki, T., Zhang, Z.-G., Kyotani, T., & Tomita, A., XPS of nitrogen-containing functional groups formed during the C-NO reaction. *Energy Fuels* **1997**, *11*, 681-685.
100. Chulliyote, R., Hareendrakrishnakumar, H., Raja, M., Gladis, J. M., & Stephan, A. M., Sulfur-Immobilized nitrogen and oxygen Co-doped hierarchically porous biomass carbon for lithium-sulfur batteries: influence of sulfur content and distribution on its performance. *ChemistrySelect* **2017**, *2*, 10484-10495.
101. Manocha, S. M., Porous carbons. *Sadhana* **2003**, *28*, 335-348.
102. Frenich, A. G., Romero-Gonzalez, R., Gomez-Perez, M. L., & Vidal, J. L., Multi-mycotoxin analysis in eggs using a QuEChERS-based extraction procedure and ultra-high-pressure liquid chromatography coupled to triple quadrupole mass spectrometry. *J. Chromatogr. A* **2011**, *1218*, 4349-4356.

103. Asperger, A., Efer, J., Koal, T., & Engewald, W., On the signal response of various pesticides in electrospray and atmospheric pressure chemical ionization depending on the flow-rate of eluent applied in liquid chromatography–tandem mass spectrometry. *J. Chromatogr. A* **2001**, *937*, 65-72.
104. Brand, R. M., Charron, A. R., Dutton, L., Gavlik, T. L., Mueller, C., Hamel, F. G., Chakkalakal, D., & Donohue, T. M., Jr., Effects of chronic alcohol consumption on dermal penetration of pesticides in rats. *J. Toxicol. Environ. Health Part A* **2004**, *67*, 153-161.
105. Struger, J., Thompson, D., Staznik, B., Martin, P., McDaniel, T., & Marvin, C., Occurrence of glyphosate in surface waters of Southern Ontario. *Bull Environ Contam Toxicol* **2008**, *80*, 378-384.
106. Adams, R. M., McAdams, B. C., Arnold, W. A., & Chin, Y. P., Transformation of chlorpyrifos and chlorpyrifos-methyl in prairie pothole pore waters. *Environ Sci Process Impacts* **2016**, *18*, 1406-1416.
107. Pospisil, L., Trskova, R., Fuoco, R., & Colombini, M. P., Electrochemistry of s-triazine herbicides: reduction of atrazine and terbutylazine in aqueous solutions. *J. Electroanal. Chem.* **1995**, *395*, 189-193.
108. Pospisil, L., Trskova, R., Zalis, S., Colombini, M. P., & Fuoco, R., Decomposition products of s-triazine herbicides by electron-transfer in acidic aqueous media. *Microchem. J.* **1996**, *54*, 367-374.
109. Ragab, M. T. H., & McCollum, J. P., Colorimetric methods for the determination of simazine and related chloro-s-triazines. *J. Agric. Food Chem.* **1968**, *16*, 284-289.
110. Gohar, G. A., & Habeeb, M. M., Proton transfer equilibria, temperature and substituent effects on hydrogen bonded complexes between chloranilic acid and anilines. *Spectrosc.* **2000**, *14*, 99-107.
111. Xu, Z., Hu, C., & Guoxin, H., Layer-by-layer self-assembly of multilayer films based on humic acid. *Thin Solid Films* **2011**, *519*, 4324-4328.
112. Arneli, Safitri, Z. F., Pangestika, A. W., Fauziah, F., Wahyuningrum, V. N., & Astuti, Y., The influence of activating agents on the performance of rice husk-based carbon for sodium lauryl sulfate and chrome (Cr) metal adsorptions. *Mater. Sci. Eng. C* **2017**, *172*, 012007.

113. Nuilerd, T., Pongyeela, P., & Chungsiriporn, J., Pellet activated carbon production using parawood charcoal from gasifier by KOH activation for adsorption of iron in water. *Warasan Songkhla Nakharin* **2018**, *40*, 264-270.
114. Zhou, Q., Mao, J., Xiao, J., & Xie, G., Determination of paraquat and diquat preconcentrated with N doped TiO<sub>2</sub> nanotubes solid phase extraction cartridge prior to capillary electrophoresis. *Anal. Methods* **2010**, *2*, 1063-1068.



**VITA**

<b>NAME</b>	Miss Anna Prukjareonchook
<b>DATE OF BIRTH</b>	15 Feb 1992
<b>PLACE OF BIRTH</b>	Phra Phutthabat, Saraburi, Thailand
<b>INSTITUTIONS ATTENDED</b>	<p>She graduated with high school degree from Pibulwittayalai Lopburi in 2009. She graduated with a Bachelor's degree from the Department of Chemistry, Faculty of Science, Srinakharinwirot University in 2013. Then, she has become a Ph.D. student in the Analytical field at the Department of Chemistry, Faculty of Science, Chulalongkorn University since 2014. She received the scholarship from Graduate School, Chulalongkorn University to commemorate the 72nd anniversary of his Majesty King Bhumibala Aduladeja. In 2018, she had a great opportunity to join Sakura Science Program at Meiji University, Ikuta campus, Japan.</p>